THE EFFECT OF HEAT TRANSFER ON THE LAMINAR BOUNDARY LAYER AND LAMINAR SEPARATION OF WATER FLOWING PAST A FLAT PLATE AND A SPHERE

Thesis for the Degree of Ph. D.
MICHIGAN STATE UNIVERSITY
SURINDER KAPUR
1972

This is to certify that the

thesis entitled

THE EFFECT OF HEAT TRANSFER ON THE LAMINAR BOUNDARY LAYER AND LAMINAR SEPARATION OF WATER FLOWING PAST A FLAT PLATE AND A SPHERE

presented by

Surinder Kapur

has been accepted towards fulfillment of the requirements for

Ph.D. degree in Mechanical Engineering

M C Smith

Major professor

Date January 17, 1972

O-7639

ABSTRACT

THE EFFECT OF HEAT TRANSFER ON THE LAMINAR BOUNDARY LAYER AND LAMINAR SEPARATION OF WATER FLOWING PAST A FLAT PLATE AND A SPHERE

By

Surinder Kapur

The effect of heating a body, which is in a uniform flow of water, is investigated numerically and experimentally. Primary interest is in the effect of heat transfer on the laminar boundary layer separation. Since the variation of viscosity with temperature is large for water, the velocity and temperature fields interact. This necessitates the simultaneous solution of the momentum and energy equations. Numerical results for various flow configurations are presented. Experimental results are presented for the flow of water past a three-inch sphere in a ten-inch square horizontal test section. Flow visualization techniques, hydrogen bubble, and the shadowgraph methods, were used to locate the separation point experimentally.

Numerical results indicate that heating does substantially shift the separation point backward for the

linearly retarded flow past a heated flat plate. The effect of heating on the position of the separation point, for flow past a sphere, is small. Experimental results tend to confirm the small influence of heating on the position of the separation point on the heated sphere.

Numerical results also include the effect of heating on the various boundary layer parameters such as displacement thickness, thermal boundary layer thickness, and wall shear.

THE EFFECT OF HEAT TRANSFER ON THE LAMINAR BOUNDARY LAYER AND LAMINAR SEPARATION OF WATER FLOWING PAST A FLAT PLATE AND A SPHERE

By

Surinder Kapur

A THESIS

Submitted to
Michigan State University
in partial fulfillment of the requirements
for the degree of

DOCTOR OF PHILOSOPHY

Department of Mechanical Engineering

1972

A DEDICATION

This thesis is dedicated to my mother, without whose encouragement and confidence this work would not have been completed.

This is also dedicated to my wife, Rani, who has displayed great patience and tolerance during the last year of this work.

Finally, I dedicate this thesis to my son, Sanjay.

ACKNOWLEDGMENTS

The author wishes to express his sincere thanks to his major professors Drs. Merle C. Potter and Mahlon C. Smith for their valuable guidance throughout the course of this study. Special thanks to Dr. Potter for his constructive comments during the preparation of this manuscript.

The author wishes to thank Dr. Norman L. Hills and Dr. George E. Mase for their time spent while serving on the guidance committee.

The author wishes to thank the Mathematics and Science Teaching Center at Michigan State University for providing a graduate teaching assistantship during the course of this study.

TABLE OF CONTENTS

		Page
LIST OF TABLES		vi
LIST OF FIGURES		vii
Chapter		
1.	INTRODUCTION	1
2.	MATHEMATICAL FORMULATION	14
3.	NUMERICAL SOLUTIONS	24
	3.1 Introduction	24
	3.2 Procedure for Solving the Boundary Layer Equations	29
	3.3 Method for Solving the Momentum Equation	30
	3.4 Method for Solving the Energy Equation	35
	3.5 Finite-Difference Representation of ξ-Derivatives	39
	3.6 Method of Integration	40
	3.7 Starting the Solution	47
	3.8 Boundary Layer Parameters	48
	3.9 Computer Program	52
4.	EXPERIMENTAL APPARATUS AND PROCEDURE	53
	4.1 Introduction	53
	4.2 Description of the Heated Sphere	53
	4.3 Description of the Test Section Loop	55
	4.4 Flow Visualization Techniques	56
	4.5 Operating Procedures	57

Chapter Page

5. NUMERICAL AND EXPERIMENTAL RESULTS . . . 59

5.1 Introduction. 59
5.2 Verification of the Numerical Technique. 60

A. Similar Flows on a Flat Plate. . 60
B. Adverse Pressure Gradient Flows . 63
C. Flow Over a Sphere 64

5.3 Flow Past an Unheated Sphere: Hydrogen Bubble Experiment 67
5.4 Effect of Heat Transfer in Linearly Retarded Flows on a Flat Plate. . . 68
5.5 Effect of Heating a Sphere 70

A. Simple Potential Flow ("Above Critical") 70
B. Experimentally Determined Velocity Distribution ("Below Critical") 71
C. Effect of Introducing the Buoyancy Force Term ("Below Critical") 72
D. Experimental Results. 74

5.6 Effect of Treating Viscosity Constant in Linearly Retarded Flow 76
5.7 Conclusions 77

TABLES. 80

FIGURES 87

BIBLIOGRAPHY. 152

APPENDIX 156

LIST OF TABLES

Table		Page
1.	Similarity Solutions ($U_e - x^m$)	80
2.	Calculated Separation Point for the Case $U_e/U_\infty = 1 - x$	80
3.	Values of γ at the Point of Separation (Illingworth [10])	80
4.	Summary of Principal Methods for Solving the Laminar Boundary Layer Equations	81
5.	Steps in the Procedure for Starting Integration at Wall	82
6.	Value of ϕ''_w for Similar Flows	83
7.	Effect of Heating and Cooling a Flat Plate on Skin Friction and Heat Transfer Parameters	83
8.	Calculated Values of ϕ''_w for Howarth's Retarded Flow $U_e/U_\infty = 1 - \xi/8$.	84
9.	Separation Point Calculated for the Flow $U_e/U_\infty = 1 - \xi$	85
10.	Comparison of Values of ϕ''_w on a Sphere as Calculated by the Present Author and Smith and Clutter [37]	85
11.	The Effect of Heating the Sphere on the Separation Point "Above Critical" Flow	86
12.	The Effect of Heating the Sphere on the Separation Point "Below Critical" Flow	86

LIST OF FIGURES

Figure		Page
1.	Velocity Profile Near the Separation Point.	87
2.	Boundary Layer Profiles	87
3.	Drag Coefficient for a Sphere as a Function of Reynolds Number	88
4.	Boundary Layer on a Body of Revolution-- Coordinate System	88
5.	Nondimensional Fluid Properties for Water	89
6.	Notation for Velocity and Temperature Profiles in the Boundary Layer on a Body of Revolution.	90
7.	Notation for Finite Difference Representation.	90
8.	Brass Sphere with Heating Element and Location of Thermocouples.	91
9.	Photograph of the Sphere with the Support Rod	91
10.	Schematic Diagram of Test Loop.	92
11.	Velocity Profiles for Similar Flows $U_e \sim \xi^m$.	93
12.	The Effect of Heating and Cooling on the Velocity Profiles on a Flat Plate	94
13.	The Effect of Heating and Cooling on the Temperature Profile on a Flat Plate	95
14.	The Effect of Buoyancy Forces on the Velocity Profiles on a Heated Vertical Plate, Two Feet from Leading Edge.	96

Figure Page

15. The Effect of Buoyancy Forces on the Temperature Profiles on a Heated Vertical Plate, Two Feet from Leading Edge 97

16. Velocity Distribution Around a Sphere . . . 98

17. Pressure Distribution for Flow Over a Sphere 98

18. Velocity Gradient at the Wall for Two Cases of Potential Flow Around the Sphere . . . 99

19. Photograph of Hydrogen Bubbles Visualized on Unheated Sphere 100

20. Graphical Procedure for Extrapolating Separation Point from Hydrogen Bubble Pictures 100

21. Velocity Profiles for a Heated Flat Plate $U_e/U_\infty = 1 - \xi/8$; $\xi = 0$. 101

22. Velocity Profiles for a Heated Flat Plate $U_e/U_\infty = 1 - \xi/8$; $\xi = .575$. 102

23. Velocity Profiles for a Heated Flat Plate $U_e/U_\infty = 1 - \xi/8$; $\xi = .7863$ 103

24. The Effect of Heating and Cooling a Flat Plate on the Velocity Gradient at the Wall $U_e/U_\infty = 1 - \xi/8$ 104

25. The Effect of Heat Transfer on Separation Point. $U_e/U_\infty = 1 - \xi/8$ 105

26. Temperature Profiles for a Heated Flat Plate $U_e/U_\infty = 1 - \xi/8$, $\xi = 0$. 106

27. Temperature Profiles for a Heated Flat Plate $U_e/U_\infty = 1 - \xi/8$, $\xi = .575$. 107

28. Temperature Profiles for a Heated Flat Plate $U_e/U_\infty = 1 - \xi/8$, $\xi = .786$. 108

29. Velocity Profiles for a Heated Flat Plate $U_e/U_\infty = 1 - \xi$, $\xi = 0$ 109

30. Velocity Profiles for a Heated Flat Plate $U_e/U_\infty = 1 - \xi$, $\xi = .083$ 110

Figure		Page
31.	Velocity Profiles for a Heated Flat Plate $U_e/U_\infty = 1 - \xi$, $\xi = .118$	111
32.	The Effect of Heating and Cooling a Flat Plate on the Velocity Gradient at the Wall $U_e/U_\infty = 1 - \xi$	112
33.	The Effect of Heat Transfer on Separation Point. $U_e/U_\infty = 1 - \xi$.	113
34.	Displacement Thickness Over Heated Flat Plate $U_e/U_\infty = 1 - \xi$	114
35.	Momentum Thickness Over a Heated Flat Plate $U_e/U_\infty = 1 - \xi$	115
36.	Temperature Profiles for a Heated Flat Plate $U_e/U_\infty = 1 - \xi$, $\xi = .047$	116
37.	Temperature Profiles for a Heated Flat Plate $U_e/U_\infty = 1 - \xi$, $\xi = .083$	117
38.	Temperature Profiles for a Heated Flat Plate $U_e/U_\infty = 1 - \xi$, $\xi = .118$	118
39.	The Effect of Heating and Cooling a Flat Plate on the Local Nusselt Number $U_e/U_\infty = 1 - \xi$	119
40.	Velocity Profiles for a Heated Sphere. "Above Critical" Flow, $\alpha = 0°$	120
41.	Velocity Profiles for a Heated Sphere. "Above Critical" Flow, $\alpha = 47.5°$	121
42.	Velocity Profiles for a Heated Sphere. "Above Critical" Flow, $\alpha = 67.8°$	122
43.	The Effect of Heating and Cooling a Sphere on the Velocity Gradient at the Wall. "Above Critical" Flow.	123
44.	The Effect of Heating and Cooling a Sphere on the Local Skin Friction Parameter. "Above Critical" Flow.	124
45.	Temperature Profiles for a Heated Sphere. "Above Critical" Flow, $\alpha = 0°$	125

Figure Page

46. Temperature Profiles for a Heated Sphere. "Above Critical" Flow, α = 47.5° 126

47. Temperature Profiles for a Heated Sphere. "Above Critical" Flow, α = 67.8° 127

48. The Effect of Heating and Cooling a Sphere on the Local Heat Transfer Parameters. "Above Critical" Flow. 128

49. Velocity Profiles for a Heated Sphere. "Below Critical" Flow, α = 40°. 129

50. Velocity Profiles for a Heated Sphere. "Below Critical" Flow, α = 62.6° 130

51. Velocity Profiles for a Heated Sphere. "Below Critical" Flow, α = 82°. 131

52. Displacement Thickness Over a Heated Sphere. "Below Critical" Flow. 132

53. Momentum Thickness Over a Heated Sphere. "Below Critical" Flow. 133

54. The Effect of Heating and Cooling a Sphere on the Velocity Gradient at the Wall. "Below Critical" Flow. 134

55. Temperature Profiles for a Heated Sphere. "Below Critical" Flow, α = 40°. 135

56. Temperature Profiles for a Heated Sphere. "Below Critical" Flow, α = 62.6° 136

57. Temperature Profiles for a Heated Sphere. "Below Critical" Flow, α = 82°. 137

58. The Effect of Heating and Cooling a Sphere on the Local Heat Transfer Parameter. "Below Critical" Flow. 138

59. Definition of Positive and Negative Buoyancy Forces. 139

60. The Effect of Buoyancy Forces on the Velocity Profiles, When the Sphere is Cooled. "Below Critical" Flow, α = 82°, ΔT = -80°F. 140

Figure Page

61. The Effect of Buoyancy Forces on the Velocity Gradient at the Wall, When the Sphere is Cooled. "Below Critical" Flow, $\Delta T = -80°F$. 141

62. The Effect of Buoyancy Forces on the Velocity Gradient at the Wall, When the Sphere is Heated. "Below Critical" Flow, $\Delta T = 80°F$. 142

63. Comparison of Local Nusselt Number with Experimental Results of Brown [27]. $T_{wall} = 80°F$; $T_{water} = 70°F$, Uniformly Heated Sphere 143

64. Comparison of Local Nusselt Number with Experimental Results of Brown [27]. $T_{wall} = 190°F$, $T_{water} = 180°F$, Uniformly Heated Sphere 144

65. Comparison of Heat Transfer Parameter with Experimental Results of Brown [27] . . . 145

66. Shadowgraph Picture of the Heated Sphere $\Delta T = 20°F$. 146

67. Shadowgraph Picture of the Heated Sphere $\Delta T = 40°F$. 146

68. Shadowgraph Picture of the Heated Sphere $\Delta T = 70°F$. 147

69. Shadowgraph Picture of the Heated Sphere $\Delta T = 100°F$ 147

70. The Effect of Treating Viscosity Constant and Variable on the Velocity Profile $U_e/U_\infty = 1 - \xi$, $\xi = .083$, $\Delta T = 80°F$ . . . 148

71. The Effect of Treating Viscosity Constant and Variable on the Temperature Profile $U_e/U_\infty = 1 - \xi$, $\xi = .083$, $\Delta T = 80°F$ . . . 149

72. The Effect of Greating Viscosity Constant and Variable on the Velocity Gradient at the Wall. $U_e/U_\infty = 1 - \xi$, $\Delta T = 80°F$ . . . 150

73. The Effect of Treating Viscosity Constant and Variable on the Local Heat Transfer Parameter. $U_e/U_\infty = 1 - \xi$, $\Delta T = 80°F$. . . 151

CHAPTER 1

INTRODUCTION

The concept of flow separation is as old as that of boundary layer theory. Ludwig Prandtl, the originator of the boundary layer theory was concerned about flow separation before he formulated his ideas on the boundary layer. As a young engineer Prandtl found that the computed pressure recovery could not be achieved in actual diffusors [1]. He spent considerable time, prior to his presentation of the boundary layer theory, attempting to understand flow separation and the pressure losses in the diffusor. In 1904 Prandtl [2] presented his new theoretical concept of the boundary layer in a paper entitled "Fluid Motion with Very Small Friction." In this paper he discussed flows over objects for which the Reynolds number was large. For such flows he made the following observations:

1. Frictional effects are confined to a very thin layer, called the boundary layer, near the surface of the object.

2. The flow external to the boundary layer can be considered frictionless.
3. The pressure variation from the mainstream is "impressed" upon the boundary layer, i.e., $\partial p/\partial y = 0$.

Because flow separation is caused by viscous effects confined in the boundary layer, it is often expressed as "boundary layer separation." Prandtl [3] states clearly that the necessary condition for separation from the wall is the increasing pressure in the direction of flow, i.e., positive (or adverse) pressure gradient along the flow path. The statement holds for compressible flow as well as incompressible flow.

Within the boundary layer, the effect of viscosity is such that the velocity parallel to the wall changes along the distance perpendicular to the surface, i.e., the velocity gradient $\partial u/\partial y$ exists (u is the streamwise velocity and y is the distance normal to the surface). Since the flow velocity at the wall is zero u increases and finally reaches U_e, the inviscid flow velocity at the outer edge of the boundary layer. The momentum of flow near the wall is small and the ability of the fluid to move forward against the pressure rise is also limited. Downstream, this small amount of momentum along the body surface is used up to overcome the pressure rise, and, finally, the fluid particles are brought to rest at the

"separation point." The point, at which the velocity gradient $\partial u/\partial y$ at the wall is zero, is defined as the separation point. At a point downstream of separation, because of the existing adverse pressure gradient, reverse flow occurs as shown in Fig. 1, and, owing to this reverse flow, the flow in the boundary layer is forced away from the wall. At the point of separation, the flows begin to leave the surface at a small angle, maintaining the adverse pressure gradient.

It has been demonstrated [1] that a laminar boundary layer can support only a very small adverse pressure gradient without the occurrence of separation. In the case where the boundary layer is turbulent, the danger of separation is intrinsically reduced, compared with laminar flow, because the turbulent flow boundary layer contains much more momentum and hence is able to resist the adverse pressure gradient for a greater distance than the laminar flow boundary layer. Typical velocity profiles of laminar and turbulent boundary layers are shown in Fig. 2.

It is this transition from laminar to turbulent boundary layer flow around the sphere which explains the abrupt change in the drag coefficient around a Reynolds Number of 3×10^5 in Fig. 3. It is well known that for Reynolds Number less than 3×10^5, the boundary layer flow around the sphere is laminar until 84° where it separates and that for Reynolds Number above 3×10^5, the boundary

layer flow undergoes transition to turbulence and the flow does not separate until it reaches 110°. This sudden backward shift in the separation point reduces the size of the wake which accomplishes the decreased drag coefficient. Thus by changing the shape of the velocity profile in the boundary layer (from a laminar to a turbulent one, see Fig. 2) a delay in the separation point is achieved.

There are in existence several methods which have been developed for the purpose of artificially controlling the behavior of boundary layers, i.e., to delay or eliminate separation. Of the most popular ones are:

1. Blowing--acceleration of the boundary layer by injecting fast moving fluid parallel to the wall.
2. Suction--removal of slow moving layer of fluid in the boundary layer near the wall.
3. Reduction in Viscosity of Fluid Near the Wall--by heating the wall for liquids and cooling the wall for gases.

It is obvious that the first method would give the fluid particles in the boundary layer the momentum they need to overcome the adverse pressure gradient, while in the second method the slow moving fluid in the boundary layer is removed which again increases the boundary layer momemtum thus delaying separation.

It is the third method, that of controlling the fluid viscosity near the wall by heating the wall, that

is the subject of the present investigation. Only liquids will be considered.

There has been some interest in the last twenty years in the effect of heat transfer on laminar separation particularly in flows involving gases. Work with liquids has been very limited.

A number of general qualitative conclusions on laminar separation with heat transfer in gases [4], which have been established (more or less independently) by various investigators are:

1. Cooling the wall tends to lessen the direct* effect of the pressure gradient.
2. Cooling the wall tends to delay separation.
3. Cooling the wall tends to diminish the skin friction for a favorable pressure gradient but tends to increase it for an unfavorable pressure gradient.

All of the above conclusions were reached by Morduchow and Galorion [5] on the basis of a Karman-Pohlhausen type of analysis with a fourth degree velocity profile and were subsequently confirmed by the use of higher degree profiles by Morduchow and Grape [6]. Moreover, these conclusions have also been reached on the basis

---

*By "direct" effect is meant here the influence of the gradient term proportional to dU_e/dx. The influence of a pressure gradient, however, appears "indirectly" also, mainly, through the dependence of U_e and T_e on x (cf., e.g., Refs. 5 and 6).

of similarity solutions by Cohen and Reshotko [7] and Li and Nagamatsu [8], through the use of the Illingworth-Stewartson transformation [9], and by the analysis of Illingworth [10], Luxton and Yonug [11] and Low [1]].

By far, most of the solutions on the laminar boundary layer with heat transfer in gases which have been considered are the similarity solutions [7, 13] in which $U_e \sim x^m$, and adverse pressure gradients are represented by negative values of m.

In connection with the effect of heat transfer on separation, the results of the similar solutions of primary interest are the value of m, as a function of wall temperature, required for a zero-skin-friction boundary layer. These are shown in Table 1. It is noted that, as the wall is cooled, a larger negative m, corresponding to a larger adverse pressure gradient, is required for separation.* This may be considered to illustrate the tendency of cooling to delay or prevent separation in gases.

The case where the external velocity may be represented by

$$\frac{U_e}{U_\infty} = 1 - x$$

---

*A comparison between entries $T_w/T_\infty = .2$ and .25 slightly contradict this trend, but this seems to be due to use of Pr = 1 in Ref. 7 and Pr = .7 in Ref. 13.

may almost be regarded as the prototype of an adverse pressure gradient. It has probably been the most frequently studied case of an adverse pressure gradient. A number of investigators: Illingworth [10]; Morduchow and Grape [6]; Gadd [14]; Curle [15]; and Poots [16], have investigated the effect of heat transfer on the separation point for such a flow of gas on a flat plate. Table 2 shows their results and confirms the result that "cooling the wall tends to delay separation."

In addition to the similarity solutions and the various solutions for the case of $U_e/U_\infty = 1 - x$, there have been a few other cases for which the effect of heat transfer on laminar separation has been calculated. Poots [16] considered the case $U_e/U_\infty = 1 - \frac{x}{8}$ and calculated the case of zero heat transfer ($T_w/T_\infty = 1$) and of a heated wall ($T_w/T_\infty = 2$). The results showed, that for low Mach Number, an upstream movement of the separation point when the wall is heated. Morduchow and Grape [6] have considered the case in which a stagnation flow is followed by an adverse pressure gradient and have calculated the adverse pressure requirement for "immediate" separation as a function of wall temperature. Gadd [14] gives corresponding results if the initial region is one of zero pressure gradient, instead of stagnation flow. Baxter and Flügge-Lotz [17] have calculated somewhat similar cases, in which a zero pressure gradient is

followed by either a step pressure gradient or a ramp pressure gradient and found in each case that separation would occur sooner with a hotter wall. Fannelop and Flügge-Lotz [18] have calculated the boundary layer over a flat-plate leading edge section followed by a semi-infinite wavy wall and found that separation occurred earlier for a heated wall than for an adiabatic wall, whereas cooling considerably delayed separation.

Illingworth [10] presented an approximate analytical solution to show the effect of uniformly heating and cooling a circular cylinder, uniformly in motion in a gas. The results are presented in Table 3 where the position of laminar separation is γ and A is defined as

$$A = 1 - \frac{h_w(x)}{H_e}$$

h and H_e being specific static and specific total enthalphy respectively.

From Table 3, it is evident that there would be no appreciable difference in the position of separation between the two cases (1) the temperature of the cylinder 0°C (A = .0521) and (2) 100°C (A = -,2951). Chang [1] explains this result of Illingworth by noting "that with the cylinder the effect of heat transfer on separation is small, due to the fact that the flow over the first 90% of the unseparated boundary layer is accelerated; consequently the deceleration region is short. Furthermore,

the skin friction has taken time (see Table 4, Ref. 10) to reach a considerably larger value at the minimum pressure than for the unheated case. Thickening subsequently takes place more rapidly with a heated wall than with an unheated cylinder, but not enough to cause much change in the position of separation."

One should also note that viscosity for a gas is quite insensitive to small changes in temperature, an increase of 100°C produces only a 30% change in the viscosity.

Because the viscosity in liquids decreases with increasing temperature, the influence of viscosity variation on the velocity profile is opposite to that for gases. Consequently, heating should delay separation and lessen the "direct" effect of pressure gradient, while cooling should do the reverse.

Surprisingly few solutions for liquids with variable viscosity have been presented. Schuh [19], Hanna [20], and Seban [21] solved the flat plate case (similarity solution, m = 0) with an inverse power law for the viscosity-temperature relationship, holding other fluid properties constant. Schuh calculated by successive approximation two flows having high Prandtl Number; one representing cooling and the other heating. Hanna presented an approximate solution achieved by integral methods in which polynomical profiles were used for the

velocity and temperature. Hanna presented results where the Prandtl Number ranged from 0.25 to 1000. Seban extended Schuh's results for a wide range of wall Prandtl Number.

The three works reveal the effect of heating and cooling the wall in that they show that the skin friction decreases when the wall is heated and increases when the wall is cooled.

Poots and Raggett [22], using experimental values (in the range of 0-100°C) for the viscosity, conductivity, specific heat and density, solved two different laminar boundary layer configurations. First the case of the heated flat plate and secondly the heat transfer effect on an infinite rotating disk is analyzed. Their results confirm the effect of heating and cooling on the skin friction and also indicate that heating tends to increase the heat transfer rate. Poots and Raggett have also presented an analytical expression for the local heat transfer at the wall.

The only other theoretical work that appears in the literature where the effect of heat transfer in liquids is treated is that of Kaups and Smith [23]. They have extended the method of Smith and Clutter [24], which solves the boundary layer equations, for calculating the laminar boundary layer in liquids having variable fluid properties, including viscosity. Kaups and Smith have,

like the previous researchers, presented numerical results for the flat plate case. They also present results of a flow past a semi-infinite body of revolution and indicate that by heating the body, the flow is stabilized, i.e., heating eliminates the inflection point from the velocity profile. They state: "In adverse pressure gradients, a heated wall appears to delay separation." However, they present no results which indicate the relationship between heating and the delay of separation.

It should be noted that in the cases where the temperature difference brings about a difference in the density of the fluid, it becomes necessary to consider buoyancy effects also. Even though the density differences in liquids are relatively small, see Fig. 5, the buoyancy effects are often considerable. Of the five references just cited [19 through 23] where the investigators have studied the effect of heating a body in liquids, only Kaups and Smith [23] have considered the effect of buoyancy. They present the cases of a heated vertical plate for both positive and negative buoyancy forces. The negative buoyancy force appears to have an effect similar to that of an adverse pressure gradient, while the positive buoyancy force has an opposite effect. This implies that the buoyancy force in the direction of fluid motion (positive buoyancy) tends to delay separation.

While there has been experimental work done on flows around spheres in air to determine the effect of heating the sphere, there exist only three papers cited in literature on the experimental results of flows around spheres in water; Kramers [25], Vliet and Leppert [26], and Brown [27].

Kramers measured the heat transfer from an induction heated steel sphere to water and to oil in forced convection. The Reynolds Number ranged from 0.4 to 2100. These experiments were conducted with small sphere to water temperature differences.

Vliet and Leppert measured heat transfer coefficients from an induction heated copper sphere transfering heat to water in the Reynolds Number range of 10^3 to 6×10^4 with substantial temperature differences (up to 130°F measured experimentally).

Whereas Kramers [25] and Vliet and Leppert [26] have made measurements on a heated sphere that has a constant temperature surface, Brown [27] has measured the heat transfer coefficients for a uniformly heated sphere. Brown has presented results indicating the relationship between Nusselt Number and Reynolds Number for flow around a uniformly heated sphere. From his data on heat transfer and shadowgraph pictures, Brown points out that, for laminar flow around a uniformly heated sphere the separation point occurs at 90° (note: as mentioned earlier,

the separation point for unheated sphere for laminar flow is 84°). Thus Brown's work shows a backward shift of the separation point.

In the experimental papers just cited above [25, 26, 27] the heated spheres were suspended in vertical test sections with upward fluid motion, which means that the buoyancy forces were positive.

In the present investigation a computer program is used to show numerically the effect of heating on the separation point and the various boundary layer parameters for various flow configurations. This is done by treating the viscosity as a temperature dependent variable. Buoyancy effects are included also. Flow of water about a heated sphere also is studied experimentally.

CHAPTER 2

MATHEMATICAL FORMULATION

Formulation of the incompressible laminar boundary layer problem with heat transfer in liquids is complicated by the strong dependence of viscosity on temperature. The equations necessary to describe such a flow are those of continuity, momentum, and energy. Also, the relations describing the dependence of viscosity and density of the fluid on temperature are needed. Axisymmetric, steady flow about a body of revolution will be considered. The simpler problem of plane two-dimensional flow is included in the equations by letting r, the body radius, be a constant.*

The basic notation and coordinate system is shown in Fig. 4. U_∞ is the reference velocity and $U_e(x)$ is the velocity of the main flow just outside the "velocity" boundary layer. T_∞ is the reference temperature and $T_e(x)$ is the temperature of the main flow field just outside the

---

*This will be illustrated later.

"thermal" boundary layer.* g_x is the gravitational acceleration in the free stream direction.

In the curvilinear coordinate system x is the distance along the surface of the body, measured from the forward stagnation point and the dimension y is measured perpendicular to x. The velocity components are u and v, u being parallel to x and positive when moving in the direction of increasing x. The velocity component v bears similar relation to the y-direction. The body radius r_o is as shown and it may vary with x.

The boundary layer equations for the axisymmetric case in the above coordinate system were first developed by Boltz [28] and Millikan [29]. They are listed as follows:**

Continuity:

$$\frac{1}{r}\left[\frac{\partial}{\partial x}(ru) + \frac{\partial}{\partial y}(rv)\right] = 0 \quad ; \tag{2.1}$$

Momentum:

$$\rho\left[u\,\frac{\partial u}{\partial x} + v\,\frac{\partial u}{\partial y}\right] = -\frac{dp}{dx} + \rho g_x + \frac{\partial}{\partial y}\left(\mu\frac{\partial u}{\partial y}\right) + \frac{\mu}{r}\,\frac{\partial r}{\partial y}\,\frac{\partial u}{\partial y} \quad ; \tag{2.2}$$

*In all the numerical examples to be presented in the subsequent chapters, $T_e(x)$ is considered constant and equal to T_∞.

**One can observe that if r = const the equations are identical to the boundary layer flow for plane 2 - D flow.

Energy:

$$\rho C_p \left[u \frac{\partial T}{\partial x} + v \frac{\partial T}{\partial y}\right] = k \frac{\partial^2 T}{\partial y^2} + \frac{k}{r} \frac{\partial r}{\partial y} \frac{\partial T}{\partial y} \quad . \tag{2.3}$$

In the above equations C_p and k are considered to be constant. Also the viscous dissipation and the compression effects are neglected. Eqs. (2.2) and (2.3) differ from the equations obtained for plane flow when the Prandtl boundary layer approximations are made in that they contain the transverse curvature terms $(\mu/r)\ (\partial r/\partial y)\ (\partial u/\partial y)$ in eq. (2.2) and $(k/r)\ \partial r/\partial y\ \partial T/\partial y$ in (2.3).

The transverse curvature terms are important when the boundary layer thickness is of the same order of magnitude as the radius of the contour of the body (i.e., $\delta \sim r_o$), which would be the case for any long, slender body as indicated by Schlichting [30]. If $\delta << r_o$ everywhere, then the transverse curvature terms could be neglected.

This investigation will be limited to various flows over a flat plate plus the axisymmetric flow around a sphere. Tomotika [31] has shown that for the case of the sphere $\delta << r_o$ and thus the transverse curvature terms may be neglected. The condition that δ is very small compared with r_o is not necessarily satisfied at the nose. It was proved by Millikan [29] for a blunt-nosed body of revolution, that the transverse curvature terms may be

legitimately neglected even in the neighborhood of the forward stagnation point at the nose where $r_o \to 0$.

Thus if $\delta/r_o << 1$ (as in the case of a sphere), then the transverse curvature terms can be neglected in both the momentum and energy equations, so that they assume the two-dimensional form. This is equivalent to replacing $r(x,y)$ by $r_o(x)$ in the continuity equation.

Thus the equations to be treated in this investigation take the forms:

$$\frac{\partial}{\partial x}(r_o u) + r_o \frac{\partial v}{\partial y} = 0 \tag{2.4}$$

$$\rho\left[u \frac{\partial u}{\partial x} + v \frac{\partial u}{\partial y}\right] = -\frac{dp}{dx} + \rho g_x + \frac{\partial}{\partial y}\left(\mu \frac{\partial u}{\partial y}\right) \tag{2.5}$$

$$\rho C_p\left[u \frac{\partial T}{\partial x} + v \frac{\partial T}{\partial y}\right] = k \frac{\partial^2 T}{\partial y^2} \tag{2.6}$$

Using the subscript w, to denote the wall, the boundary conditions are

$$\left.\begin{aligned} &\text{at } y = 0 && u_w = 0 \\ & && v_w = 0 \\ & && T_w = \text{given} \\ &\text{at the edge of the boundary layer} && \\ & && u = U_e(x) \\ & && T = T_\infty . \end{aligned}\right\} \tag{2.7}$$

Eqs. (2.4) and (2.5) may be combined into a single third order equation in terms of the stream function ψ by use of the relation

$$u = \frac{1}{r_o} \frac{\partial}{\partial y} (\psi r_o) = \frac{\partial x}{\partial y} \tag{2.8}$$

$$v = - \frac{1}{r_o} \frac{\partial}{\partial x} (\psi r_o) = - \frac{\partial \psi}{\partial x} - \frac{\psi}{r_o} \frac{\partial r_o}{\partial x} \tag{2.9}$$

From the definition of ψ, the continuity equation is automatically satisfied, thus, the momemtum equation, using eq. (2.8) and (2.9) becomes

$$\rho \left[\frac{\partial \psi}{\partial y} \frac{\partial^2 \psi}{\partial x \partial y} - \left(\frac{\partial \psi}{\partial x} + \frac{\psi}{r_o} \frac{\partial r_o}{\partial x} \right) \frac{\partial^2 \psi}{\partial y^2} \right]$$

$$= - \frac{dp}{dx} + \rho g_x + \frac{\partial}{\partial y} \left(\mu \frac{\partial^2 \psi}{\partial y^2} \right) \tag{2.10}$$

or

$$\rho_\infty \left[\frac{\partial \psi}{\partial y} \frac{\partial^2 \psi}{\partial x \partial y} - \frac{\partial \psi}{\partial x} \frac{\partial^2 \psi}{\partial y^2} - \frac{\psi}{r_o} \frac{\partial r_o}{\partial x} \frac{\partial^2 \psi}{\partial y^2} \right]$$

$$= \rho_\infty U_e \frac{dU_e}{dx} + \rho_\infty \beta g_x (T - T_\infty) + \frac{\partial}{\partial y} \left(\mu \frac{\partial^2 \psi}{\partial y^2} \right) \tag{2.11}$$

In eq. (2.11) use has been made of Euler's equation which is given by

$$\frac{1}{\rho_\infty}\frac{dp}{dx} + U_e\frac{dU_e}{dx} + g\frac{dz}{dx} = 0 \qquad (2.12)$$

where the density gradient $d\rho_\infty/dx$ is neglected. The relationship

$$\rho = \rho_\infty[1 - \beta(T - T_\infty)]$$

is used and certain terms in eq. (2.11) are neglected because β is very small.

Eq. (2.11) is transformed to a more convenient coordinate system by stretching the y-coordinate. The transformation from the (x,y) coordinate system to the (ξ,y) coordinate system is a modified Howarth-Dorotnitsyn transformation as used in reference [23] given by

$$\xi = x/L$$

$$\eta = \left(\frac{U_e\rho_\infty}{\mu_\infty x}\right)^{1/2} y = \left(\frac{U_e\rho_\infty}{\mu_\infty \xi L}\right)^{1/2} y \qquad (2.13)$$

where L is the characteristic length (for the sphere L = radius).

Furthermore, it is convenient to introduce a dimensionless stream function f, such that

$$\frac{\partial f}{\partial \eta} = f' = \frac{u}{U_e} \qquad (2.14)$$

The relation between f and ψ is

$$\psi = \left(\frac{U_e \mu_\infty x}{\rho_\infty}\right)^{1/2} f(\xi,\eta) \tag{2.15}$$

In order to transform the boundary layer equation above from the (x,y) coordinate system to the (ξ,η) coordinate system, the following relations are used:

$$\frac{\partial}{\partial x} = \frac{\partial \xi}{\partial x}\frac{\partial}{\partial \xi} + \frac{\partial \eta}{\partial x}\frac{\partial}{\partial \eta}$$

$$\frac{\partial}{\partial x} = \frac{1}{L}\frac{\partial}{\partial \xi} - \frac{1}{2L}\frac{\eta}{\xi}\frac{\partial}{\partial \eta} + \frac{1}{2}\frac{\eta}{U_e}\frac{dU_e}{d\xi}\frac{\partial}{\partial \eta} \tag{2.16}$$

$$\frac{\partial}{\partial y} = \frac{\partial \xi}{\partial y}\cdot\frac{\partial}{\partial \xi} + \frac{\partial \eta}{\partial y}\frac{\partial}{\partial \eta}$$

$$\frac{\partial}{\partial y} = \left(\frac{U_e \rho_\infty}{\mu_\infty \xi L}\right)^{1/2}\frac{\partial}{\partial y} \tag{2.17}$$

After transformations the momentum equation becomes

$$\left.\begin{aligned} &\frac{\partial}{\partial \eta}(cf'') + P[1 - f'^2] + \left(\frac{P+1}{2} + R\right)ff'' \\ &\qquad + \frac{\xi L}{U_e^2} g_x \beta (T - T_\infty) = \xi\left[f'\frac{\partial f'}{\partial \xi} - f''\frac{\partial f}{\partial \xi}\right] \end{aligned}\right\} \tag{2.18}$$

where the primes denote differentiation with respect to η, and

$$c = \frac{\mu}{\mu_\infty}$$

$$P = \frac{\xi}{U_e}\frac{dU_e}{d\xi} = \text{Pressure Parameter}$$

$$R = \frac{\xi}{r_o}\frac{dr_o}{d\xi} = \text{Radius Parameter.} \qquad (2.19)$$

The boundary conditions now become

$$\left.\begin{aligned} &\eta = 0 \quad f'_w = 0 \quad ; \quad f_w = 0 \\ &\text{for large } \eta,\ f' \to 1 \end{aligned}\right\} \qquad (2.20)$$

The energy equation is rewritten here

$$\rho C_p\left[u\frac{\partial T}{\partial x} + v\frac{\partial T}{\partial y}\right] = k\frac{\partial^2 T}{\partial y^2} \qquad (2.21)$$

Define g(x,y) as

$$g = \frac{T}{T_\infty} \qquad (2.22)$$

Then eq. (2.21) becomes

$$\rho C_p\left[u\frac{\partial g}{\partial x} + v\frac{\partial g}{\partial y}\right] = k\frac{\partial^2 g}{\partial y^2}\ . \qquad (2.23)$$

To transform the above equation from the (x,y) coordinate system to the (ξ,η) one, use is made of the same transformations, eqs. (2.13) to (2.17). Thus the energy equation along with the boundary conditions now become

$$\frac{1}{Pr_\infty}\frac{\partial}{\partial\eta}(g') + (\frac{P+1}{2} + R)fg' = \xi[f'\frac{\partial g}{\partial\xi} - g'\frac{\partial f}{\partial\xi}] \qquad (2.24)$$

where Pr_∞ is the Prandtl Number at infinity defined by

$$Pr_\infty = \frac{\mu_\infty C_p}{k} . \qquad (2.25)$$

The boundary conditions necessary for the energy equation are

$$\eta = 0 \qquad g_w = T_w/T_\infty$$

$$\text{for large } \eta \quad g \to 1. \qquad (2.26)$$

Equations (2.13) through (2.26) have been previously given by Smith and Clutter [24].

In this investigation, the only property of water that is assumed to be a function of temperature is viscosity, thus limiting the application to moderate pressures. The temperature range used in this study varies from 32°F to 212°F, a range in which viscosity decreases monotonically with increasing temperatures.

The fluid property data (eq. 2.27 and 2.28) was taken from [23]. The data is nondimensionalized by dividing through by values at 32°F. The viscosity and density variation are given by

$$\mu/\mu_{ref} = 1./[35.16 - 106.98(T/T_{ref}) + 107.77(T/T_{ref})^2 - 40.6(T/T_{ref})^3 + 5.64(T/T_{ref})^4]$$

$$\rho/\rho_{ref} = 0.8039 + 0.4615(T/T_{ref}) - 0.2869(T/T_{ref})^2 + 0.0235(T/T_{ref})^3 \qquad (2.27)$$

The Prandtl Number at infinity is needed in the calculations and is calculated by using the following expression (again taken from [23]):

$$Pr/Pr_{\infty} = 1/[73.38 - 208.75(T/T_{ref}) + 197.76(T/T_{ref})^2 - 68.86(T/T_{ref})^3 + 7.48(T/T_{ref})^4] \qquad (2.28)$$

In (2.27) and (2.28) T is expressed in degrees Rankin so that T_{ref} = 491.69°F.

Fig. 5 shows the graph of these equations and the reference values are also given in the figure.

CHAPTER 3

NUMERICAL SOLUTIONS

3.1 Introduction

The momentum and energy equations, which must be solved simultaneously, are summarized here for convenience:

$$(Cf'')' + P[1 - f'^2] + \left(\frac{P+1}{2} + R\right)ff'' + \frac{\xi L}{U_e^2} \cdot g_x\beta(T - T_\infty) = \xi\left[f'\frac{\partial f'}{\partial \xi} - f''\frac{\partial f}{\partial \xi}\right] \qquad (3.1)$$

$$\frac{1}{Pr_\infty}\frac{\partial}{\partial \eta}(g') + \left(\frac{P+1}{2} + R\right)fg' = \xi\left[f'\frac{\partial g}{\partial \xi} - g'\frac{\partial f}{\partial \xi}\right] \qquad (3.2)$$

The boundary conditions are:

$$\text{at } \eta = 0 \quad : \quad f'_w = f_w = 0 \text{ and } g_w = T_w/T_\infty$$

$$\text{for large } \eta: \quad f' = 1 \text{ and } g = 1 \qquad (3.3)$$

The momentum equation (3.1) is a third order, non-linear equation. Once the momentum equation is solved, the energy equation becomes linear. Solution of these equations is also made difficult by the fact that one of the boundary conditions lies at "large η," a rather poorly defined boundary condition.

The fundamental idea for the method of solution used in the present investigation was advanced by Hartree and Womersley [32]. They proposed replacing the ξ-derivatives, which here are only of first order, by finite difference approximations. The remainder of the equations is left unchanged and as a consequence the equations are converted to ordinary differential-difference equations. A far more common procedure is to approximate the derivatives in both directions by finite difference formulas, thereby obtaining the usual network of elements. The present procedure combines both procedures as will be examined in more detail later.

To eliminate the problem of the boundary condition that lies at "large η," the present procedure changes this two-point boundary value problem to an initial value problem, where another boundary condition at the wall is arbitrarily chosen, i.e., f''_w for eq. (3.1) and g'_w for eq. (3.2). It is then necessary to search through the possible values of f''_w and g'_w to find the ones that satisfy the outer boundary conditions.

Later in this chapter this method of solution, which was initially advanced by Hartree and Womersley [32] and since has been used by Clutter and Smith [24], will be developed but first it is felt that some explanation should be given for the preference of this method over the other available techniques for solving the equations.

To justify the preference of the so-called "Hartree-Womersley Method," two essential aspects must be discussed. The first is the form of the boundary layer equations to be solved; the second is the question of the method to be used in solving the particular equations.

Consider the form of the equations. In the original equations of continuity, momentum, and energy, u, v, and T are functions of the independent variables x and y. Not all the methods of solution retain the independent variables x and y. In certain methods the variable x and y, are stretched by certain rules, while there are other methods which involve transformations such that x and y are no longer the independent variables. The most popular of these latter type transformations is that by Crocco [33], where x and u are the independent variables and τ, the shear stress is the dependent variable in the momentum equation. Crocco's form of equation receives a great deal of attention because the variable in the y-direction is replaced by u and is therefore bounded. These equations become attractive for the network method because the location of the secondary boundary is known. In the majority of problems τ is a smooth regular, single valued function of u, but on occasion τ can be double valued, as in the case of accelerating flow past a hot wall. While techniques may be found to handle this problem it presents a real difficulty when using Crocco's method.

Methods of solution fall into two classes. In one class some simplifying approximation is made in the original equations in the interest of obtaining a more convenient solution. When this is done, even if the solution of the resulting equation is exact, the answer is usually in substantial error because the equation itself is approximate. In the second class, the equation is solved by some numerical finite difference technique. Even though the equation is not compromised, the answers are not exact because of the use of finite increments instead of infinitesimals. In the finite difference class itself there are two procedures, the explicit and the implicit. In the explicit method, a finite difference formula is so written that the results at a downstream point are given in terms of certain small number of known upstream values. In the implicit method, the results entirely across the boundary layer are found simultaneously by solving a system of algebraic equations for the full set of values at all the y-stations involved.

Table 4, which was arranged by Smith and Clutter [24], presents a summary of the principal methods for solving the laminar boundary layer equations. It is presented without comment except for certain points which merit emphasis.

Numbers 1 and 2 are definitely approximate procedures, in the sense that the original equation has been

compromised. Though they are rapid and convenient, accuracy is only good for certain particular external velocity distributions (wedge flows).

Method 3 is exact in the limit, that is, for an infinite number of terms. For incompressible flows it has the advantage that certain universal solutions can be found once and for all, and when they are available, calculations of a particular boundary layer flow becomes trivial. It is not so attractive for variable properties because of difficulties in obtaining these universal solutions.

The next three methods, 4, 5, and 6 are various applications of classical finite difference procedures. Conceptually, the Hartree-Womersley Method (7) is different because it divides the region of the boundary layer into vertical strips, whereas methods 4, 5, and 6 divide it into rectangular elements.

Finally, it is worth noting certain important properties of the momentum equation (3.1), which is the difficult equation to solve because of its non-linearity. If the edge velocity is of the form $U_e = C_1\xi^m$ (wedge flows), the pressure parameter $(\xi/U_e)(dU_e/d\xi)$ is identically m. If $r_o = C_2\xi^n$, the radius parameter $(\xi/r_o)(dr_o/d\xi)$ is equal to n. If m and n are constant and if buoyancy forces can be neglected, it is known [30] that the equation is independent of ξ and provides the so-called similar solutions. The equation takes the form:

$$\frac{\partial}{\partial \eta}(cf'') + P[1 - f'^2] + \left(\frac{P+1}{2} + R\right)ff'' = 0 \qquad (3.4)$$

Equation (3.1) has another very important property. Most other forms of the equations are singular at $\xi = 0$ and thus require that an initial profile be specified, but at $\xi = 0$, eq. (3.1) becomes eq. (3.4), if buoyancy forces are absent, and the solution can be started with a similar flow. Hence, Clutter and Smith [24] refer to the ξ-derivative terms in the bracket in eq. (3.1), as the "non-similarity" terms.

The addition of the buoyancy term does not present any difficulty at $\xi = 0$. For the flat plate case the buoyancy term is identically equal to zero at $\xi = 0$. For the case of the uniform stream flowing past the sphere, where the direction of uniform stream and buoyancy force are the same, the term representing the buoyancy force becomes $g\beta(T - T_\infty)$. Thus this term is added on to the right-hand side of eq. (3.4) and is solved numerically.

3.2 Procedure for Solving the Boundary Layer Equations

The Hartree-Womersley Method [32], as modified by Clutter and Smith [24], will be used to solve the boundary layer equations; this will be discussed in the following sections. In this section only a brief outline of the procedure for solving the equations simultaneously will be given. The major steps employed in the solution are as follows:

1. Initially the viscosity variation across the boundary layer, which exists because of temperature variation, is assumed. At the first station, a linear form is used. At the stations that follow, the solution of the fluid flow properties from the previous station is used. (Since $\mu = \mu(T)$, the temperature profile is used from the previous station to solve the momentum equation at the station of interest.)

2. Using μ from Step 1, a first solution of the momentum equation is obtained.

3. The energy equation, which now is linear because of the solution from Step 2, is solved.

4. Using the solution of the energy equation, i.e., the temperature profile, corrected values of μ are calculated.

5. The momentum equation is again solved.

6. Steps 3 to 5 are repeated until convergency of both the momentum and energy equation is obtained.

3.3 Method for Solving the Momentum Equation

The momentum and energy equations will be solved simultaneously by the method of Hartree-Womersley [24] as modified. The ξ-derivative in the momentum and energy

equations are replaced by finite differences, so that the partial differential equations are approximated by ordinary differential-difference equations at each ξ-station. The region of solution is thus divided in stations in the ξ-direction as shown in Fig. 6. Each equation must be solved step-by-step as the calculation proceeds in the ξ-direction.

Consider the momentum equation for the boundary layer:

$$\frac{\partial}{\partial \eta}(cf'') + P[1 - f'^2] + \left(\frac{P+1}{2} + R\right)ff'' + \frac{\xi L}{U_e^2} g_x \beta (T - T_\infty) = \xi \left| f' \frac{\partial f'}{\partial \xi} - f'' \frac{\partial f}{\partial \xi} \right| \qquad (3.5)$$

In the studies conducted by Clutter and Smith [24], it was found that round-off errors in the computation were reduced by making the following substitution in the momentum equation

$$\left.\begin{aligned} \phi &= f - \eta \\ \phi' &= f' - 1 \\ \phi'' &= f'' \\ \phi''' &= f''' \end{aligned}\right\} \qquad (3.6)$$

The same substitution is made here. Introduction of eq. (3.6) into (3.5) gives

$$\frac{\partial}{\partial\eta}(c\phi'') = P[(\phi' + 1)^2 - 1] - \left(\frac{P+1}{2} + R\right)(\phi + \eta)\phi'' - \frac{\xi L}{U_e^2} g_x\beta(T - T_\infty) + \xi\left[(\phi' + 1)\frac{\partial\phi'}{\partial\phi} - \phi''\frac{\partial\phi}{\partial\xi}\right] \tag{3.7}$$

with boundary conditions

$$\left.\begin{array}{ll} \eta = 0 & \phi_w = 0 \quad ; \quad \phi_w' = -1 \\ \text{for large} & \eta' \to 0 \end{array}\right\}$$

The momentum equation is of third order and non-linear. Solution is made difficult by both the non-linearity and the boundary that lies at very large η. To solve eq. (3.7) an initial value problem is created using arbitrary values of ϕ_w'' as the third boundary condition. Thus it becomes necessary to search through possible values of ϕ_w'' until one is found that satisfies the outer boundary condition $\phi' = 0$ at large η. Thus the boundary conditions now become

$$\left.\begin{array}{ll} \eta = 0 \quad , & \phi_w = 0,\ \phi_w' = -1,\ \phi_w'' = \text{arbitrary} \\ \text{for large } \eta & \phi' \to 0 \end{array}\right\} \tag{3.8}$$

The procedure for performing the search is described below, but first consider the solution of the momentum equation as an initial value problem. We must first determine

$$c\phi'' = \int_0^\eta \frac{\partial}{\partial\eta}(c\phi'')d\eta + c_w\phi_w'' \tag{3.9}$$

where $\partial/\partial\eta(c\phi")$ is given by the right-hand side of eq. (3.7). c_w is known and $\phi"_w$ is "searched" for. The method of integration used in eq. (3.9) will be described in Section 3.6. Other quantities needed in eq. (3.7) are

$$\phi" = \frac{c\phi"}{c} \tag{3.10}$$

$$\phi' = \int_0^\eta \phi"d\eta - 1 \tag{3.11}$$

$$\phi = \int_0^\eta \phi'd\eta \tag{3.12}$$

The steps in the procedure for searching for the correct value of $\phi"_w$ are:

1. Initially, $\phi"_w = (\phi"_w)$ input, where the latter is an input into the program for the first station $\xi = 0$; for the following stations, it is the value of $\phi"_w$ from the previous station. Integrate outwards and determine if the trial solution exceeds $\phi' = 0$ or not.

2. If ϕ' exceeds zero, it implies that the trial value of $\phi"_w$ that was used in Step 1 is high and a second solution is used to integrate out, using a lower $\phi"_w$. The procedure is continued until both a high and a low value of $\phi"_w$ are obtained.

3. Once a (ϕ''_w) high and a (ϕ''_w) low are known, a new value of ϕ''_w is obtained by splitting the difference between the high and low value of ϕ''_w and the procedure is continued.

4. This "splitting" is continued until three solutions are obtained such that ϕ' at $\eta_{max} = \eta_\infty$ is between the bounds of $-k \leq \phi'(\eta_\infty) \leq k$ where $k << 1$. (Both k and η_∞ are inputs.) At least one of the solutions is a high one and one a low one. A three-point interpolation procedure is used to determine the value of ϕ''_w that satisfies the outer boundary condition.

Once the interpolated value of ϕ''_w has been determined, it is now used to provide the correct solution to eq. (3.7), from which the velocity profile and its derivatives can be determined.

A similarity solution exists at the first station ($\xi = 0$), so the correct value of ϕ''_w at $\xi = 0$ is known a priori also, since ϕ''_w is a relatively smooth function of ξ, the searching procedure does not take long because the value of ϕ''_w does not change radically from one station to the next.

The interpolation procedure is now described. Consider the three solutions which have been obtained by the searching procedure to be ϕ_1, ϕ_2, ϕ_3. The interpolated

value of ϕ''_w obtained by three-point Langrangian interpolation which meets the outer boundary condition $\phi'(\eta_\infty) = 0$ is

$$\phi''_w = A_1\phi''_1(\eta=0) + A_2\phi''_2(\eta=0) + A_3\phi''_3(\eta=0) \tag{3.13}$$

where the coefficients are given by

$$A_1 = \frac{\phi'_2\phi'_3}{[\phi'_1 - \phi'_2][\phi'_1 - \phi'_3]}$$

$$A_2 = \frac{\phi'_1\phi'_3}{[\phi'_2 - \phi'_1][\phi'_2 - \phi'_3]} \tag{3.14}$$

$$A_3 = \frac{\phi'_3\phi'_2}{[\phi'_3 - \phi'_1][\phi'_3 - \phi'_2]}$$

All values in eq. (3.14) of ϕ' are evaluated at η_∞.

3.4 Method for Solving the Energy Equation

Before solving the energy equation, it is convenient to use the function ϕ, introduced in the preceding section, and to introduce the function θ, defined as

$$\theta = g - 1 \tag{3.15}$$

for the same reason that ϕ was introduced in the momentum equation. Substitutions of the functions in eq. (3.2) gives

$$\theta'' = Pr_\infty\left[\frac{P+1}{2} + R\right](\phi+\eta)\theta' + \xi\left[(\phi'+1)\frac{\partial\theta}{\partial\xi} - \theta'\frac{\partial\phi}{\partial\xi}\right] \quad (3.16)$$

The boundary conditions are

$$\eta = 0 \quad \theta_w = g_w - 1 \quad \text{(constant wall temperature)}$$

$$\text{or} \quad \theta'_w = g'_w \quad \text{(constant heat flux)}$$

$$\text{for large } \eta \quad \theta \to 0$$

$$\theta' \to 0. \quad (3.17)$$

The method of solution of eq. (3.16) is similar to that of the momentum equation. The region is divided into ξ-wise stations as shown in Fig. 6. Again the ξ-derivatives are replaced by finite differences, these will be defined in the next section. When solving eq. (3.16), the previous solution of the momentum equation is known. Thus in eq. (3.16) the only unknown is θ. The equation is linear.

The solution of equation (3.16) is as follows:

$$\theta' = \int_0^\eta \theta''d\eta + \theta'_w \quad (3.18)$$

The right-hand side of eq. (3.16) gives the value of θ''. θ_w is known from the prescribed wall temperature. In this case θ'_w is arbitrarily chosen and

$$\theta = \int_0^\eta \theta'd\eta + \theta_w \quad (3.19)$$

The method of integration to be used for eqs. (3.18) and (3.19) is the same as for the momentum equation and is described in Section 3.6. Since eq. (3.16) is linear, its solutions may be linearly combined. Thus eq. (3.16) is solved twice, and the two solutions combined to meet the outer boundary conditions. The exact procedure is dependent upon whether g_w or g_w' is known. Consider both cases:

Case 1: g_w is known. Both solutions begin with the same given value of θ_w, the one imposed by the boundary condition

$$\theta_w = g_w - 1$$

Equation (3.16) is solved using a trial value of $\theta_w' = g_w'$. Let this solution be denoted by $\theta_1(\eta)$.

If $\theta_1(\eta_\infty)$ is greater than zero, a lower value of θ_w' is chosen, if it is less, a higher value of θ_w'. The second solution is denoted by $\theta_2(\eta)$. The two solutions are added to produce the general solution which can be made to meet the boundary conditions. The general solution is

$$\theta(\eta) = A\theta_1(\eta) + B\theta_2(\eta) \qquad (3.20)$$

The boundary conditions are

$$\theta(\eta_\infty) = A\theta_1(\eta_\infty) + B\theta_2(\eta_\infty)$$

$$\theta'(\eta_\infty) = A\theta_1'(\eta_\infty) + B\theta_2'(\eta_\infty)$$

and $$\theta_w = A\theta_{1w} + B\theta_{2w} \tag{3.21}$$

But, the solutions were started using

$$\theta_w = \theta_{1w} = \theta_{2w}$$

so that

$$A + B = 1 \quad \text{or} \quad B = 1 - A.$$

Thus boundary conditions (3.21) gives

$$A = \frac{-\theta_2(\eta_\infty)}{\theta_1(\eta_\infty) - \theta_2(\eta_\infty)} \tag{3.22}$$

Thus, the correct solution becomes:

$$\theta(\eta) = A\theta_1(\eta) + (1 - A)\theta_2(\eta)$$

$$\theta'(\eta) = A\theta_1'(\eta) + (1 - A)\theta_2'(\eta) \tag{3.23}$$

Case 2: g_w' is known. The procedure is similar to that of Case 1, but now the energy equation is solved using two trial values of g_w instead of g_w'. Again the two trial values are denoted as $\theta_1(\eta)$ and $\theta_2(\eta)$. Relations (3.22) and (3.23) then gives the correct solution.

3.5 Finite-Difference Representation of ξ-Derivatives

The fundamental idea for the method of solution, that of replacing the ξ-derivatives by finite differences to approximate the partial differential equation by an ordinary differential-difference equation, was advanced by Hartree and Womersley [32]. Note that all the ξ-derivatives that appear in the momentum and energy equations are only of first order.

The notation for the finite-difference representation is presented in Fig. 7. The space is divided into a number of rectangular strips of variable thickness $\Delta\xi$. The corners of the strips are located at "ξ_{n+1}, ξ_n, ξ_{n-1}, ξ_{n-2}, ξ_{n-3}." The momentum and energy equations, being "parabolic" are solved by proceeding in the direction of positive ξ. It is assumed that the solution has been obtained at all previous stations up to and including ξ_{n-1}, which of course means that $\phi(\eta)$ and $\theta(\eta)$ and their derivatives are fully known at these stations. The problem is to find $\phi(\eta)$ and $\theta(\eta)$ at the new station ξ_n.

In solving the boundary layer equations the calculations must start at $\xi = 0$. For the $\xi = 0$ station the terms with the ξ-derivatives in both momentum and energy equations disappear. At the second station the two-point form of finite difference is used, but, at all stations farther downstream the three-point form is used.

For two points:

$$\frac{\partial \phi n}{\partial \xi} = \frac{\phi_n - \phi_{n-1}}{\xi_n - \xi_{n-1}} \tag{3.24}$$

The error in this expression is of order $\frac{\Delta \xi}{2} \frac{\partial^2 \phi}{\partial \xi^2}$.

For three points:

$$\frac{\partial \phi n}{\partial \xi} = \left[\frac{1}{(\xi_n - \xi_{n-1})} + \frac{1}{(\xi_n - \xi_{n-2})}\right]\phi_n - \left[\frac{(\xi_n - \xi_{n-2})}{(\xi_n - \xi_{n-1})(\xi_{n-1} - \xi_{n-2})}\right]\phi_{n-1} + \left[\frac{(\xi_n - \xi_{n-1})}{(\xi_n - \xi_{n-2})(\xi_{n-1} - \xi_{n-2})}\right]\phi_{n-2} \tag{3.25}$$

The error here is of order $\frac{(\Delta \xi)^2}{3} \frac{\partial^3 \phi}{\partial \xi^3}$.

Because of the errors being of order $\Delta \xi$ for two point and $(\Delta \xi)^2$ for three point, the first step must be suitably reduced in order to have the same accuracy in the solution at all stations.

The other ξ-derivatives $\partial \phi'/\partial \xi$ and $\partial \theta/\partial \xi$ are replaced by similar expressions as (3.24) and (3.25).

All of the above relations are given in Ref. [24].

3.6 Method of Integration

The method of solution of both the momentum and energy equations is outlined in Sections 3.3 and 3.4. The problem of solution is one of integration. There are several methods of performing the integrations that

are available in computer libraries for example, Milne's fourth-order predictor corrector method; but, because of their generality, they require long computing time to solve the present problem. In the present investigation, a method developed by Clutter and Smith [24], will be used and is discussed below. It uses a four-point form of the Falkner extrapolation formulas and the Adams interpolation formulas [24].

Consider first the general situation where the solution is known up to η_S and the problem is to find the values of ϕ and θ and their derivatives at η_{S+1} $(= \eta_S + \Delta\eta)$ by use of eqs. (3.9 to 3.12) and eqs. (3.18) and (3.19). A special procedure is used to get started near the wall and is described later in this section.

Consider the momentum equations first where the integration indicated in (3.9, 3.11, 3.12) will be approximated by the Falkner's extrapolation and Adams' interpolation formulas. The extrapolation formulae use values of $(c\phi'')'$ and ϕ'' at the S, S-1, S-2, S-3 stations to determine values of ϕ, ϕ', ϕ'', and $(c\phi'')'$ at the S+1 station. The formulas are

$$(c\phi'')_{S+1)E} = (c\phi'')_S + \frac{\Delta\eta}{24}[55(c\phi'')'_S - 59(c\phi'')'_{S-1} + 37(c\phi'')'_{S-2} - 9(c\phi'')'_{S-3}] \qquad (3.26)$$

where the subscript E denotes extrapolation. The step size $\Delta\eta$ is constant.

The extrapolation formulae for ϕ' and ϕ are

$$\phi'_{S+1)E} = \phi'_S + \frac{\Delta\eta}{24}[55\phi''_S - 59\phi''_{S-1} + 37\phi''_{S-2} - 9\phi''_{S-3}] \tag{3.27}$$

and

$$\phi_{S+1)E} = \phi_S + \Delta\eta\phi'_S + \frac{(\Delta\eta)^2}{360}[323\phi''_S - 264\phi''_{S-1} + 159\phi''_{S-2} - 39\phi''_{S-3}] \tag{3.28}$$

The quantity $(c\phi'')'_{S+1}$ can now be determined by using the momentum equation (3.7) and the extrapolated values of ϕ''_E, ϕ'_E, ϕ_E. The result will be denoted by

$$(c\phi'')'_{S+1)E} = F(\phi''_E, \phi'_E, \phi_E)_{S+1} \tag{3.29}$$

The interpolation formulae are now used to determine more exact values of ϕ'', ϕ', ϕ, and $(c\phi'')'$ at the S+1 station. The formulae are

$$(c\phi'')_{S+1} = (c\phi'')_S + \frac{\Delta\eta}{24}[9(c\phi'')'_{S+1)E} + 19(c\phi'')'_S - 5(c\phi'')'_{S-1} + (c\phi'')'_{S-2}] \tag{3.30}$$

and

$$\phi'_{S+1} = \phi'_S + \frac{\Delta\eta}{24}[9\phi''_{S+1)E} + 19\phi''_S - 5\phi''_{S-1} + \phi''_{S-2}] \tag{3.31}$$

and

$$\phi_{S+1} = \phi_S + \Delta\eta\phi'_S + \frac{(\Delta\eta)^2}{360}[38\phi''_{S+1)E} + 171\phi''_S - 36\phi''_{S-1} + 7\phi''_{S-2}] \tag{3.32}$$

A comparison of the error terms for the extrapolated and interpolated formulas show that not only are the interpolation errors much less than the extrapolation ones but they are also opposite in sign [24]. Thus, the errors tend to cancel rather than add up. The solution can be made as exact as desired by choosing a small enough step size.

The formulas for performing the integration required in the solution of the energy equation are similar to those above. The extrapolation formulae are

$$\theta'_{S+1)E} = \theta'_S + \frac{\Delta\eta}{24}[55\theta''_S - 59\theta''_{S-1} + 37\theta''_{S-2} - 9\theta''_{S-3}] \tag{3.33}$$

and

$$\theta_{S+1)E} = \theta_S + \frac{\Delta\eta}{24}[55\theta'_S - 59\theta'_{S-1} + 37\theta'_{S-2} - 9\theta'_{S-3}] \tag{3.34}$$

and then using eq. (3.16)

$$\theta''_{S+1)E} = G_1(\theta'_E, \theta_E)_{S+1} \tag{3.35}$$

The interpolation formulas are given by

$$\theta'_{S+1} = \theta'_S + \frac{\Delta\eta}{24}[9\theta''_{S+1)E} + 19\theta''_S - 5\theta''_{S-1} + \theta''_{S-2}] \quad (3.36)$$

$$\theta_{S+1} = \theta_S + \frac{\Delta\eta}{24}[9\theta'_{S+1)E} + 19\theta'_S - 5\theta'_S + \theta'_{S-2}] \quad (3.37)$$

and finally, using (3.16)

$$\theta''_{S+1} = G(\theta',\theta)_{S+1} \quad (3.38)$$

The extrapolation-interpolation formulae above require values of the functions ϕ and θ along with their derivatives at four previous ξ stations. To get started at the wall Taylor's Series will be used, with a step size of $\Delta\eta/16$; $\Delta\eta$ is the step size used in the four-point extrapolation-interpolation formulas. The step size is gradually built up to the full length step $\Delta\eta$ by using two-point and three-point extrapolation formulae using step sizes of $\Delta\eta/8$, $\Delta\eta/4$, and $\Delta\eta/2$, respectively.

The steps to be used in the procedure are shown in Table 5. The equations to be used are given below.

<u>Taylor Series--Step Size $\Delta\eta/16$</u>

$$(c\phi'')_{\Delta\eta/16} = (c\phi'')_w + \frac{\Delta\eta}{16}(c\phi'')'_w \quad (3.39)$$

$$\phi'_{\Delta\eta/16} = \phi'_w + \frac{\Delta\eta}{16}\phi''_w \quad (3.40)$$

$$\phi_{\Delta\eta/16} = \phi_w - \frac{\Delta\eta}{16} + \frac{(\Delta\eta)^2}{512}\phi''_w \quad (3.41)$$

$$\theta'_{\Delta\eta/16} = \theta'_w + \frac{\Delta\eta}{16}\,\theta''_w \tag{3.42}$$

$$\theta_{\Delta\eta/16} = \theta_w + \frac{\Delta\eta}{16}\,\theta'_w \tag{3.43}$$

Two-Point Formulas--Step Size $\Delta\eta/16$

$$(c\phi'')_{\Delta\eta/8} = (c\phi'')_{\Delta\eta/16} + \frac{\Delta\eta}{32}[3(c\phi'')'_{\Delta\eta/16} - c\phi'')'_w] \tag{3.44}$$

$$\phi'_{\Delta\eta/8} = \phi'_{\Delta\eta/16} + \frac{\Delta\eta}{32}[3\phi''_{\Delta\eta/16} - \phi''_w] \tag{3.45}$$

$$\phi_{\Delta\eta/8} = \phi_{\Delta\eta/16} + \frac{\Delta\eta}{16}\,\phi'_{\Delta\eta/16} + \frac{(\Delta\eta)^2}{1536}[4\phi''_{\Delta\eta/16} - \phi''_w] \tag{3.46}$$

$$\theta'_{\Delta\eta/8} = \theta'_{\Delta\eta/16} + \frac{\Delta\eta}{32}[3\theta''_{\Delta\eta/16} - \theta''_w] \tag{3.47}$$

$$\theta_{\Delta\eta/8} = \theta_{\Delta\eta/16} + \frac{\Delta\eta}{32}[3\theta'_{\Delta\eta/16} - \theta'_w] \tag{3.48}$$

Two-Point Formulas--Step Size $\Delta\eta/8$

$$(c\phi'')_{\Delta\eta/4} = (c\phi'')_{\Delta\eta/8} + \frac{\Delta\eta}{16}[3(c\phi'')'_{\Delta\eta/8} - (c\phi'')'_w] \tag{3.49}$$

$$\phi'_{\Delta\eta/4} = \phi'_{\Delta\eta/8} + \frac{\Delta\eta}{16}[3\phi''_{\Delta\eta/8} - \phi''_w] \tag{3.50}$$

$$\phi_{\Delta\eta/4} = \phi_{\Delta\eta/8} + \frac{\Delta\eta}{8}\,\phi'_{\Delta\eta/8} + \frac{(\Delta\eta)^2}{384}[4\phi''_{\Delta\eta/8} - \phi''_w] \tag{3.51}$$

$$\theta'_{\Delta\eta/4} = \theta'_{\Delta\eta/8} + \frac{\Delta\eta}{16}[3\theta''_{\Delta\eta/8} - \theta''_w] \tag{3.52}$$

$$\theta_{\Delta\eta/4} = \theta_{\Delta\eta/8} + \frac{\Delta\eta}{16}[3\theta'_{\Delta\eta/8} - \theta'_w] \tag{3.53}$$

Two-Point Formulas--Step Size $\Delta\eta/4$

$$(c\phi'')_{r+1} = (c\phi'')_r + \frac{\Delta\eta}{8}[3(c\phi'')'_r - (c\phi'')'_{r-1}] \tag{3.54}$$

$$\phi'_{r+1} = \phi'_r + \frac{\Delta\eta}{8}[3\phi''_r - \phi''_{r-1}] \tag{3.55}$$

$$\phi_{r+1} = \phi_r + \frac{\Delta\eta}{4}\phi'_r + \frac{(\Delta\eta)^2}{96}[4\phi''_r - \phi''_{r-1}] \tag{3.56}$$

$$\theta''_{r+1} = \theta'_r + \frac{\Delta\eta}{8}[3\theta''_r - \theta''_{r-1}] \tag{3.57}$$

$$\theta_{r+1} = \theta_r + \frac{\Delta\eta}{8}[3\theta'_r - \theta'_{r-1}] \tag{3.58}$$

Three-Point Formulas--Step Size $\Delta\eta/2$

$$(c\phi'')_{r+1} + (c\phi'')_r + \frac{\Delta\eta}{24}[23(c\phi'')'_r - 16(c\phi'')'_{r-1} + 5(c\phi'')'_{r-2}] \tag{3.59}$$

$$\phi'_{r+1} = \phi'_r + \frac{\Delta\eta}{24}[23\phi''_r - 16\phi''_{r-1} + 5\phi''_{r-2}] \tag{3.60}$$

$$\phi_{r+1} = \phi_r + \frac{\Delta\eta}{2}\phi'_r + \frac{(\Delta\eta)^2}{96}[19\phi''_r - 10\phi''_{r-1} + 3\phi''_{r-2}] \tag{3.61}$$

$$\theta'_{r+1} = \theta_r + \frac{\Delta\eta}{24}[23\theta''_r - 16\theta''_{r-1} + 5\theta''_{r-2}] \tag{3.62}$$

$$\theta_{r+1} = \theta_r + \frac{\Delta\eta}{24}[23\theta'_r - 16\theta'_{r-1} + 5\theta'_{r-2}] \tag{3.63}$$

All of the above expressions may be found in Reference [24].

3.7 Starting the Solution

At $\xi = 0$, the ξ-dependent terms disappear in both the momentum and energy equation, when buoyancy forces are excluded. The momentum equation reduces to

$$(c\phi'')' = P[(\phi' + 1)^2 - 1] - \left(\frac{P+1}{2} + R\right)(\phi+\eta)\phi'' \qquad (3.64)$$

and energy equation to

$$\theta'' = Pr_\infty\left[\frac{P+1}{2} + R\right](\phi+\eta)\theta' \qquad (3.65)$$

Hence, values of ϕ and θ at previous stations are not required. The ξ-dependent terms also disappear for similar type flows. Such flows occur when P and R and the wall boundary condition are constant for all ξ. These include flow over a flat plate with constant pressure and wedge type flows (buoyancy forces not included).

The procedure of solution described earlier requires that the momentum equation be solved first, but to do so requires the values of viscosity. To get started at the $\xi = 0$ station, a linear temperature profile that satisfies the inner and outer boundary conditions for temperature is assumed. The viscosity obtained from this temperature profile is then used to start the solution. After the first solution of the momentum equation at any

particular station is found, the viscosity obtained from the last solution of the energy equation is used.

At $\xi = 0$, the value of P, the pressure parameter is known. For the flat plate with zero pressure gradient, $P = 0$, while for a sphere, $P = 1$. At $\xi = 0$, the value of R, the radius parameter, for any conical body is zero, while for a flat plate $R = 0$ for any ξ.

3.8 Boundary Layer Parameters

Once the momentum and energy equations have been solved at a particular ξ-station, the conventional boundary layer parameters are calculated.

1. Displacement Thickness.

A physically meaningful measure for the boundary layer thickness is the displacement thickness δ_1, which is the distance by which the external potential flow is displaced outwards as a consequence of the decrease in the velocity gradient in the boundary layer.

$$\delta_1 = \int_0^\infty (1 - \frac{u}{U_e}) dy \tag{3.66}$$

Using the transformation equations (2.13), the definition of δ_1, equation (3.65) transformed into the (ξ,η) coordinates is

$$\delta_1 = \sqrt{\frac{\nu_\infty x}{U_e}} \int_0^\infty (1 - \frac{u}{U_e}) dy$$

$$\delta_1 = \sqrt{\frac{\nu_\infty x}{U_\infty}} \sqrt{\frac{U_\infty}{U_e}} \int_o^\infty (1 - f')dy \tag{3.67}$$

A dimensionless displacement thickness may be defined as in Smith and Clutter [24]

$$\delta_1^* = \sqrt{\frac{U_\infty L}{\nu_\infty}} \frac{\delta_1}{R} \tag{3.68}$$

Substituting (3.67) into (3.68)

$$\delta_1^* = \frac{\eta_\infty - f_{\eta=\infty}}{\sqrt{\frac{U_e}{U_\infty}} \sqrt{\frac{L}{x}}} \tag{3.69}$$

2. Momentum Thickness.

The momentum thickness is defined as

$$\delta_2 = \int_o^\infty \frac{u}{U_e}(1 - \frac{u}{U_e})dy \tag{3.70}$$

In the (ξ,η) coordinates, δ_1 may be written as

$$\delta_2 = \sqrt{\frac{\nu_\infty \xi L}{U_\infty}} \sqrt{\frac{U_\infty}{U_e}} \int_o^\infty f'(1 - f')dy$$

A dimensionless momentum thickness is defined [24] as

$$\delta_2^* = \sqrt{\frac{U_\infty R}{\nu_\infty}} \frac{\delta_2}{R} . \tag{3.71}$$

or

$$\delta_2^* = \frac{f_{\eta=\infty} - \int_0^\infty f'^2 d\eta}{\sqrt{\frac{U_e}{U}}\ \sqrt{\frac{R}{x}}} \tag{3.72}$$

3. Shear Stress at the Wall.

The shear stress at the wall is defined as

$$\tau_w = \mu_w \left(\frac{\partial u}{\partial y}\right)_w$$

or in (ξ,η) coordinates as

$$\tau_w = \sqrt{\frac{U_e}{\nu_\infty \xi L}}\ \mu_w\ U_e f''_w \tag{3.73}$$

Introducing the local skin friction coefficient defined [23] as:

$$c_f = \frac{\tau_w}{\frac{1}{2}\rho_\infty U_e^2} \tag{3.74}$$

or

$$c_f = 2\sqrt{\frac{\nu_\infty}{U_e \xi L}} \left(\frac{\mu_w}{\mu_\infty}\right) f''_w$$

Define the local Reynolds Number Re_ξ to be

$$Re_\xi = \frac{U_e \xi}{\nu_\infty}$$

Thus

$$c_f (Re_\xi)^{\frac{1}{2}} = \frac{2}{\sqrt{L}} \left(\frac{\mu_w}{\mu_\infty}\right) f''_w \tag{3.74}$$

A conventional shear parameter is defined [23] as

$$c_f^* = c_f \sqrt{\frac{U_\infty L}{\nu_\infty}}$$

which with (3.74) becomes

$$c_f^* = \frac{2}{\sqrt{U_e/U_\infty}} \sqrt{\frac{L}{x}} \left(\frac{\mu_e}{\mu_\infty}\right) f''_w \tag{3.75}$$

4. Heat Transfer Parameter.

The heat transfer rate at the wall is given by

$$q_w = - \left(k \frac{\partial T}{\partial y}\right)_w$$

or in (ξ,η) coordinates

$$q_w = - k_w \sqrt{\frac{U_e}{\nu_\infty \xi L}}\, g'_w T_\infty \tag{3.76}$$

Let the local Nusselt Number be defined as (for flat plates)

$$Nu_x = \frac{q_w\, x}{k_w (T_w - T_\infty)}$$

or with (3.76) and definition of Re_x,

$$Nu_x/Re_x = \frac{g'_w}{1 - g_w} \tag{3.77}$$

For the sphere, Nusselt Number is defined as

$$Nu_D = \frac{q_w\, D}{k_w (T_w - T_\infty)} \tag{3.78}$$

Since the external velocity field U_e is a function of ξ, it may be written as

$$U_e = U_\infty f(\xi) \ .$$

Thus

$$Nu_D/\sqrt{Re}_R = 2\sqrt{\frac{f(\xi)}{\xi}} \left(\frac{g_w'}{1 - g_w} \right) \tag{3.79}$$

3.9 Computer Program

A computer program was written to solve the momentum and energy equations simultaneously by the method described in the proceeding sections. This program was run on the CDC 6500 and is reproduced in the Appendix. The results of the runs made are given in Chapter 5.

CHAPTER 4

EXPERIMENTAL APPARATUS AND PROCEDURE

4.1 Introduction

The experiments were conducted to provide a qualitative estimate of the effect of heating a sphere on the separation point. A brass sphere was placed in a square horizontal test section of a loop designed to circulate water. The sphere was heated electrically by means of a heating element placed inside the hollow brass sphere. The temperature difference between the water upstream from the sphere and the wall of the sphere was measured with the use of thermocouples. Hydrogen bubbles generated off a fine wire placed on the surface of the sphere were used to visualize the flow around the unheated sphere, while the shadowgraph method was employed when the sphere was heated.

A description of the sphere, test loop, and the flow visualization techniques follow.

4.2 Description of the Heated Sphere

A sketch of the sphere with the heating element installed inside it, is shown in Fig. 8. The 3.00"

(±.004) external diameter hollow brass sphere consisted of two hemispheres joined together. The wall of the sphere was 0.25 inches thick resulting in a constant temperature sphere. The heating element consisted of 21 feet of Nichrome wire with asbestos insulation. The heating wire was held in a plastic cage inside the sphere, as shown in Fig. 8.

Four, 30-gage iron-constantine thermocouples were soft-soldered into the inside wall of the sphere at the position shown, i.e., No. 1 at 70°, No. 2 at 45°, No. 3 at 0°, No. 4 at 315° (all angles measured clockwise from the forward stagnation point). The thermocouples, when inbedded into the wall, were 1/16" from the outside surface. Since the temperature difference between the upstream water and the wall of the sphere is required, a thermocouple was placed upstream of the sphere and used as the reference junction.

The heating element lead wires and the thermocouple wires passed through the Plexiglass support tube. A photograph of the sphere with the support tube is shown in Fig. 9.

The brass sphere was marked at 2 degree intervals between 80° and 100° (measured from the forward stagnation point).

The sphere was coated with a fine coat of varnish, which insulated the brass sphere from the fine wire which

generated the hydrogen bubbles. The hollow sphere was filled with water before it was placed into the test section. The water served to improve the heat transfer to the interior walls of the sphere.

4.3 Description of the Test Section Loop

A schematic diagram of the test loop, which consists of a variable flow rate pump, two tanks and a 10-inch square plexiglass test section is shown in Fig. 10. Water was circulated by a centrifugal pump. The walls of the upstream and downstream tanks were lined with stainless steel sheets. The upstream tank contained three straightening sections. The first of these contained glass marbles sandwiched between two stainless steel screens; the second, a fine mesh stainless steel screen; and the third, a honeycomb constructed by placing 3-inch long, 0.2 inches diameter plastic soda straws between two stainless steel screens. The honeycomb was placed at the inlet of the square test section, so as to insure uniform velocity profiles in the test section. No measurement was made of the low free stream fluctions level. However, hydrogen bubbles traces showed no observable fluctions. The piping used to transport water from the downstream tank to the upstream tank through the pump was made of P.V.C., a plastic material.

Care was taken to maintain the water as free from impurities as possible. Before any tests were made, the water in the test loop was passed through a water filter at low speeds for at least 12 hours.

4.4 Flow Visualization Techniques

The two visualization techniques, the hydrogen bubble method and the shadowgraph method, used in the present work will not be discussed at any length because they have been used in the past by many researchers [40]. Mention will be made, however, of the problems encountered in using these techniques in the present situation.

The hydrogen bubble method consists of using a fine wire as one end of a d-c circuit to electrolyze the water. The tiny bubbles thus formed are visualized by means of an appropriate light source placed outside the test section. A .001-inch platinum wire was used to generate the hydrogen bubbles. A Spectra-Physics Laser beam passed through a cylindrical lens was used as a light source. The platinum wire was stretched across the top half of the meridian plane. Thus the hydrogen bubbles were generated next to the surface of the sphere, in the boundary layer and the wake region.

The shadowgraph method is based on the phenomenon that light passing through a density gradient in a fluid is deflected. It measures the second derivative, therefore allowing visualization of only those parts of the

flow where the density gradient change is sufficiently large. The shadowgraph system consists of a bright light source, a colliminating lens, and a viewing screen.

Photographs were taken of the region near the separation point using the hydrogen bubble method and of the whole flow field around the sphere using the shadowgraph method. The laser beam used to visualize the hydrogen bubbles was not photographed directly; a video recording was made with a TV camera installed with a 130 mm lens. The video pictures projected on the TV screen were then photographed. The shadowgraph pictures were directly photographed.

4.5 Operating Procedures

The test loop was filled with soft water and the brass sphere was installed in the test section. The flow rate was adjusted so that the pump circulated 94 gallons per minute through the test loop. This flow rate resulted in the flow rate of the water in the test section to be 0.3 ft/sec. The Reynolds Number, based on the diameter of the sphere, was thus 7500. This low Reynolds Number assured a laminar flow in the boundary layer prior to separation.

Before the sphere was heated, the hydrogen bubbles were generated and photographs taken to insure the occurrence of laminar separation (about 84°). The power to the heating element inside the sphere was then adjusted

to provide the desired temperature difference between the water upstream of the sphere and the wall of the sphere. The shadowgraph pictures were taken for various temperature differences.

Prior to making any tests, the sphere was heated to check the uniformity of the temperature of the sphere wall. All the thermocouples (1 thru 4) were used to check the wall temperature of the sphere and it was found that the sphere temperature was essentially constant. When the sphere was heated to make tests two thermocouples (2 and 4) were used to determine the temperature difference between the water upstream and the wall of the sphere.

The sphere reached a constant temperature within three minutes after the power was turned on.

CHAPTER 5

NUMERICAL AND EXPERIMENTAL RESULTS

5.1 Introduction

In this chapter results will be presented to show the effect of heating a body which is placed in a uniform stream of water. Numerical results will be presented for various flow cases of water flowing past a flat plate and a sphere. Experimental results, which are qualitative in nature, will be presented for the case of water flowing past a 3-inch sphere placed in a 10-inch horizontal square test section.

Though the primary objective of this investigation is to show that heating does affect separation, numerical results will include the effect of heating on the boundary layer parameters.

In Chapter 3, the numerical methods of solution, for the momentum and energy equations, were discussed. It should be emphasized that the boundary layer equations (momentum and energy) are valid only if $\delta << 1$. Near the separation point this requirement is no longer valid and hence the boundary layer equations are not applicable.

If the boundary layer equations were extended up to the separation point, a mathematical singularity would exist at the separation point. This presents a serious problem to investigators interested in locating the separation point. One way to eliminate this mathematical singularity would be to solve the full Navier-Stokes equations instead of the boundary layer equations. Since the Navier-Stokes equations are very difficult to solve, what is usually done is that the boundary layer equations are solved to a point as near the separation point as possible and then the solution is extrapolated to the separation point. The usual procedure is to use the value of ϕ''_w along the surface of the wall and to extrapolate the separation point to be the point where $\phi''_w = 0$. (This is done by fitting a curve through the ϕ''_w data points.)

5.2 Verification of the Numerical Technique

The purpose of this section is to establish the accuracy of the numerical method of solution. It will be done by comparison with known numerical and exact solutions, and experimental data.

A. Similar Flows on a Flat Plate

The only boundary layer flows which can be solved exactly are similar flows for which $U_e = \xi^m$, where constant coefficients are assumed. For such flows the momentum equation and the energy equations are uncoupled.

The momentum equation is independent of ξ, and since the flow is two-dimensional, the radius parameter R is zero; eq. (3.7) then reduces to

$$\phi''' = -\frac{P+1}{2}(\phi+\eta)\phi'' + P[(\phi' + 1)^2 - 1] \qquad (5.1)$$

In this equation P = m where $U_e = \xi^m$. The flows included in this study are for m = 1.0, 0.33, 0, -.047619, and -0.090429. m = 1.0 is the stagnation point flow; m = 0 is the Blasius type or flat plate flow; and m = 0.090429 corresponds to the separation profile. Fig. 11 shows these five profiles and in Table 6 the values of ϕ''_w are compared with exact results.

Kaups and Smith [24] present results for a flat plate ($U_e = \xi^m$, m = 0) where the plate is heated. Heating causes a viscosity variation $\mu(T)$ across the boundary layer coupling the momentum and energy equations; they are

$$\frac{\partial}{\partial\eta}(c\phi'') = -\frac{P+1}{2}(\phi+\eta)\phi'' + P[(\phi' + 1)^2 - 1]$$

$$\theta'' = Pr_\infty\left(\frac{P+1}{2}\right)(\phi+\eta)\theta' \qquad (5.2)$$

where c is the variable viscosity parameter defined by eq. (2.9).

The eqs. (5.2) are solved simultaneously. Figs. 12 and 13 show the velocity and temperature profiles respectively for the heated and the cooled flat plate.

It can be seen that the given temperature variation causes considerable deviation from the Blasius profile. As expected, the inverse viscosity-temperature relationship for liquids makes the effect of heating and cooling opposite to that for gases. Also shown in Fig. 12 is the "seventh power" turbulent profile. In Chapter 1, it was pointed out that the reason why a turbulent boundary layer around a sphere separated "later" (110°) than a laminar boundary layer (84°) was that the turbulent boundary layer contained more momentum near the wall than the laminar boundary layer and thus could better overcome the adverse pressure gradient. The "seventh power" turbulent boundary layer profile in Fig. 12 is shown to indicate that with sufficient heating the laminar profile tends to look more like the turbulent profile (i.e., contains more momentum). Figs. 12 and 13 also give a check against the calculations of Kaups and Smith [24]. Table 7 shows the effect of heating and cooling on the skin friction and the heat transfer parameters; the results are compared with Kaups and Smith.

Since buoyancy forces are to be included in the calculations for flow around a sphere, a check was made with Kaups and Smith's [24] example of flow past a vertical flat plate with T_w = 312°F, T_∞ = 40°F, and U_∞ = 6fps. Figs. 14 and 15 show the velocity and temperature profiles respectively at a distance of two feet from the leading edge.

It is concluded from the results presented for the similar flows that the numerical method of solution being used in the present investigation is sufficiently accurate. Since in this investigation, attention is focused on the separation point, a check was made on decelerated, or adverse pressure gradient, flows.

B. Adverse Pressure Gradient Flows

The development of the laminar boundary layer in a linearly retarded velocity field

$$\frac{U_e}{U_\infty} = 1 - \frac{\xi}{8} \tag{5.3}$$

has been studied by Howarth [34], Von-Karman and Millikan [35], Hartree [36], and Smith and Clutter [37]. This fluid flow case was studied without the consideration of heat transfer effects. In this investigation, a method of solution which is identical to the method of the latter two [36, 37] is used. This particular type of flow, eq. (5.3), leads to separation. Table 8 compares values of ϕ''_w calculated by the present author and those by Hartree and Smith and Clutter.

As was pointed out earlier, the boundary layer equations are not valid at the separation point, thus the separation point is extrapolated from the values of ϕ''_w. The present method extrapolated the separation point to lie at $\xi = 0.96$ for the flow given by eq. (5.3).

In addition, the retarded flow

$$\frac{U_e}{U_\infty} = 1 - \xi \tag{5.4}$$

has been studied by various authors [6, 34, 38]. Table 9 compares the separation point as calculated (extrapolated) by various workers and the present author. It is evident that the discrepancy is greater than for the retarded flow given by eq. (5.3). The reason for this seems to be that, because eq. (5.4) represents a very strong adverse pressure gradient, separation occurs very close to the leading edge. The boundary layer equations are valid in only a short region near the leading edge; hence the extrapolation procedure is assumed inaccurate.

The flows discussed in parts A and B have been two-dimensional plane flows. For axially symmetric bodies, the radius parameter $R = (\xi/r_o)(dr_o/d\xi)$ has values other than zero. The boundary layer growth on a sphere is presented next.

C. Flow Over a Sphere

Two cases for the potential flow around the sphere will be considered; in one case, the simple potential flow for an unseparated flow is employed, while in the other, use is made of a velocity distribution U_e/U_∞ which has been obtained experimentally [31] in the case when the flow separates from the forward portion of the

sphere. The two velocity distributions are shown in Fig. 16. The pressure distribution around the sphere has been reproduced from [31] and is shown in Fig. 17. "Critical flow" is defined as the flow where the flow in the boundary layer "just" becomes turbulent at the point of separation. In Fig. 17 the "above critical" curve represents the pressure distribution around the sphere when the boundary layer becomes turbulent before it separates and the "below critical" curve represents the pressure distribution when the boundary layer remains laminar up to the separation point. It is obvious from Fig. 17 that the pressure distribution measured for the "above critical" flow is similar to that of the simple potential flow. Thus the solution obtained from the potential flow theory for flow around the sphere serves as an approximation for the "above critical" flow.

The theoretical velocity distribution on the surface of a sphere as obtained from potential flow theory, is given by

$$\frac{U_e}{U_\infty} = \frac{3}{2} \sin \alpha = \frac{3}{2} \sin \xi, \tag{5.5}$$

The radius $r_o(\xi)$ is given by

$$r_o = R_1 \sin \xi$$

where R_1 is the radius of the sphere. The boundary layer calculations for the flow around the sphere, with no

heating, were carried out to determine the separation point. The value of ϕ''_w are tabulated in Table 10 and are compared with those calculated by Smith and Clutter [37]. The separation point, $\phi''_w = 0$, was extrapolated to be at 104°.

The experimentally determined velocity distribution [31] for "below critical" flow around the sphere is given by

$$\frac{U_e}{U_\infty} = 1.5\ \xi - .36402\xi^3 + .24668\xi^5. \qquad (5.6)$$

The boundary layer calculations using eq. (5.6) for the velocity distribution with no heating predicts the separation point to be at 87°. Tomotika [31] using eq. (5.6) calculated the separation point to be at 81° using a momentum integral technique. Fage [41] measured the separation point to be around 85°.

Fig. 18 shows ϕ''_w plotted against α for the two types of flows around the sphere corresponding to eqs. (5.5) and (5.6). Referring back to Fig. 17, it is evident that the point of minimum pressure lies at 74° for the "below critical" flow. It is because of this stronger adverse pressure gradient for the "below critical" flow case that the flow separates earlier (about 10° after minimum pressure point) than for the "above critical" flow case (about 20° after the minimum pressure point).

5.3 Flow Past an Unheated Sphere: Hydrogen Bubble Experiment

The purpose of this section is to present experimental results which show that the flow past the unheated sphere is laminar. This is done by showing that separation exists around 85°. The hydrogen bubbles, generated by the platinum wire placed on the surface of the sphere, made it possible to visualize the entire flow region around the sphere, i.e., the boundary layer and the wake region. Fig. 19 shows a photograph of the flow region between 80° and 100° (measured from the stagnation point). It is evident from the photograph that there is reverse flow beyond 88°, implying that the separation point must lie ahead of 88°. To define the separation point, the following procedure was employed.

A tracing of the photograph was made, as is shown in Fig. 20 (solid lines). Then a dotted line was passed through the zero velocity point of the reverse flow "path" lines and extrapolated to a point on the sphere. This point was defined as the separation point. As is evident from Fig. 20, the separation point lies near 84°.

It must be emphasized that the major problem encountered was the generation of large hydrogen bubbles. Researchers have experienced this problem in the past [41] but it was especially a nuisance in these experiments because the large bubbles would stick to the surface of the sphere thus disturbing the flow. Conventional

techniques of brushing off the bubbles and switching the polarity of the platinum wire were employed but without satisfactory results.

5.4 Effect of Heat Transfer in Linearly Retarded Flows on a Flat Plate

Consider first the flow over a heated flat plate where the external velocity flow field is given by

$$\frac{U_e}{U_\infty} = 1 - \frac{\xi}{8} \quad . \tag{5.7}$$

Since the viscosity variation is important in heated liquid flows, the momentum and energy equations are coupled and thus solved simultaneously. The free stream fluid temperature is assumed to be 70°F and the flat plate is heated to temperatures of 100°F, 150°F, and 200°F. Also considered will be the case of the cooled flat plate, where the free stream temperature is 150°F and the plate is 70°F. Thus we have three heated cases with temperature differences of $\Delta T = 30°$, 80°, 130°, and one cooled case with $\Delta T = -80°$ ($\Delta T = T_w - T_\infty$). For all the cases to be presented, the results will be given for the four temperature differences mentioned above.

Figs. 21 through 23 show the velocity profiles at various ξ-stations along the flat plate for $\Delta T = 130°$, 80°, 30°, 0°, and -80°. Fig. 24 shows how ϕ''_w varies along the plate for various ΔT. The dotted line in

Fig. 24 represents the extrapolation to ξ_s, the separation point. Fig. 25 shows the separation point location for various temperature differences. Figs. 26 through 28 are plots of the temperature profiles at various ξ-stations.

Next, the flow over a heated flat plate where the external velocity flow field is given by

$$\frac{U_e}{U_\infty} = 1 - \xi \tag{5.8}$$

was calculated. This external velocity flow field represents a stronger adverse pressure gradient than the case represented by eq. (5.7). Figs. 29 through 31 show the velocity profiles at various ξ-stations along the flat plate for different ΔT. Fig. 32 shows the variation of ϕ''_w vs. ξ and here again the dotted line shows the extrapolated values of ξ_s. Fig. 33 shows the location of the separation point for various temperature differences, ΔT.

Since heating tends to increase the ξ-component of the velocity vector (i.e., increased momentum in the boundary layer), it is obvious that as the plate is heated, there will be a corresponding decrease in the displacement thickness. Fig. 34 shows this decrease in displacement thickness by comparing the curves of various ΔTs. Note that for the cooled flat plate, the displacement thickness is the greatest. Fig. 35 gives a similar plot for the momentum thickness. Figs. 36 through 38 show the

temperature profiles for various ΔTs. It may be inferred from these plots that as the plate is heated, the thermal boundary layer decreases with correspondingly higher gradients at the wall, thus increasing the heat transfer rate. Fig. 39 is a plot of the heat transfer parameter Nu_ξ/Re_ξ, showing the increased heat transfer.

5.5 Effect of Heating a Sphere

Numerical results will be presented for the two potential flows, eq. (5.5) and eq. (5.6), around the sphere (see Section 5.2). The effect of introducing the buoyancy force term will be discussed for the case of flow of water past a heated sphere in a vertical channel. Experimental results showing the effect of heating a 3-inch sphere in a 10-inch square horizontal test section will be presented.

A. Simple Potential Flow ("Above Critical")

The velocity profiles for the temperature differences, ΔT = 130°, 80°, 30°, 0°, -80°, at various α locations along the surface of the sphere are shown in Figs. 40 through 42. Fig. 43 shows the variation of ϕ''_w vs. α for the temperature differences mentioned above. The dotted line shows the extrapolation to the separation point α_s. Fig. 44 is a plot of the local skin friction coefficient along the surface of the sphere. Referring back to Fig. 17, it is evident that the pressure distribution represented by the "theoretical" curve is such

that the pressure gradient is favorable (negative) from the stagnation point ($\alpha = 0°$) to $\alpha = 90°$ and that beyond $\alpha = 90°$, the pressure gradient is unfavorable (positive). Fig. 44 shows that heating the sphere diminishes the skin friction before $\alpha = 90°$ and increases it beyond $\alpha = 90°$. Figs. 45 through 47 are plots of the temperature profiles for various α-locations along the surface of the sphere. Fig. 48 shows the variation of local heat transfer parameters, $Nu_x/\sqrt{Re}_x$ for the temperature differences being discussed. Table 11 gives the extrapolated values of α_s for the various temperature differences.

B. Experimentally Determined Velocity Distribution ("Below Critical")

The effect heating has on the velocity profiles in the boundary layer at various α-locations is shown in Figs. 49 through 51. It is evident that heating tends to decrease the velocity boundary layer thickness. Figs. 52 and 53 show how the displacement thickness and momentum thickness is affected by heating and cooling the sphere. Fig. 54 shows the effect of heat transfer on the velocity gradient ϕ''_w at the wall. The dotted lines indicate the extrapolation to the separation point α_s. Figs. 55 through 57 are plots of temperature profiles at various α-locations. The local heat transfer parameter $Nu_x/\sqrt{Re}_x$ is plotted in Fig. 58. Table 12 gives the extrapolated values of α_s for the various temperature differences.

C. Effect of Introducing the Buoyancy Force Term ("Below Critical")

The buoyance force term in the momentum equation (3.7) is retained to show its effect. For the potential flow around the sphere, use is made of eq. (5.6), which represents the "below critical" flow. Before the results showing the effect of the buoyancy force term are presented, a definition of positive and negative buoyancy force is given.

The buoyancy force is considered positive when it is in the same direction as the free stream velocity and negative when in a direction opposite to the free stream velocity. Fig. 59 shows the positive and negative buoyancy force in a vertical channel that exists in the boundary layer when the sphere is heated or cooled. The reason for presenting the flow in the vertical channel is that the flow remains axisymmetric and thus can be treated by the numerical solution.

It is obvious that when the buoyancy force is positive (Fig. 59a and 59d), it would delay separation, and that when the buoyancy force is negative (Fig. 59b and 59c), it would bring about separation earlier.

Calculations were made, with the buoyancy force term included for the four cases listed below, where the sphere was either heated or cooled.

Case 1. $T_w = 150°F$; $T_\infty = 70°F$ (heating)
Fig. 59a Buoyancy Force Positive

Case 2. $T_w = 150°F$; $T_\infty = 70°F$ (heating)
Fig. 59c Buoyancy Force Negative

Case 3. $T_w = 70°F$; $T_\infty = 150°F$ (cooling)
Fig. 59d Buoyancy Force Positive

Case 4. $T_w = 70°F$; $T_\infty = 150°F$ (cooling)
Fig. 59b Buoyancy Force Negative

Fig. 60 shows the effect of the positive and negative buoyancy forces on the velocity profile at an α-station on the sphere when the sphere was cooled (Case 3 and 4). Also shown in Fig. 60, for comparison, is the velocity profile when the buoyancy force was not included in the calculation. It is evident that the negative buoyancy force makes the velocity profile approach the separation profile. Figs. 61 and 62 are plots of ϕ''_w vs. α for the cases mentioned above. Both the cooled sphere (Fig. 61) and the heated sphere (Fig. 62) indicate a slight shift in the separation point when the buoyancy forces are included.

In Chapter 1, reference was made to an experimental study by Brown [27], where he studied the effect of heating a sphere in a vertical channel (as in Fig. 59a). The copper sphere was heated with a constant heat flux

such that the temperature difference between the water upstream and the stagnation point of the sphere was 10°F. The two extreme cases for which Brown presents results are: (1) water temperature = 70°F, sphere temperature = 80°F; and (2) water temperature = 180°F, sphere temperature = 190°F. Brown plotted the experimentally determined local Nusselt number along the sphere for various Reynolds numbers. Also presented was a plot of a heat transfer parameter ($Nu_D/Re_D^{\frac{1}{2}} Pr^{.36}$) vs. α.

Brown's experimental results are verified qualitatively by the present numerical solution, with the buoyancy force term included. For the purpose of simulating the potential flow around the sphere, use was made of eq. (5.6).

The local Nusselt number Nu_D is plotted in Figs. 63 and 64, and compared with Brown's results. Fig. 65 compares the heat transfer parameter used by Brown, as calculated by the present analysis.

The results show that Brown's experimental data agree within 10% of the results calculated by the present work.

D. Experimental Results

Hydrogen bubble method: The hydrogen bubble method was unsuccessful in visualizing the flow past the heated sphere. It was evident that the platinum wire generated large bubbles very rapidly and that these bubbles remained

on the wire thus disturbing the flow field. Attempts to brush off the bubbles fast enough and record only the tiny bubbles were unsuccessful. Repeatedly, a new platinum wire was used with the anticipation of generating uniform bubbles but all attempts failed. It was thought that the secondary currents produced by the heating element wire (which had A.C. flowing through it) may be the cause of a large potential across the platinum wire, and reducing the input d.c. potential did not produce any different results.

Thus the hydrogen bubble method was abandoned in favor of the shadowgraph method.

Shadowgraph method: The 3-inch brass sphere was heated in a 10-inch square horizontal test section. The temperature difference between the water upstream and the wall of the sphere ranged from 20°F to 100°F. Shadowgraph pictures were taken for various temperature differences and these are presented in Figs. 66 through 69. Since shadowgraph pictures show dark lines where the derivatives of the density gradients are large, the wake region is visualized. It becomes difficult to extrapolate the separation point, since the reverse flow patterns are not visualized.

However, these pictures do merit some qualitative analysis. It is evident that as the sphere is heated to higher temperatures the flow about the sphere becomes

asymmetric, i.e., the wake region becomes asymmetric. This is probably due to the buoyancy forces. Also, note that the wake is apparently three-dimensional at higher temperatures. Even though the location of the separation point cannot be determined, it is evident that there is not a significant shift in the separation point, i.e., the separation streamline appears to lie in the same region.

As is evident from the results presented, the shadowgraph method is not suited to determine the location of the separation point.

5.6 Effect of Treating Viscosity Constant in Linearly Retarded Flow

The results presented in the preceding sections were calculated when the viscosity varied across the boundary layer. In the present section, calculations are made with the viscosity held constant across the boundary layer.

The linearly retarded flow, eq. (5.4), past a heated flat plate is examined. Calculations are made using: (1) the value of viscosity at wall temperature $\mu = \mu_w$; and (2) the value of viscosity at free stream temperature, $\mu = \mu_\infty$. These results will be compared with the results obtained previously, when the viscosity was allowed to vary, $\mu = \mu(T)$. Calculations are made for the case when the temperature of the flat plate is 150°F and that of the free stream is 70°F ($\Delta T = 80°F$).

Figs. 70 and 71 compare the velocity and temperature profiles at a typical ξ-station, when the viscosity is considered constant and variable across the boundary layer. In Figs. 72 and 73, the effect of treating viscosity constant on the velocity gradient at the wall and the heat transfer parameter Nu_x/Re_x are shown.

The plots show that the results obtained by treating viscosity constant are substantially different than those obtained by treating viscosity variable. When viscosity is considered constant, the calculations do not show any significant shift in the position of the separation point.

5.7 Conclusions

Heating substantially increases the u-component of the velocity in the laminar boundary layer. With a ΔT of 180°F the u-component of the velocity in the boundary layer increases by 100% for the linearly retarded flow past a heated flat plate, while the u-component of the velocity increases by approximately 50% in the laminar boundary layer for the flow past a heated sphere.

Heating retards the laminar boundary layer separation. The shift in the separation point is more pronounced in the linearly retarded flow past heated flat plate (30%), than for the flow past the heated sphere*

*The numerical calculations were made using the experimentally determined [31] pressure distribution from

(5%). Experimental results tend to confirm that heating a sphere has a small effect on the position of the separation point.

Heating has the effect of decreasing the displacement thickness and the momentum thickness. The displacement thickness decreased by 22% and the momentum thickness by 6% for the linearly retarded flows past the heated flat plate with $\Delta T = 180°F$. For the flow past the heated sphere, the displacement thickness decreased by 30% and the momentum thickness by 20%.

While the effect of heating and cooling is small on the velocity boundary layer thickness, cooling does substantially increase the thermal boundary layer thickness.

The effect of introducing the buoyancy terms is not significant and thus may be neglected for the flow of water past a heated sphere in a vertical channel.

The effect of heating a body subjected to a uniform flow of water on the boundary layer parameters cannot be determined with high accuracy by treating viscosity constant. The skin friction coefficient may be calculated, with up to a 10% error, using the value of viscosity at the wall temperature as constant, and the heat transfer

---

an unheated sphere. This pressure distribution was not allowed to change during the calculations; but as the separation point shifts the actual pressure distribution also changes. To properly account for this change an iteration scheme would be necessary which would undoubtedly result in a greater shift of the separation point.

coefficient may be calculated, with up to a 15% error, using the value of viscosity at the free-stream temperature as being constant.

TABLES

TABLE 1. Similarity solutions ($U_e = x^m$)

T_w/T_∞	Values of m for $\partial u/\partial y = 0$	Reference
2	-0.06	7, 13
1	-0.094	13
0.6	-0.109	7
0.5	-0.1178	13
0.25	-0.1351	13
0.2	-0.134	7

TABLE 2. Calculated separation point for the case $U_e/U_\infty = 1 - x$

T_w/T_∞	Value of x_s According to Several Authors				
	Illingworth [10]	Morduchon & Grape [6]	Gadd [14]	Curle [15]	Poots [16]
2	0.067	0.073	0.072	0.071	0.075
1.295	0.093	0.106			
0.8	0.128	0.135			
0.6		0.152	0.16		
0.5		0.168		0.195	
0.3		0.19	0.195		

TABLE 3. Values of γ at the point of separation (Illingworth [10])

A	γ
-1	1.402
0	1.429
+1	1.550

TABLE 4. Summary of principal methods for solving the laminar boundary layer equations

No.	Method	Working Form of Equation	Accuracy as Measured by Errors in τ, the Skin Friction	Advantages	Criticisms
1.	Momentum Integral	Von Kármán's momentum integral equation	3 figure accuracy possible in the most favorable cases. Greater than 100 percent error in adverse cases.	Very fast and convenient. well conditioned problems accuracy is good.*	In Accuracy entirely unsatisfactory for problems of boundary layer stability. Method insensitive to shape of upstream boundary layer. It considers only thickness.
2.	Local Similarity	Based on Similar solutions, as of Falkner-Skan equation.	About the same as above.	About the same as above.	About the same as above.
3.	Infinite Series	Various transformations of momentum equation where x,y remain essentially as the independent variables.	5 to 8 figure accuracy possible in the most favorable cases, as near stagnation point. Several hundred percent error in adverse cases.	Exact solutions can be obtained easily for certain fortuitous edge velocity distributions.	Cannot handle ordinary pressure distributions such as those of airfoils.
4.	Finite Difference, Explicit	Unmodified momentum and energy equations.	Theoretically exact, but insufficient work has been done to establish the accuracy, computing time relation.	Simple and sufficiently fast for low accuracy. Theoretically can handle any boundary layer problem exactly in limit.	Boundary layer thickness in this system varies greatly, causing computing complications. Computing time excessive where high accuracy demanded. Has numerical stability problem.
5.	Finite Difference, Explicit	Crocco's transformed equation, in which x,u are independent variables.	Theoretically exact. Accuracy high (3 to 5 figure). Computing time is long.	Theoretically exact and convenient formulation, because boundaries are at $u = 0$, $u = 1$, and Crocco's equation is second order.	Computing time great where high accuracy demanded. Crocco's equation not suitable for problems involving "overshoot." Has numerical stability problem.
6.	Finite Difference, Implicit	Crocco's transformed equation, in which x,u are independent variables.	Theoretically exact, but insufficient work has been done to establish accuracy-computing time relation, Computing time should be short.	Same as No. 5 above plus rapid computing time. Computing is fast because a "trick" good for second order equations has been used. No numerical stability problem.	Crocco's equation not suitable for problems involving "overshoot."
7.	Hartree-Womersley Finite Difference, Implicit	Simple transformation of momentum equation in which x,y remain essentially as independent variables.	Theoretically exact. Accuracy high (3 to 5 figure). Computing time now medium, but could be reduced greatly.	Theoretically can handle any boundary-layer problem, exactly in limit. Computing time is good. Has best starting procedure of any exact method. No numerical stability problem.	Probably slower than No. 6 in cases where No. 6 can handle the problem.

*By "well conditioned" is meant that the problem to be solved is similar to those for which the method is at its best.

TABLE 5. Steps in the procedure for starting integration at wall

Step in Procedure	η	Type of Formula	Step Size	Equations
0	0	Wall Values	--	--
1	$\Delta\eta/16$	Taylor's Series	$\Delta\eta/16$	(3.39) through (3.43)
2	$\Delta\eta/8$	2-Point Extrapolation	$\Delta\eta/16$	(3.44) through (3.48)
3	$\Delta\eta/4$	" "	$\Delta\eta/8$	(3.49) through (3.53)
4	$\Delta\eta/2$	" "	$\Delta\eta/4$	(3.54) through (3.58)
5	$3\Delta\eta/4$	" "	$\Delta\eta/4$	(3.54) through (3.58)
6	$\Delta\eta$	" "	$\Delta\eta/4$	(3.54) through (3.58)
7	$3\Delta\eta/2$	3-Point Extrapolation	$\Delta\eta/2$	(3.59) through (3.63)
8	$2\Delta\eta$	" "	$\Delta\eta/2$	(3.59) through (3.63)
9	$5\Delta\eta/2$	" "	$\Delta\eta/2$	(3.59) through (3.63)
10	$3\Delta\eta$	" "	$\Delta\eta/2$	(3.59) through (3.63)
11	$4\Delta\eta$	4-Point Extrapolation-	$\Delta\eta$	
	$\Delta\eta$	Interpolation	$\Delta\eta$	(3.26) through (3.38)
12	5	" "		(3.26) through (3.38)
		Etc.		
	η_∞			

TABLE 6. Value of ϕ''_w for similar flows

m	ϕ''_w Calculated	ϕ''_w Exact
1.0	1.232587	1.2325877
0.33	0.47413	0.4741
0.0	0.332057	0.3320573
-0.04	0.220325	0.220317
-0.0904285	0.00006	0.0

TABLE 7. Effect of heating and cooling a flat plate on skin friction and heat transfer parameters

T_w °F	T_∞ °F	$C_f(R_x)^{1/2}$		$N_u/R_x^{1/2}$	
		Kaups & Smith [24]	Present Method	Kaups & Smith	Present Method
312	40	0.3698	0.36985	1.0646	1.06462
130	40	0.5540	0.55401	0.8938	0.89387
40	312	0.8182	0.81823	0.2937	0.29375

TABLE 8. Calculated values of ϕ''_w for Howarth's retarded flow $U_e/U_\infty = 1 - \xi/8$

ξ	Present Author	Smith & Clutter	Hartree
0.0	.33206		
0.025		.325728	
0.04795	0.32263		
0.05		.321842	
0.100	.312	.311979	
0.1534	.30102	.301031	
0.206	.28966	.290089	
.3116	.26564	.265623	
.417	.23962	.239712	.23972
.5226	.21108		
.62808	.17922	.179232	
.73356	.14254	.142554	
.83904	.097337	.098627	.09773
.8865	.071046	.072033	
.948	.02642	.026397	.0249
.956		.014267	.0114
.958		.009534	.0059
.9589		.006469	0-extrapolated
.96	0-extrapolated	0-extrapolated	
Computing Time	106 secs	70 mins	

TABLE 9. Separation point calculated for the flow $U_e/U_\infty = 1 - \xi$

ξ Sep.	Reference
.12	Present Author
.122	6
.12	38
.12	34
.1198	39

TABLE 10. Comparison of values of ϕ''_w on a sphere as calculated by the present author and Smith and Clutter [37]

$\alpha°$	ϕ''_w	
	Smith & Clutter [37]	Present Author
0°	1.31189	1.31193
30°	1.26099	1.261
60°	1.08115	1.082
90°	0.64833	0.642
101.7°		0.2394
104°		0*
105.9°	0*	

*Value obtained by extrapolation.

TABLE 11. The effect of heating the sphere on the separation point "above critical" flow

ΔT(°F)	α°*
130	107.9
80	106.6
30	105.2
0	104
-80	101.5

*Values obtained by extrapolation.

TABLE 12. The effect of heating the sphere on the separation point "below critical" flow

ΔT(°F)	α°*
130	91°
80	90°
30	88.5°
0	87°
-80	85°

*Values obtained by extrapolation.

FIGURES

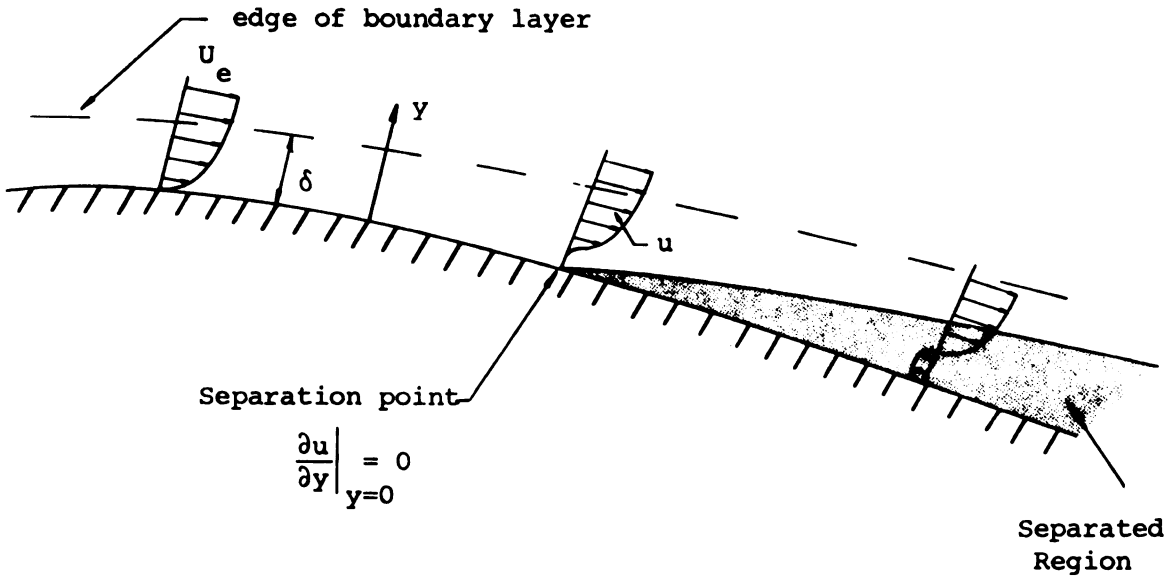

Figure 1. Velocity profile near the separation point.

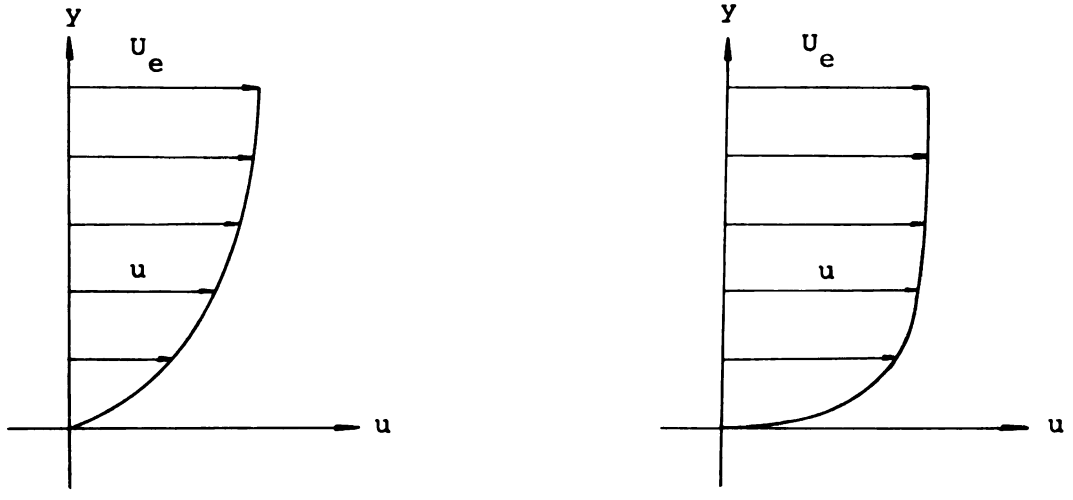

a) Laminar

b) Turbulent

Figure 2. Boundary layer profiles.

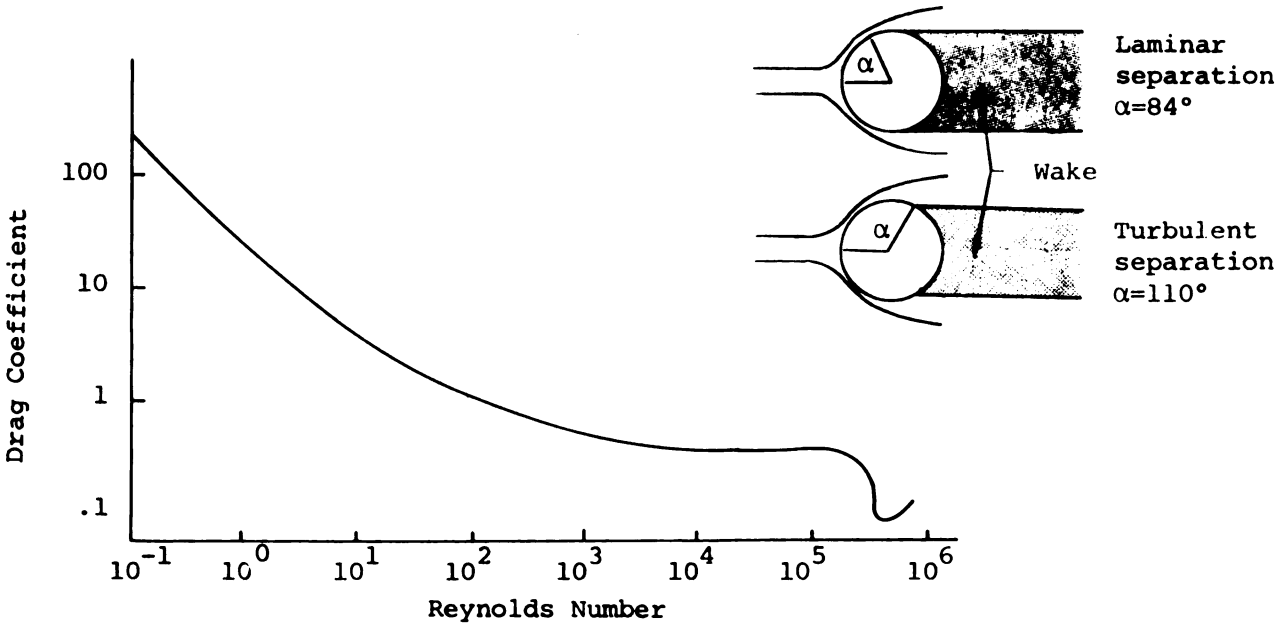

Figure 3. Drag coefficient for a sphere as a function of Reynolds Number.

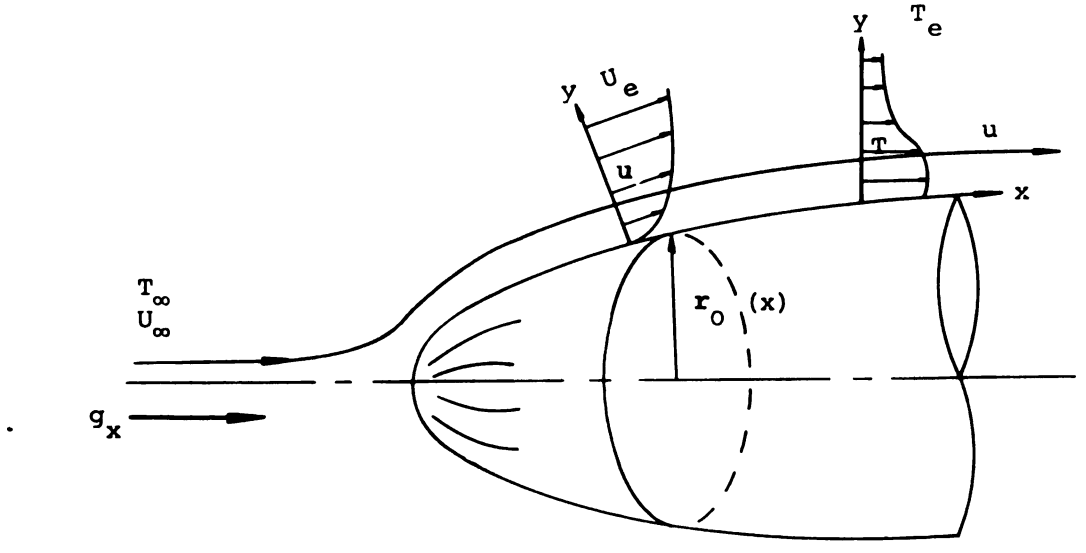

Figure 4. Boundary layer on a body of revolution--coordinate system.

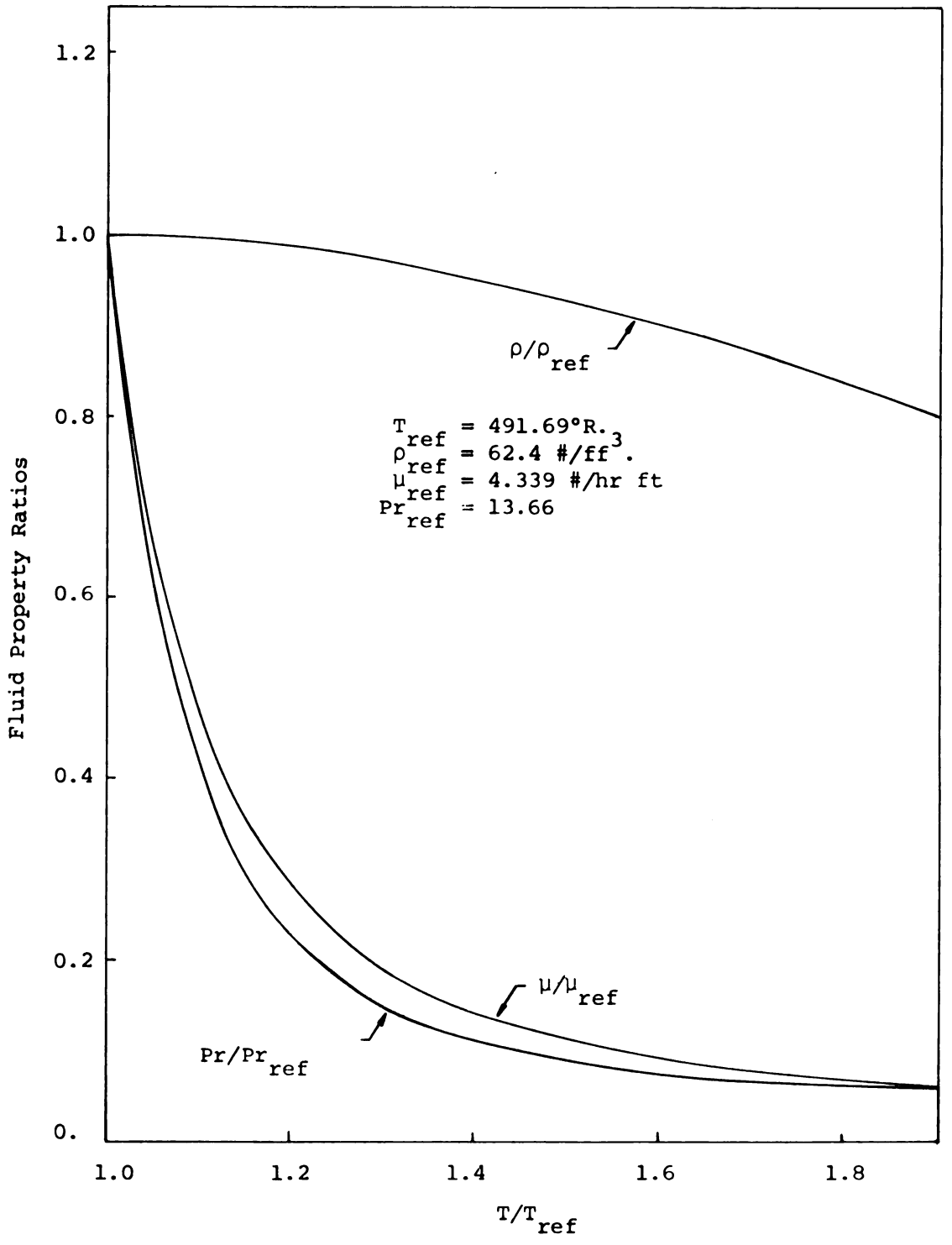

Figure 5. Nondimensional fluid properties for water.

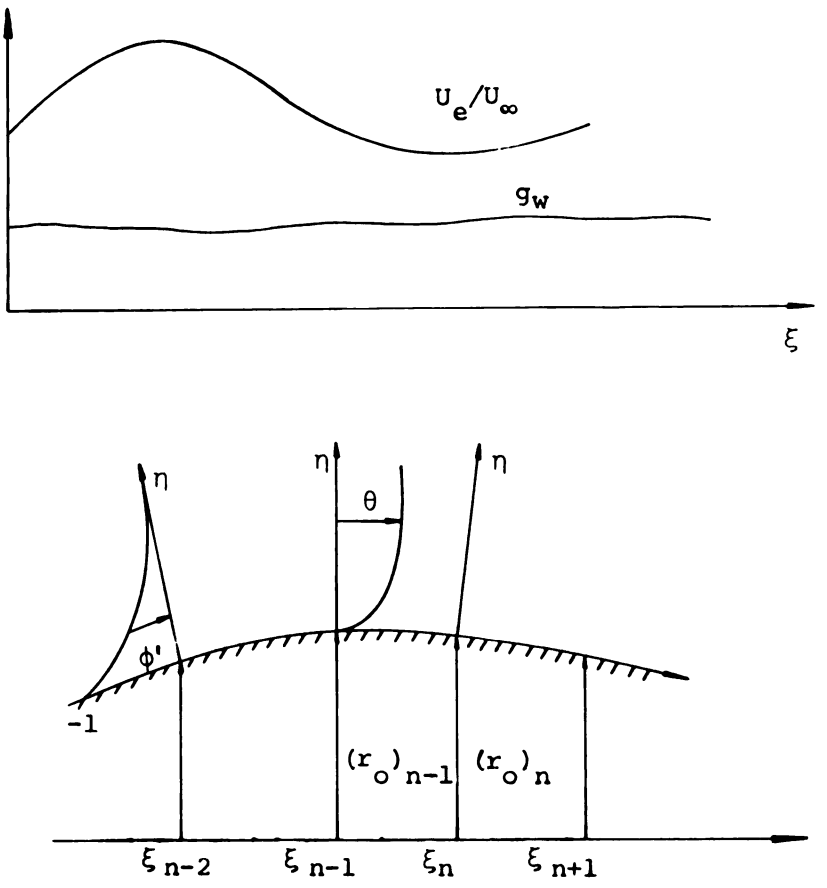

Figure 6. Notation for velocity and temperature profiles in the boundary layer on a body of revolution.

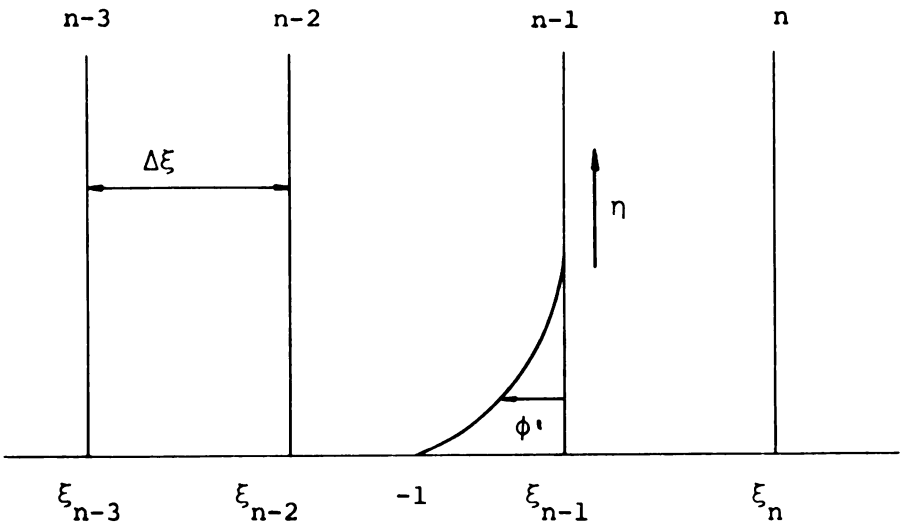

Figure 7. Notation for finite difference representation.

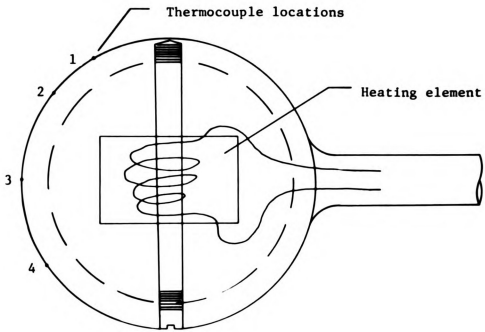

Figure 8. Brass sphere with heating element and location of thermocouples.

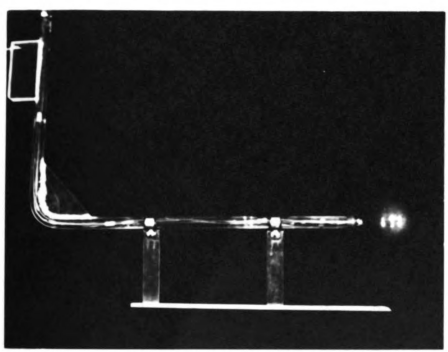

Figure 9. Photograph of the sphere with the support rod.

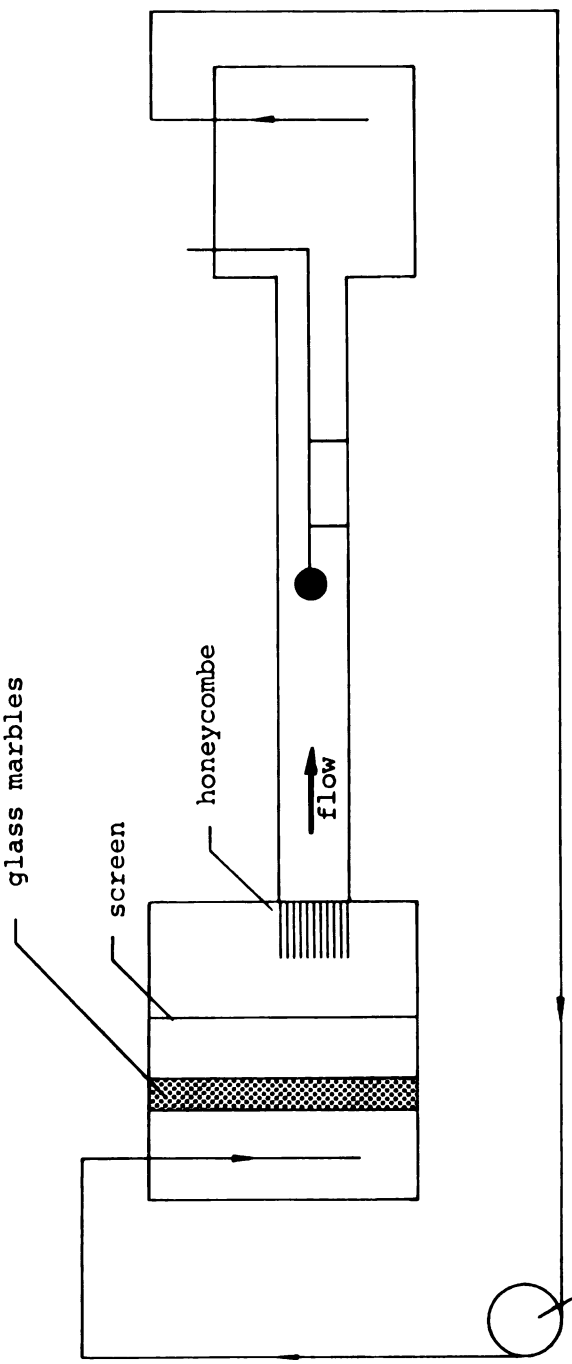

Figure 10. Schematic diagram of test loop.

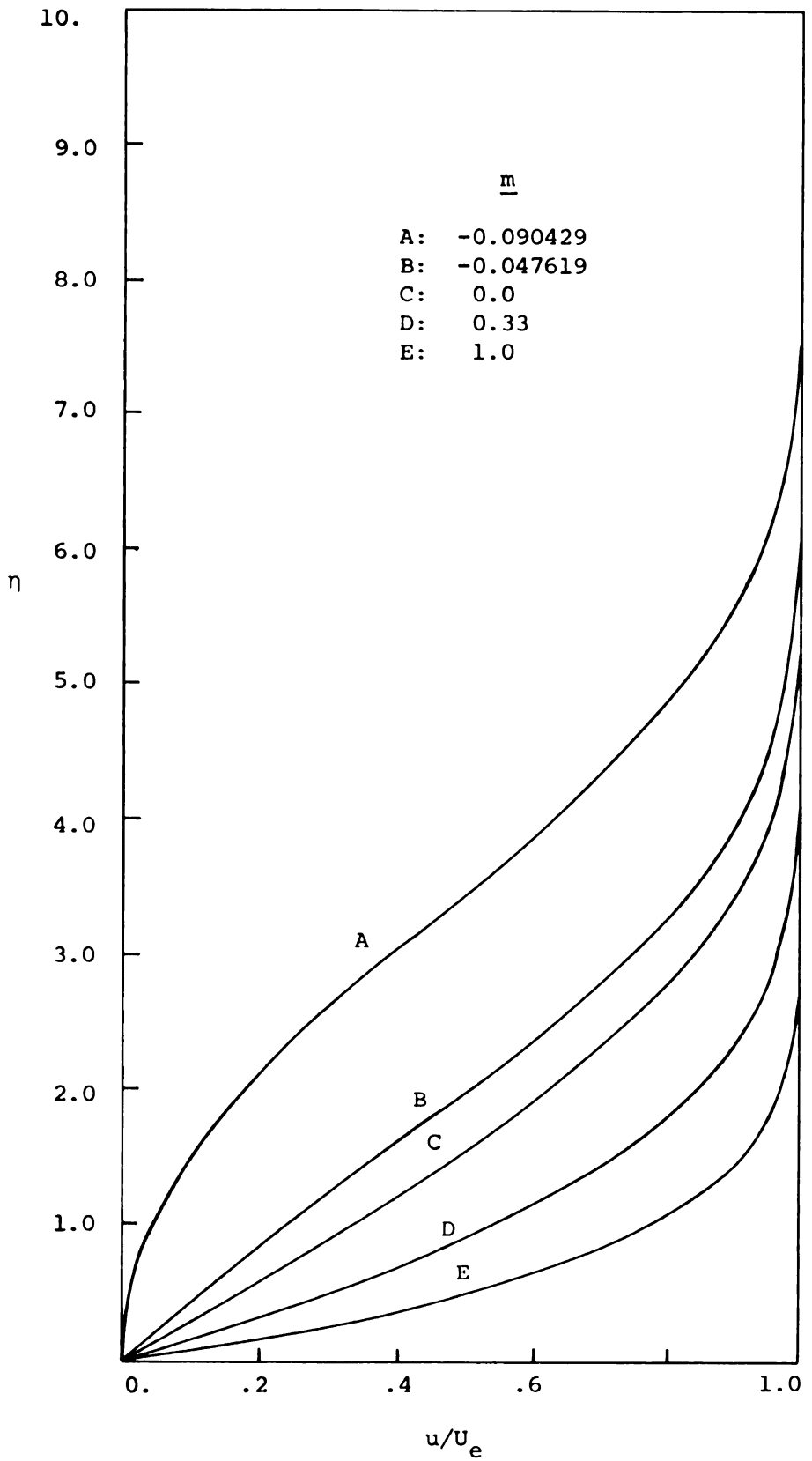

Figure 11. Velocity profiles for similar flows.
$U_e \sim \xi^m$

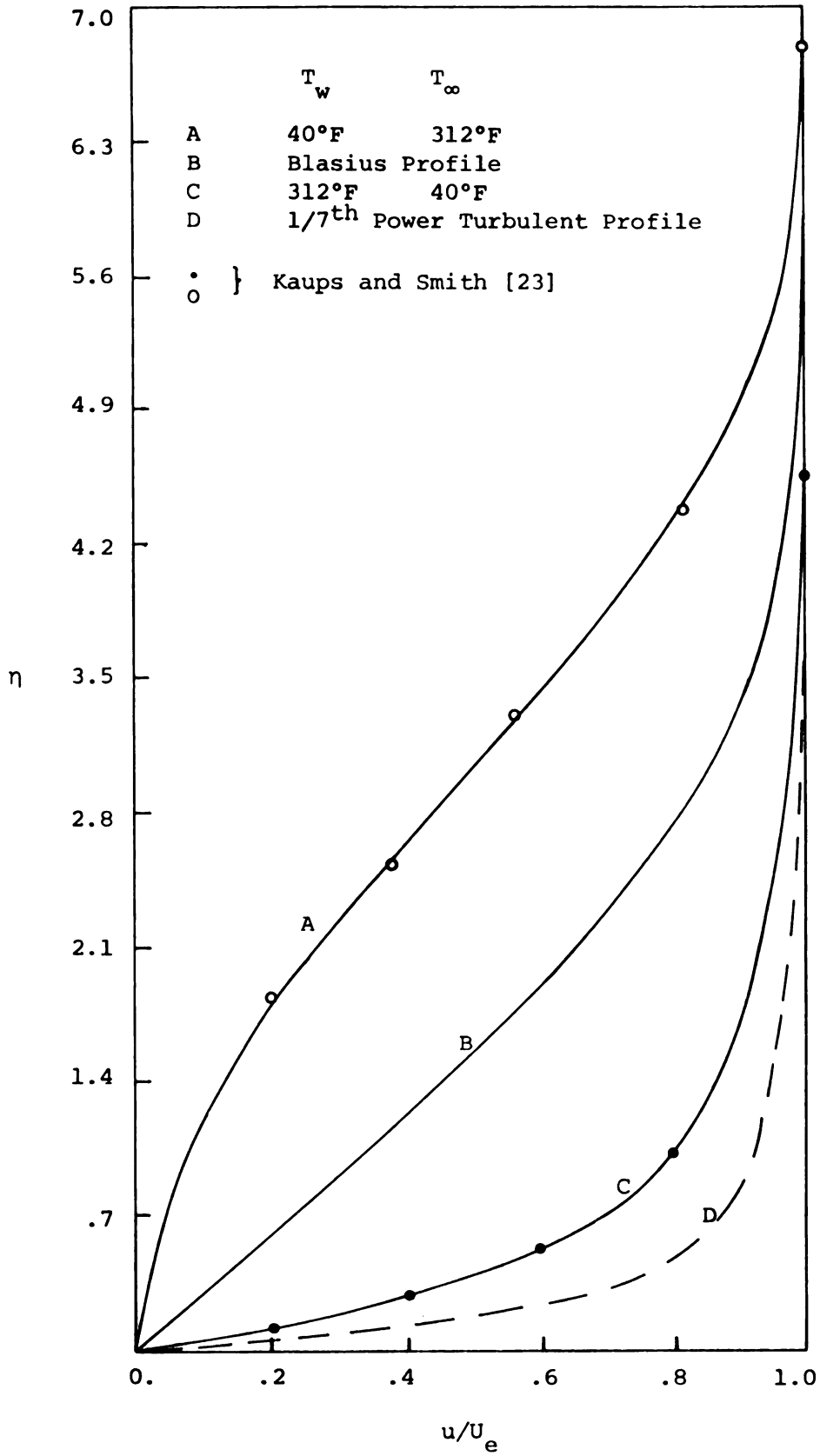

Figure 12. The effect of heating and cooling on the velocity profiles on a flat plate.

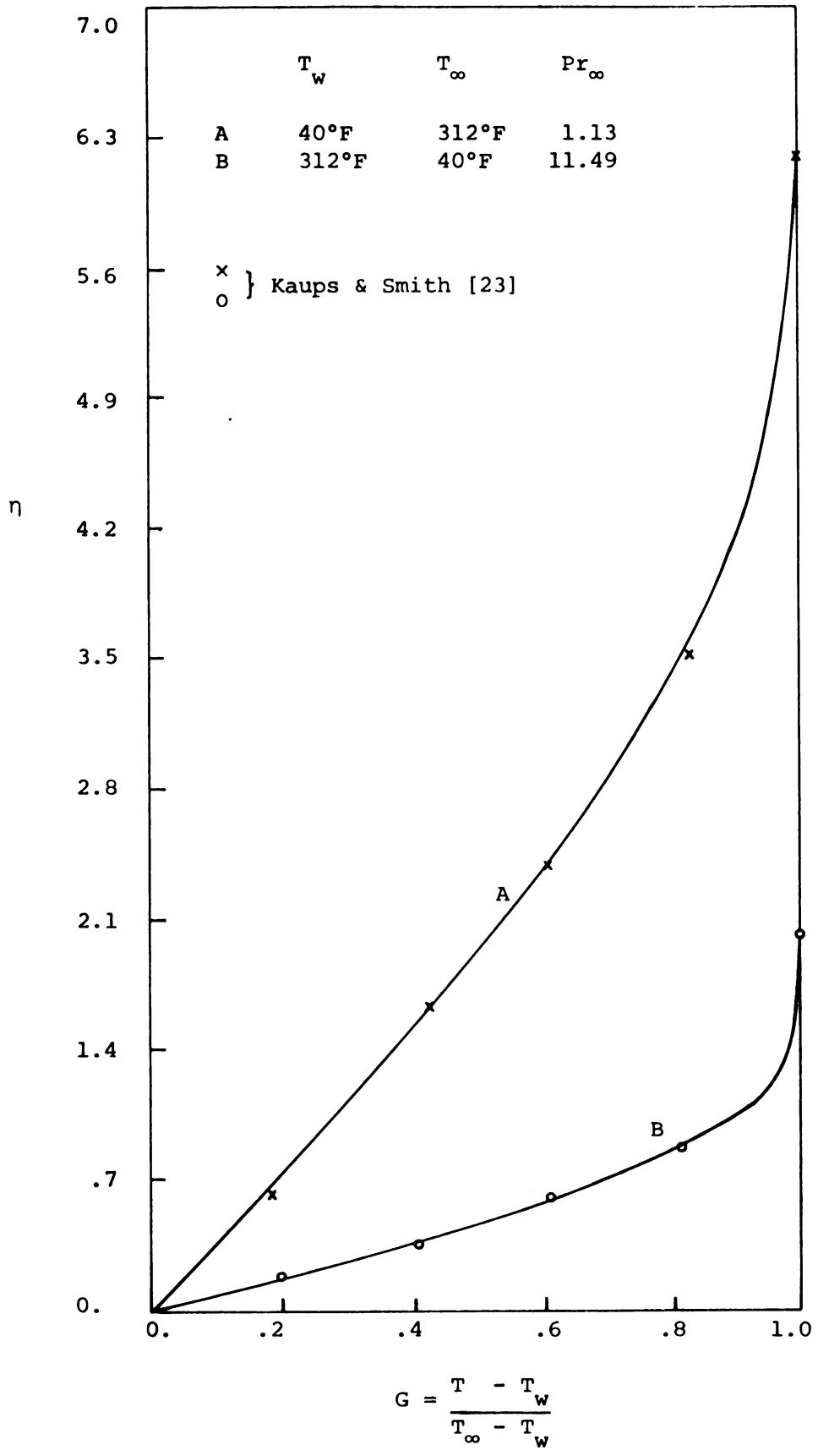

Figure 13. The effect of heating and cooling on the temperature profile on a flat plate.

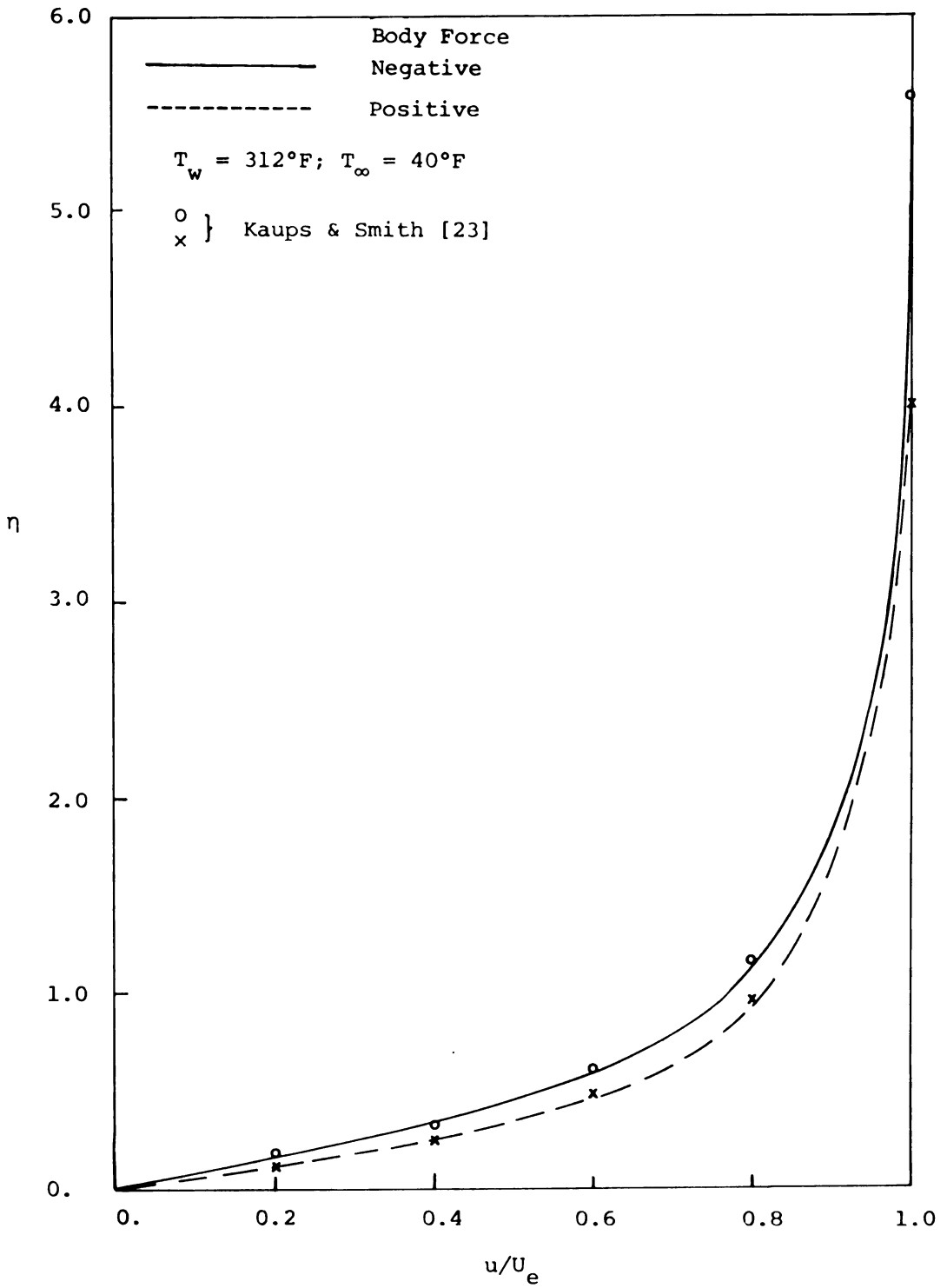

Figure 14. The effect of buoyancy forces on the velocity profiles on a heated vertical plate, two feet from leading edge.

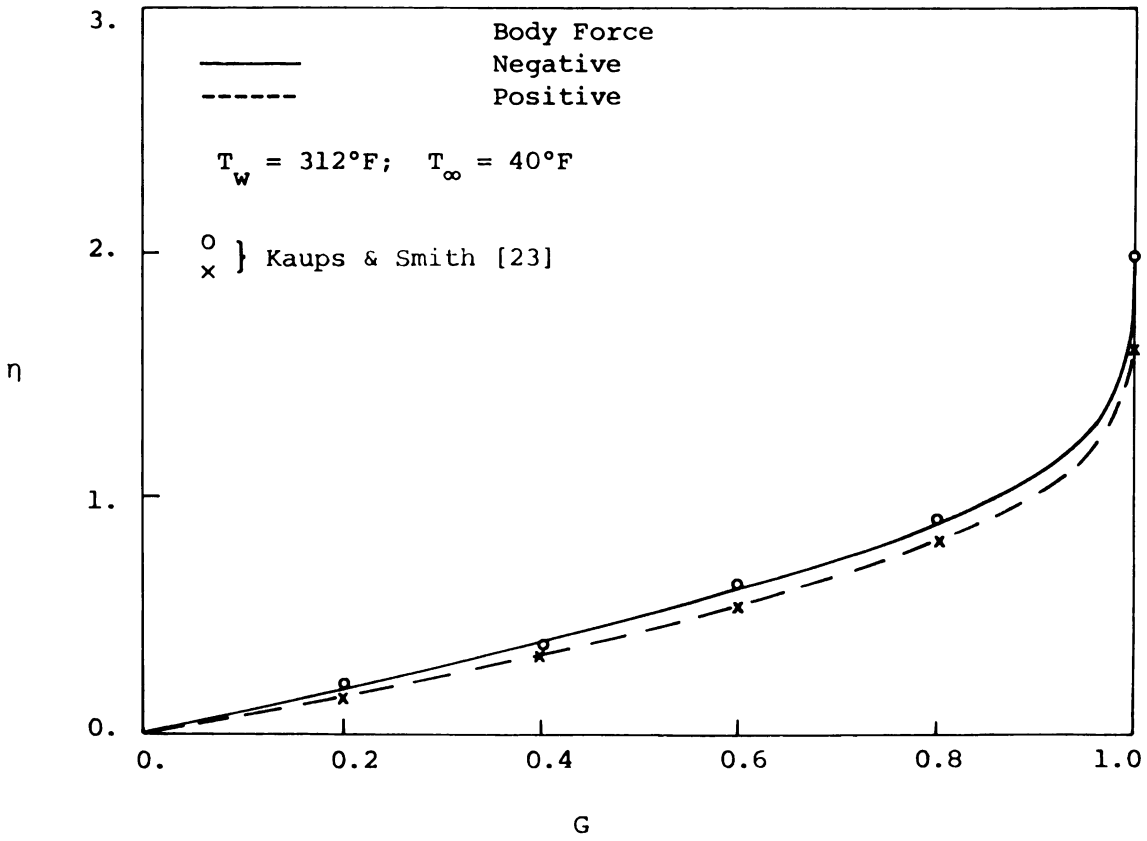

Figure 15. The effect of buoyancy forces on the temperature profiles on a heated vertical plate, two feet from leading edge.

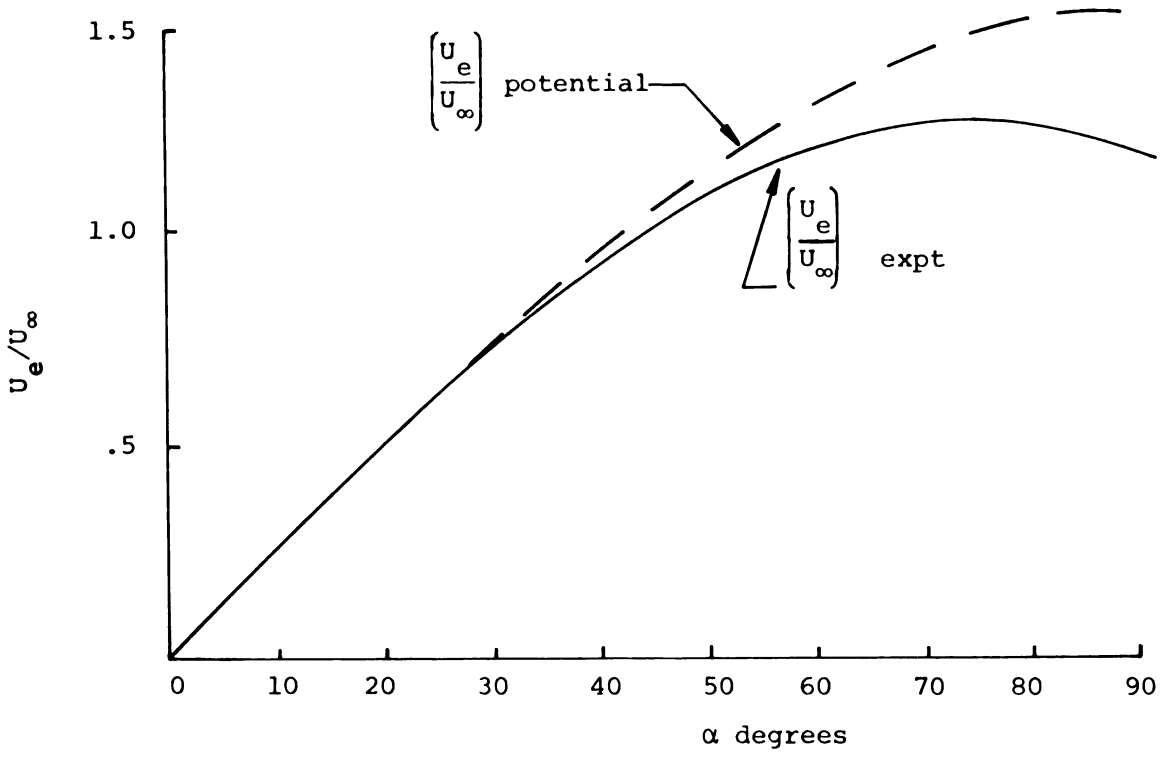

Figure 16. Velocity distribution around a sphere.

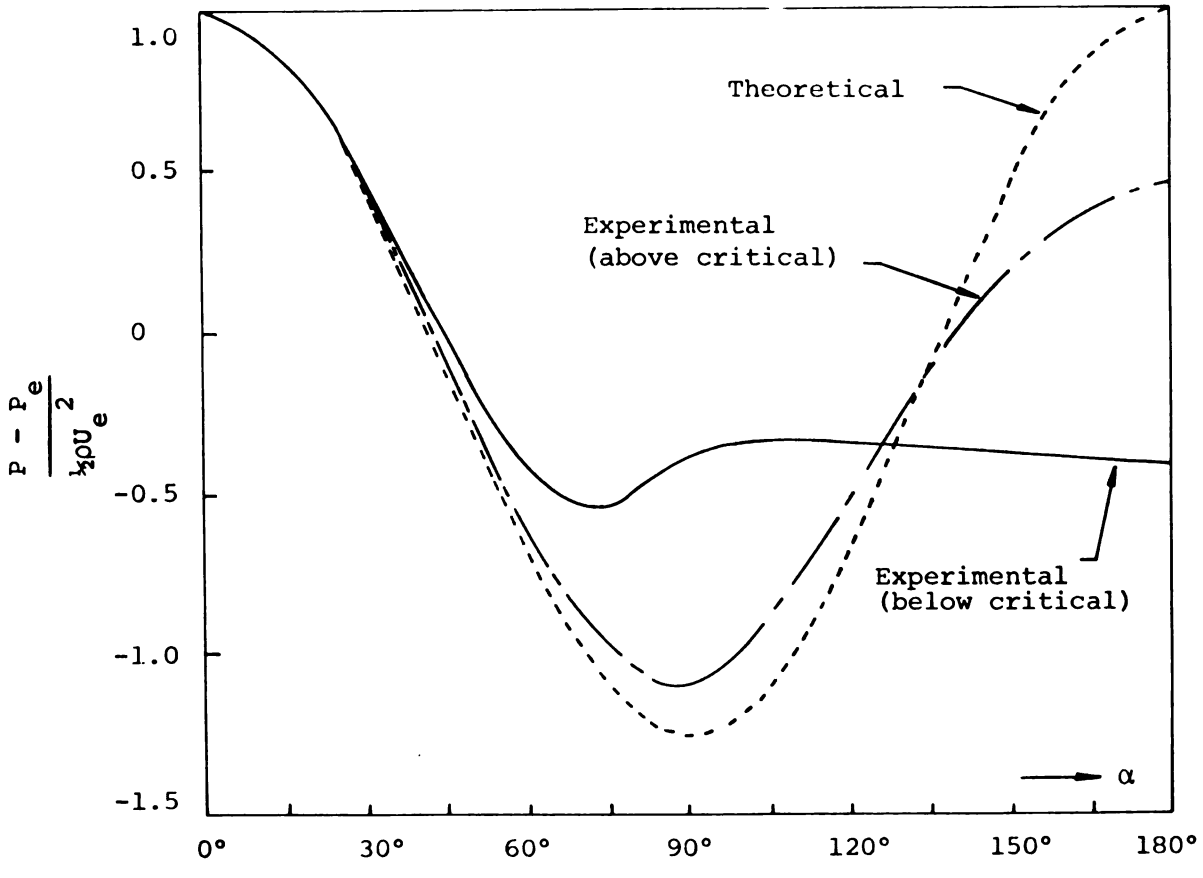

Figure 17. Pressure distribution for flow over a sphere.

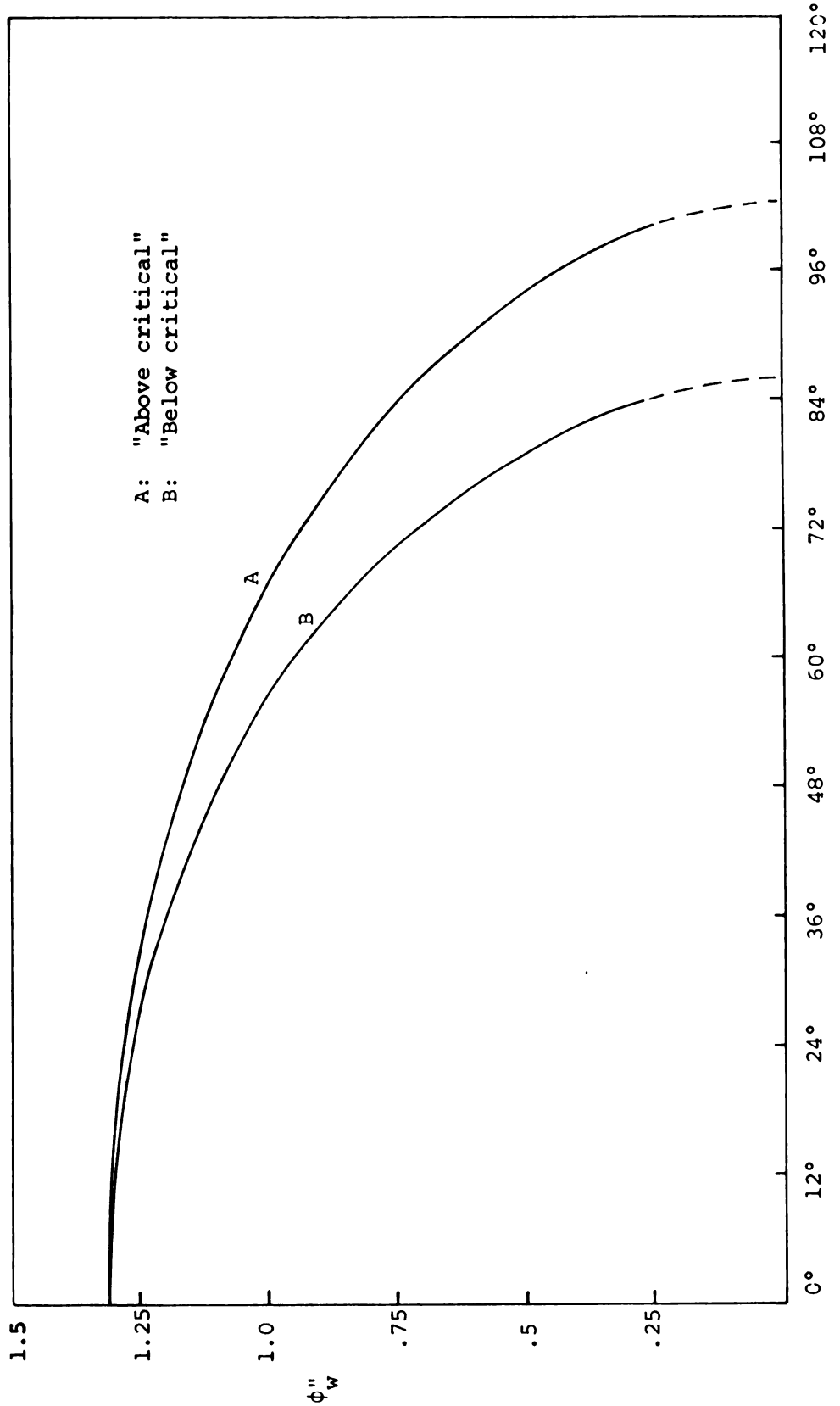

Figure 18. Velocity gradient at the wall for two cases of potential flow around the sphere.

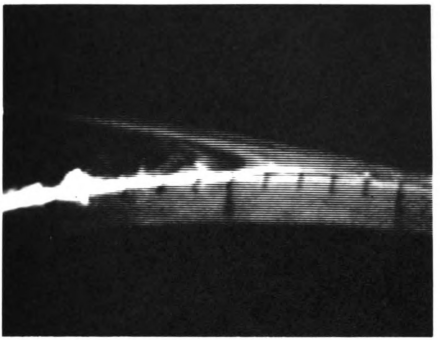

Figure 19. Photograph of hydrogen bubbles visualized on unheated sphere.

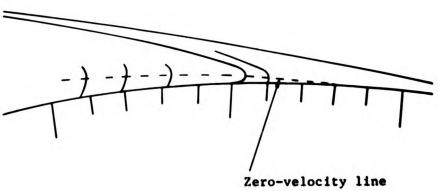

Figure 20. Graphical procedure for extrapolating separation point from hydrogen bubble pictures.

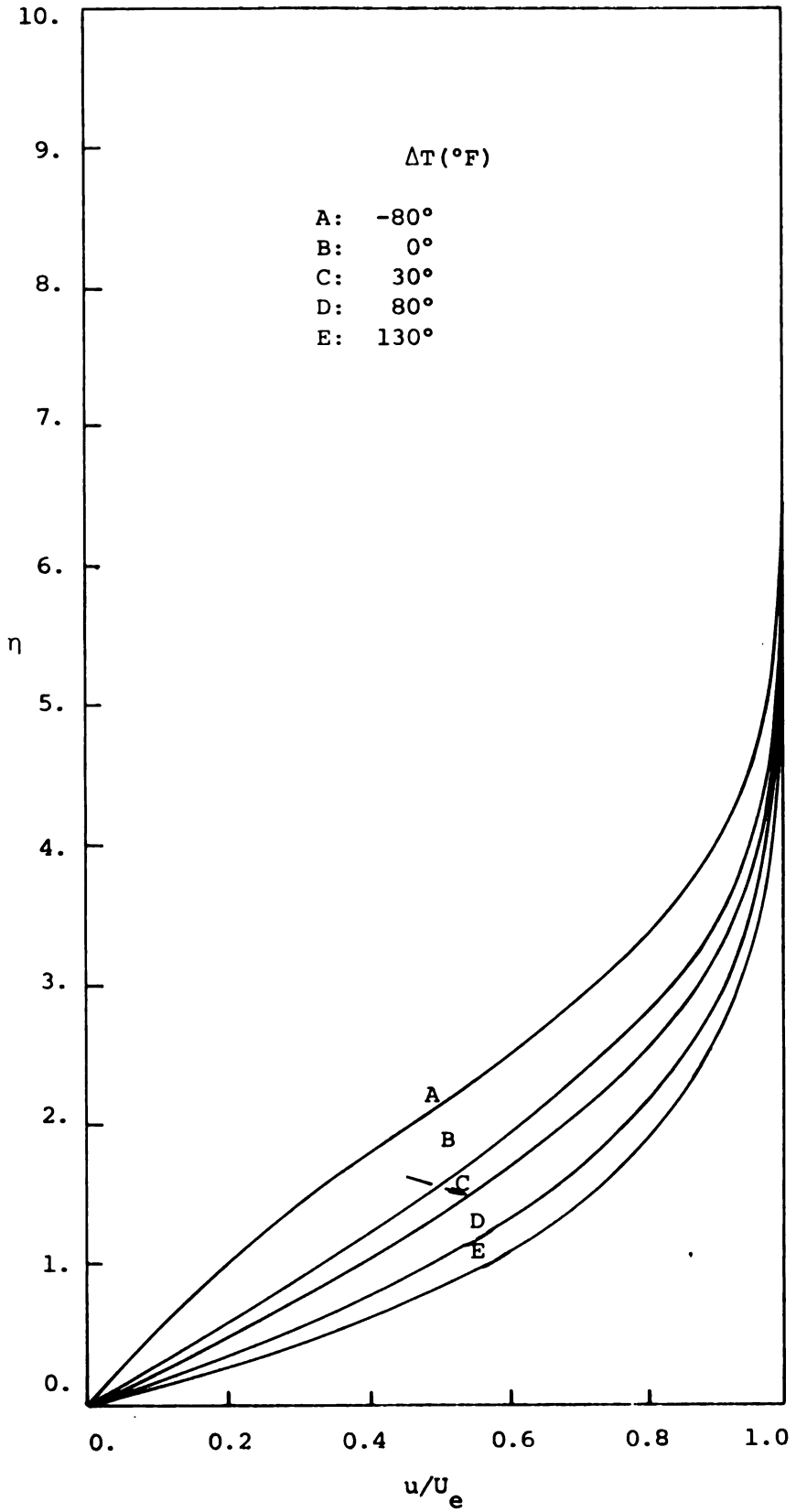

Figure 21. Velocity profiles for a heated flat plate. $U_e/U_\infty = 1 - \xi/8$; $\xi = 0$

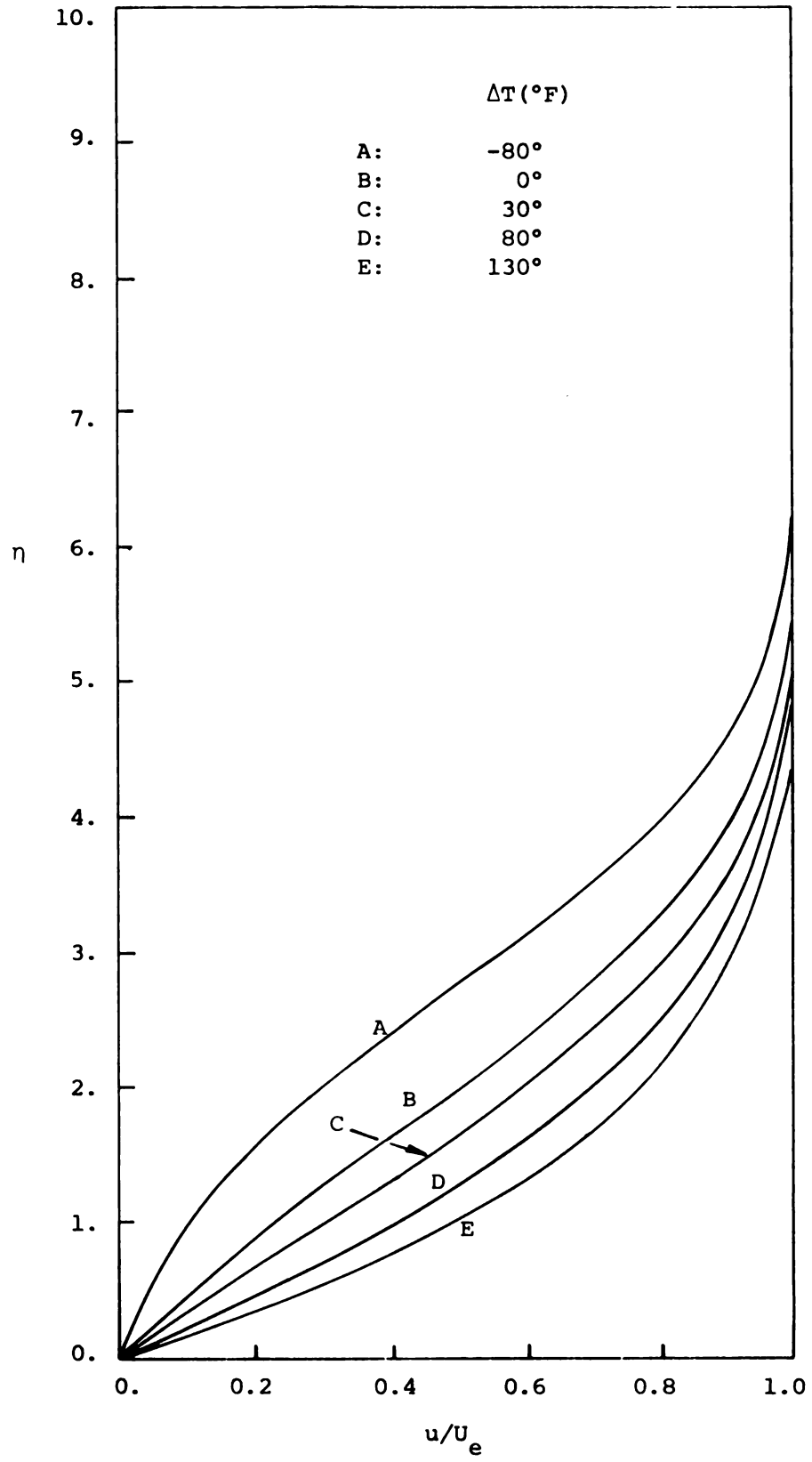

Figure 22. Velocity profiles for a heated flat plate. $U_e/U_\infty = 1 - \xi/8$; $\xi = .575$

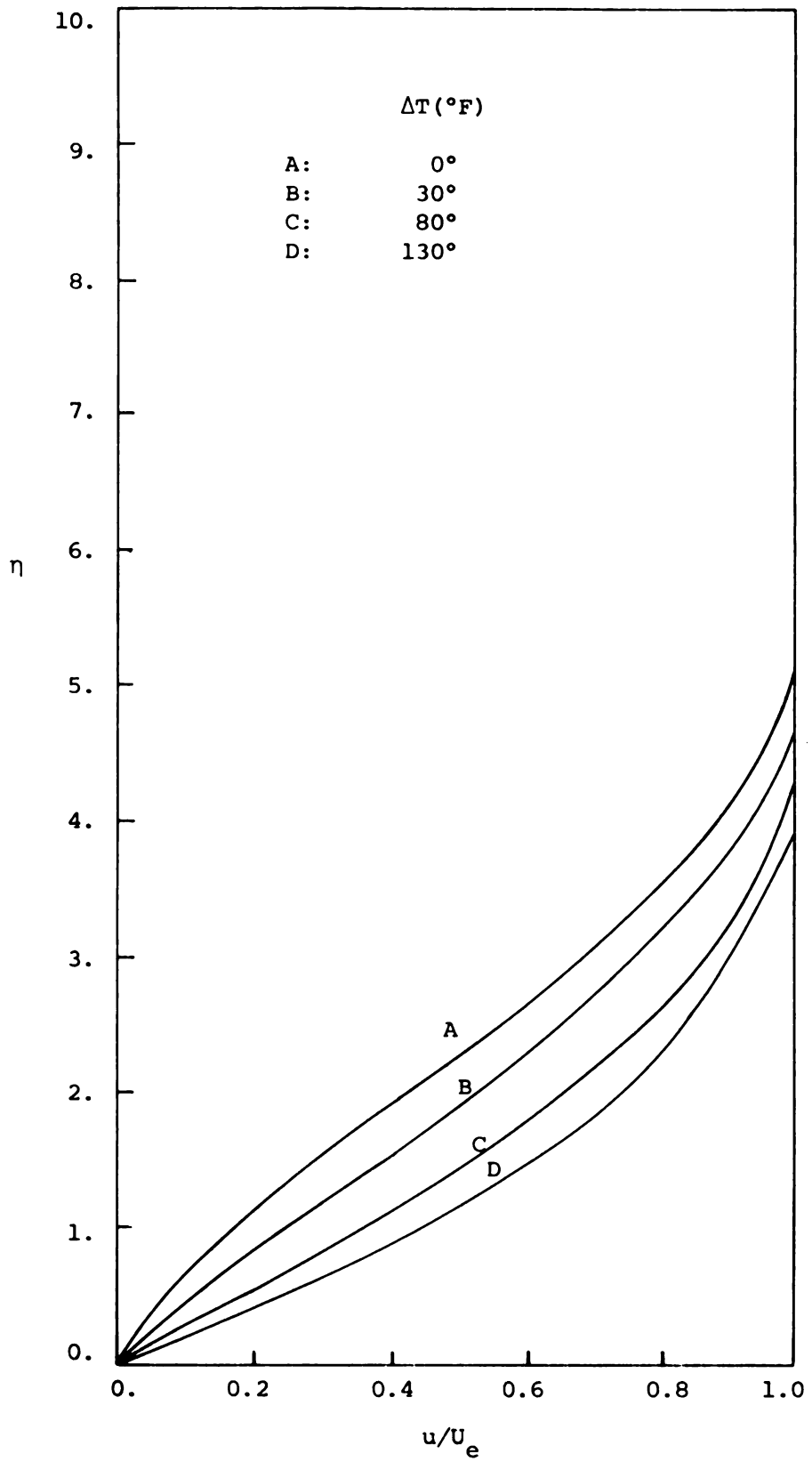

Figure 23. Velocity profiles for a heated flat plate. $U_e/U_\infty = 1 - \xi/8$; $\xi = .7863$

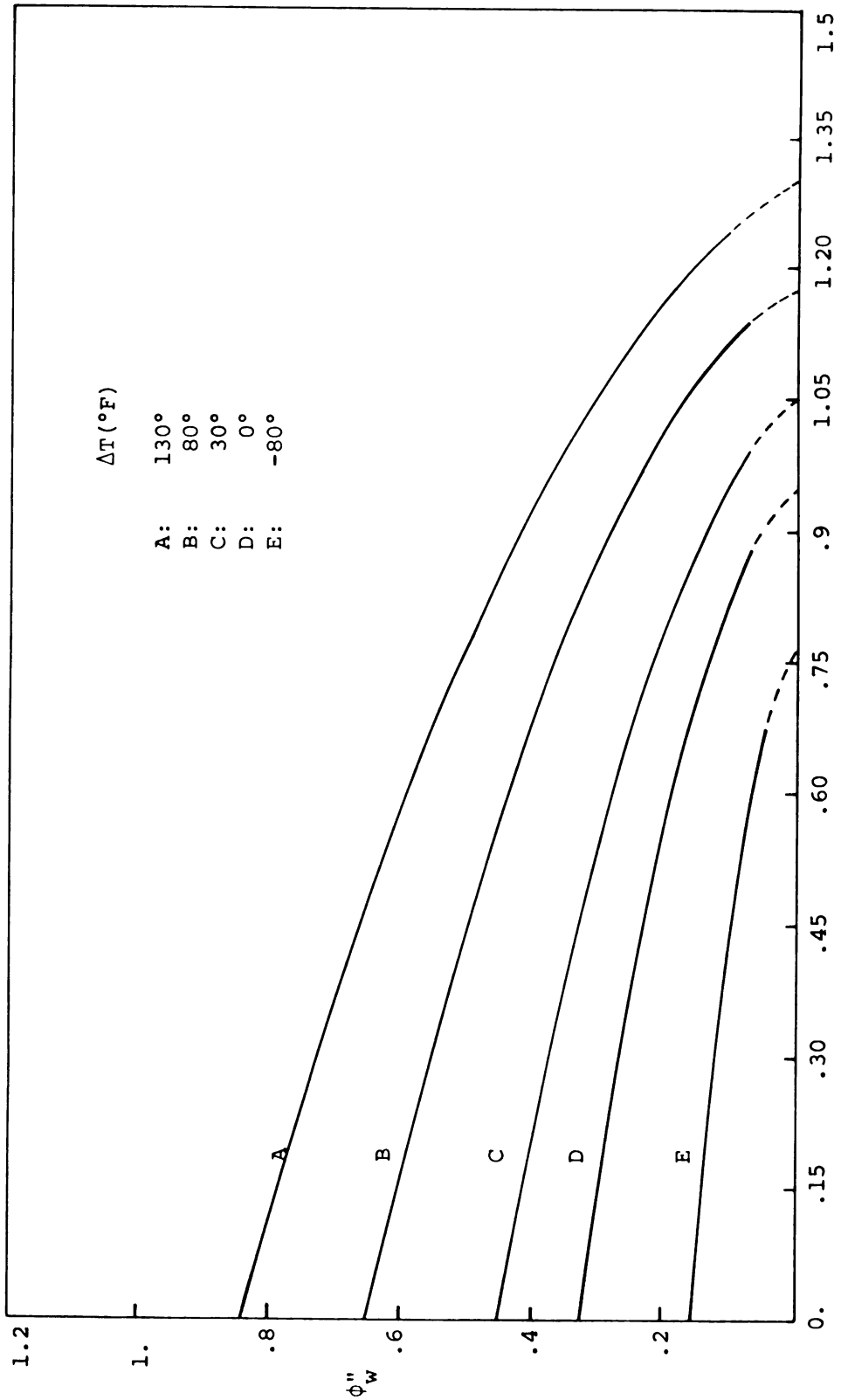

Figure 24. The effect of heating and cooling a flat plate on the velocity gradient at the wall. $U_e/U_\infty = 1 - \xi/8$

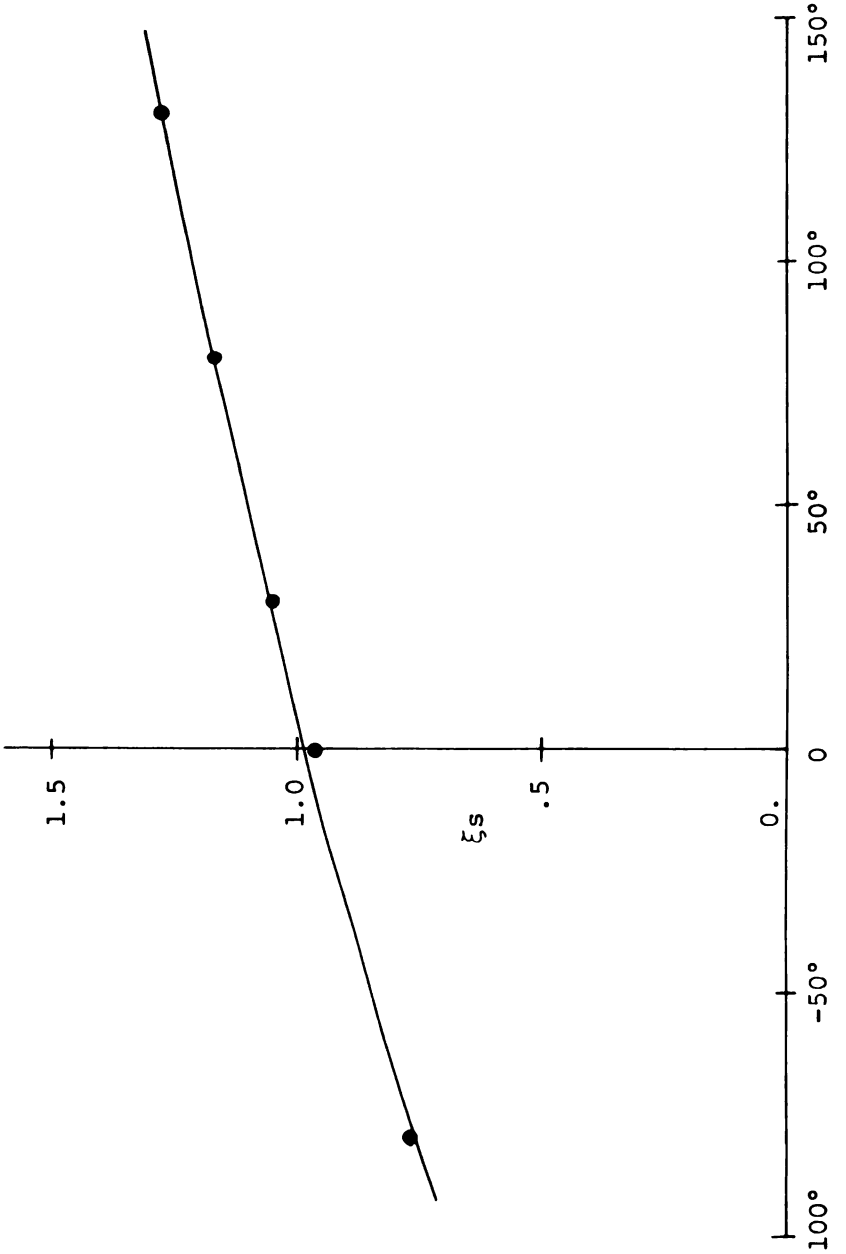

Figure 25. The effect of heat transfer on separation point. $U_e/U_\infty = 1 - \xi/8$

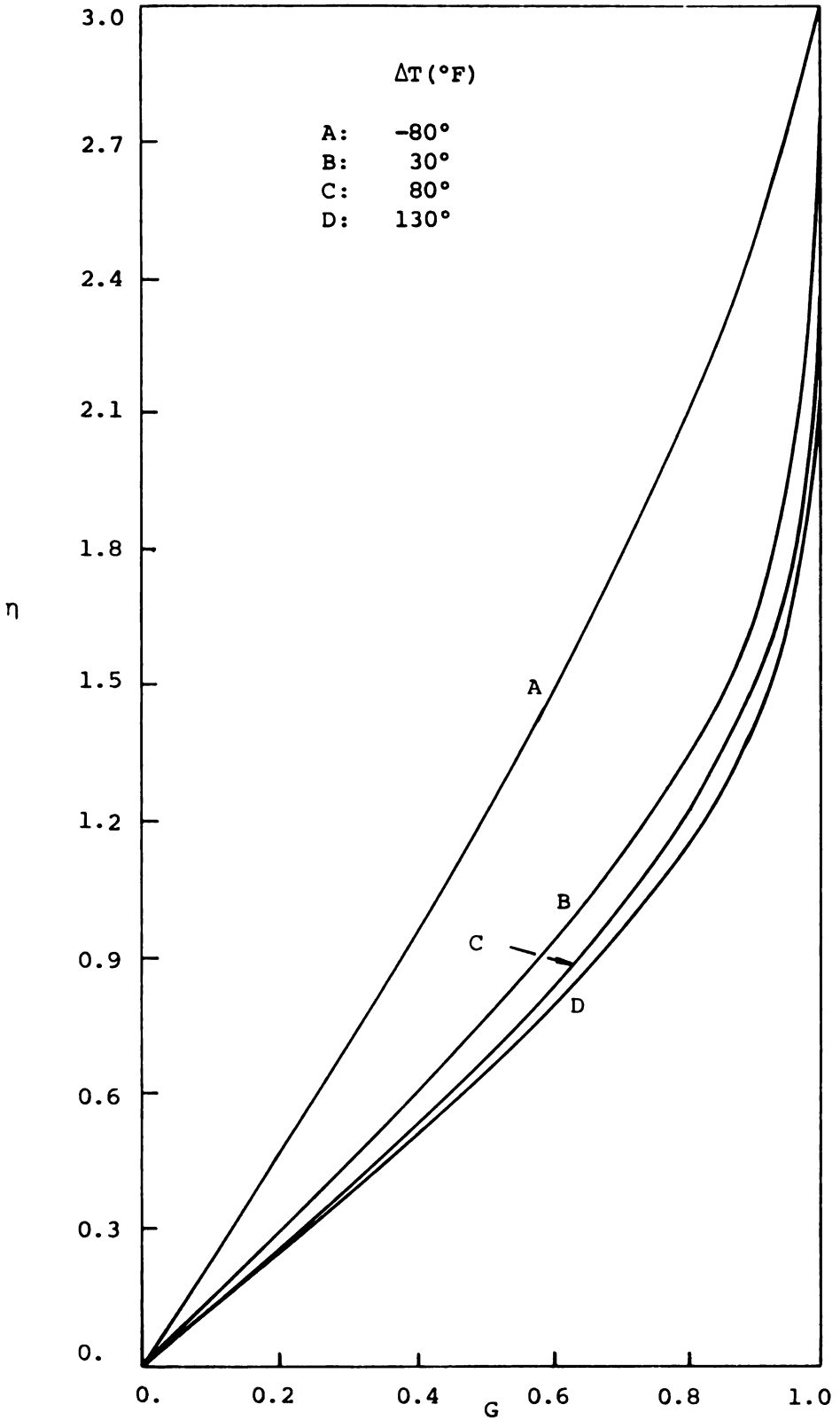

Figure 26. Temperature profiles for a heated flat plate. $U_e/U_\infty = 1 - \xi/8$, $\xi = 0$

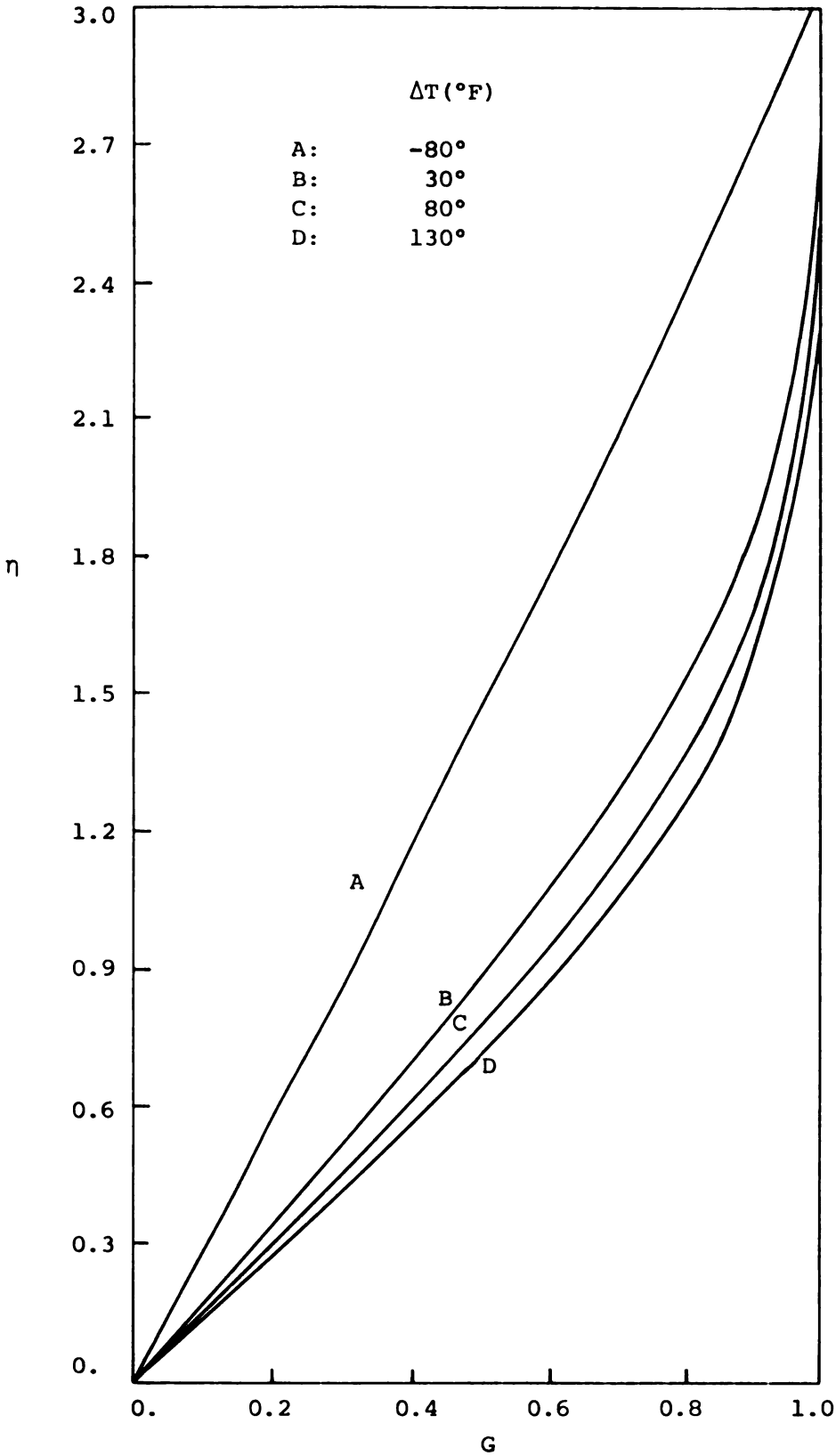

Figure 27. Temperature profiles for a heated flat plate. $U_e/U_\infty = 1 - \xi/8$, $\xi = .575$

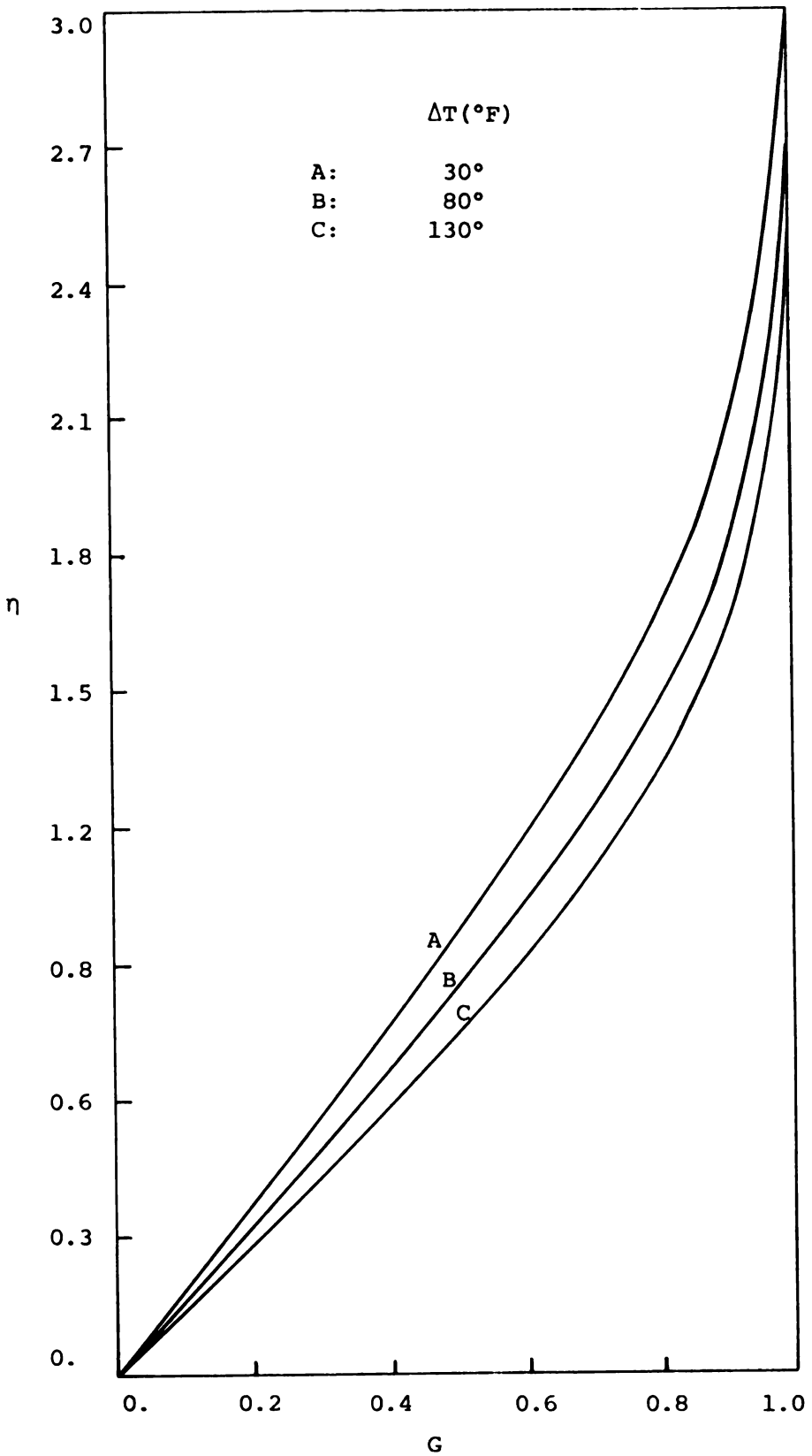

Figure 28. Temperature profiles for a heated flat plate. $U_e/U_\infty = 1 - \xi/8$, $\xi = .786$

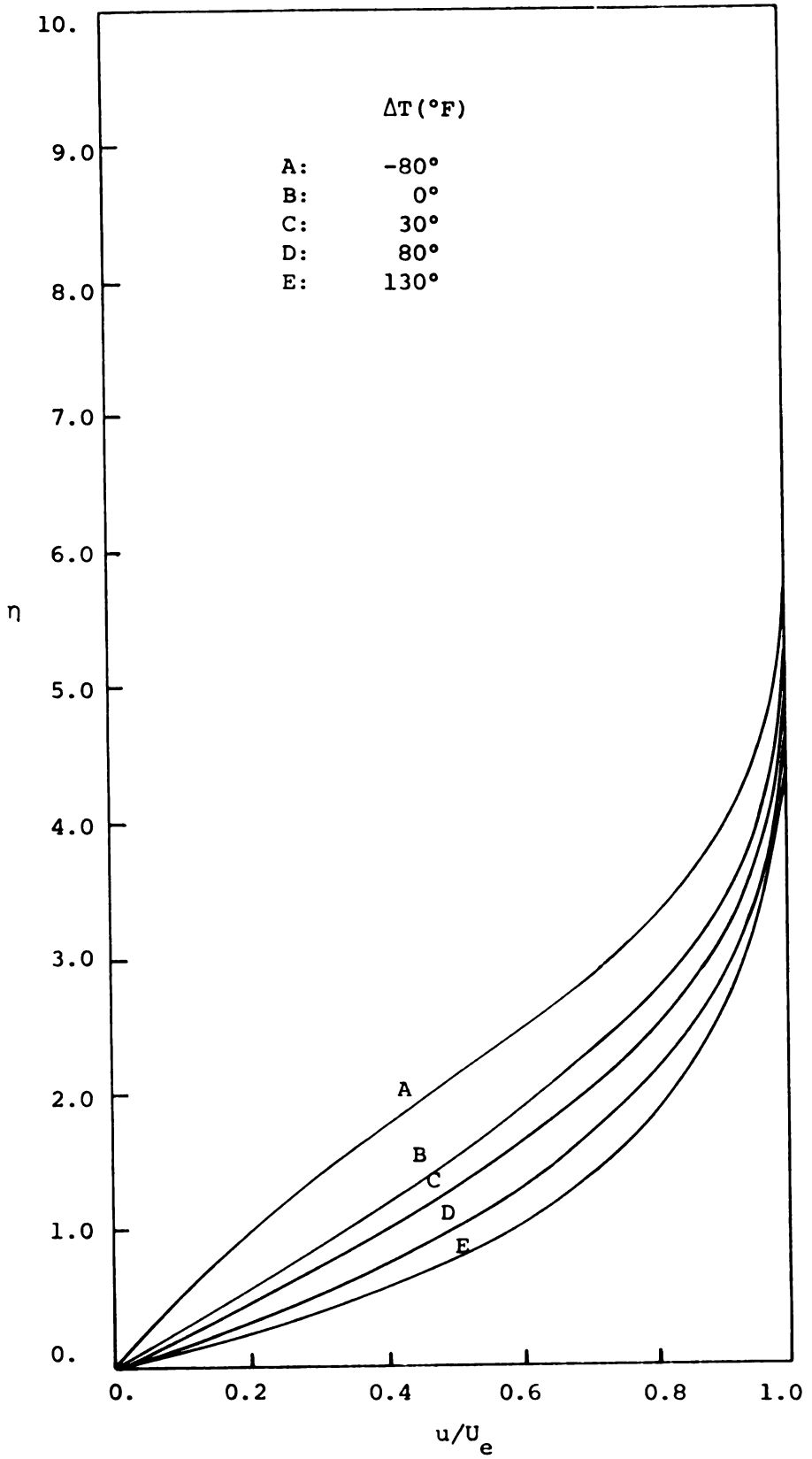

Figure 29. Velocity profiles for a heated flat plate. $U_e/U_\infty = 1 - \xi$, $\xi = 0$

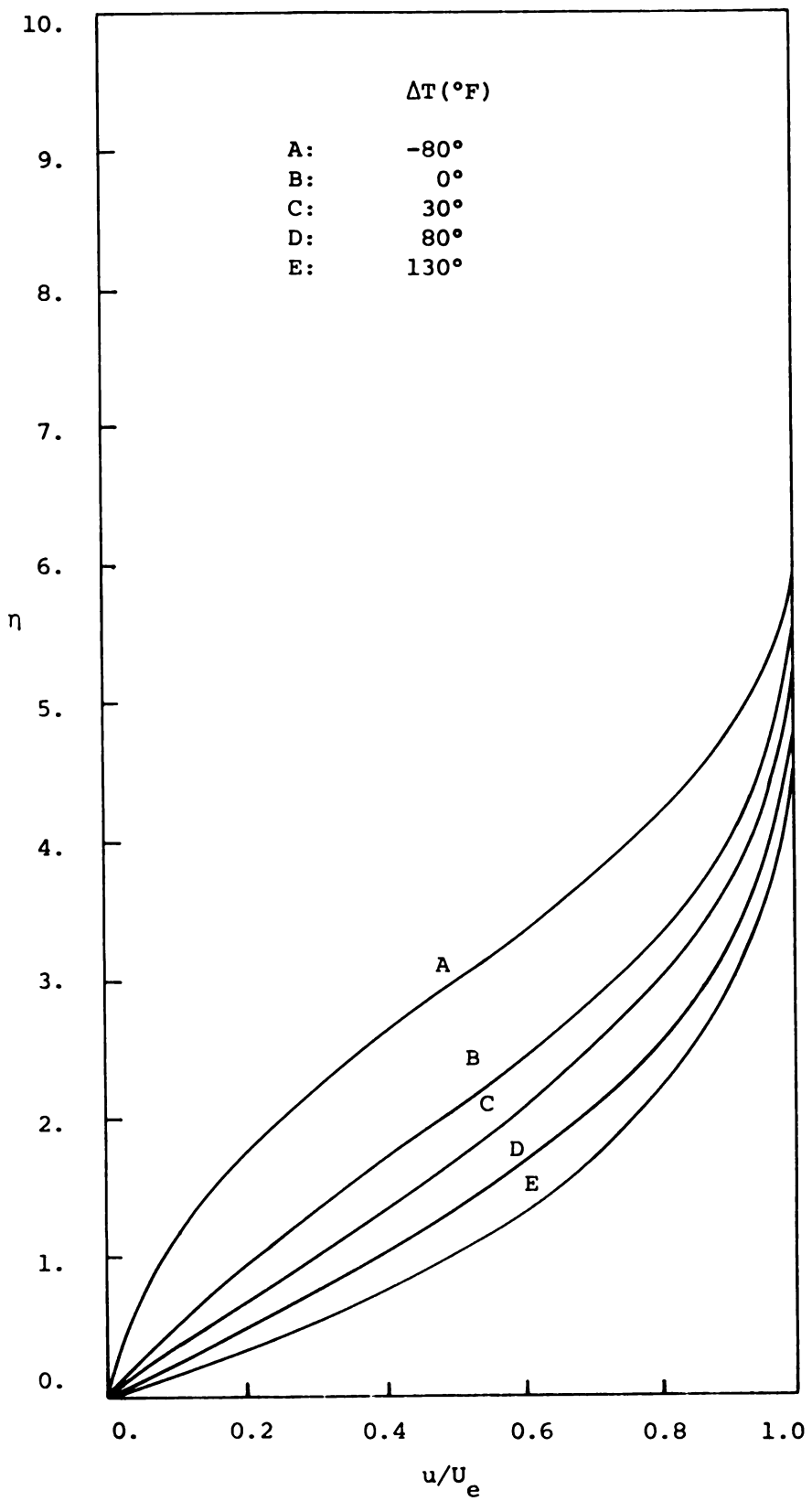

Figure 30. Velocity profiles for a heated flat plate. $U_e/U_\infty = 1 - \xi$, $\xi = .083$

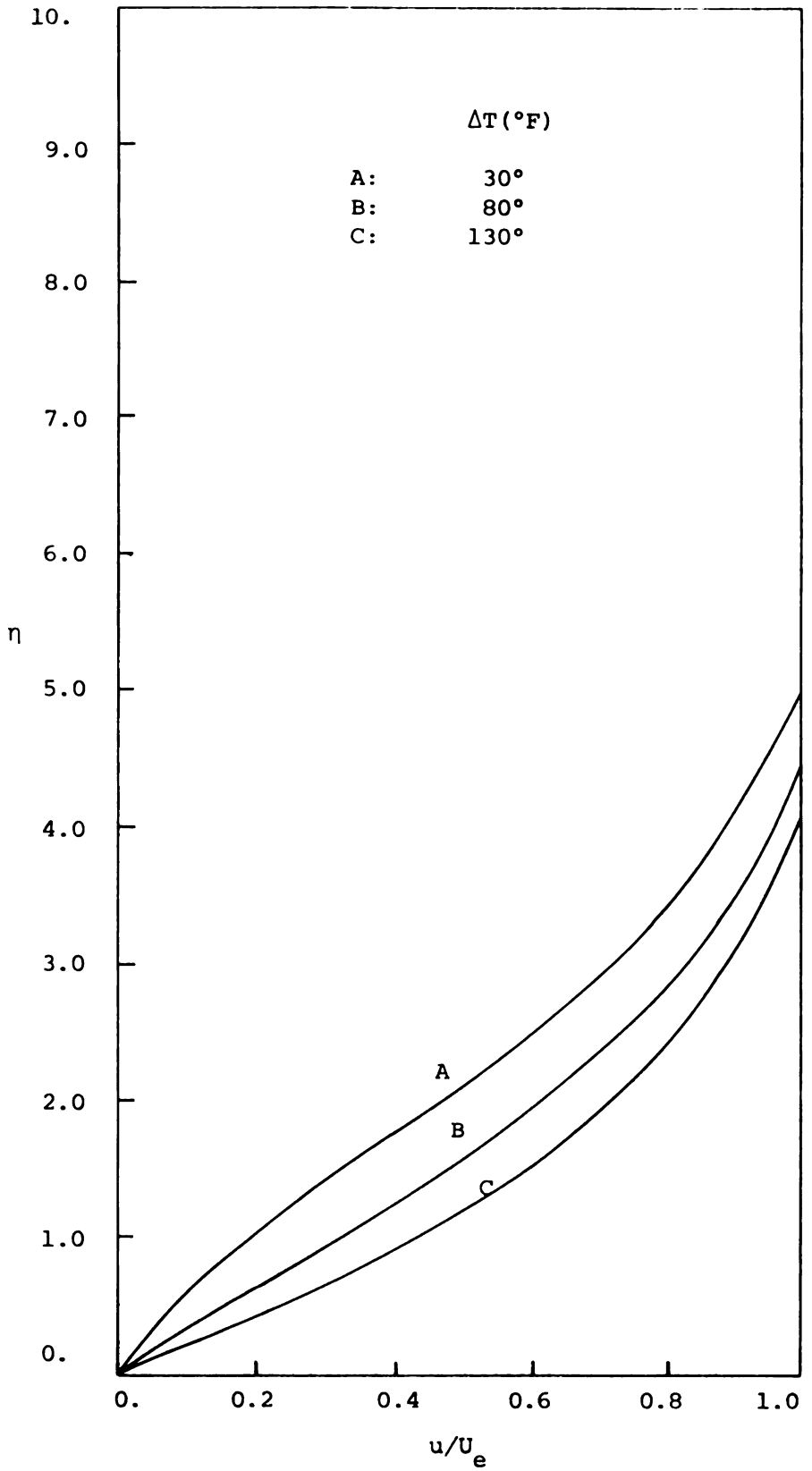

Figure 31. Velocity profiles for a heated flat plate.
$U_e/U_\infty = 1 - \xi$, $\xi = .118$

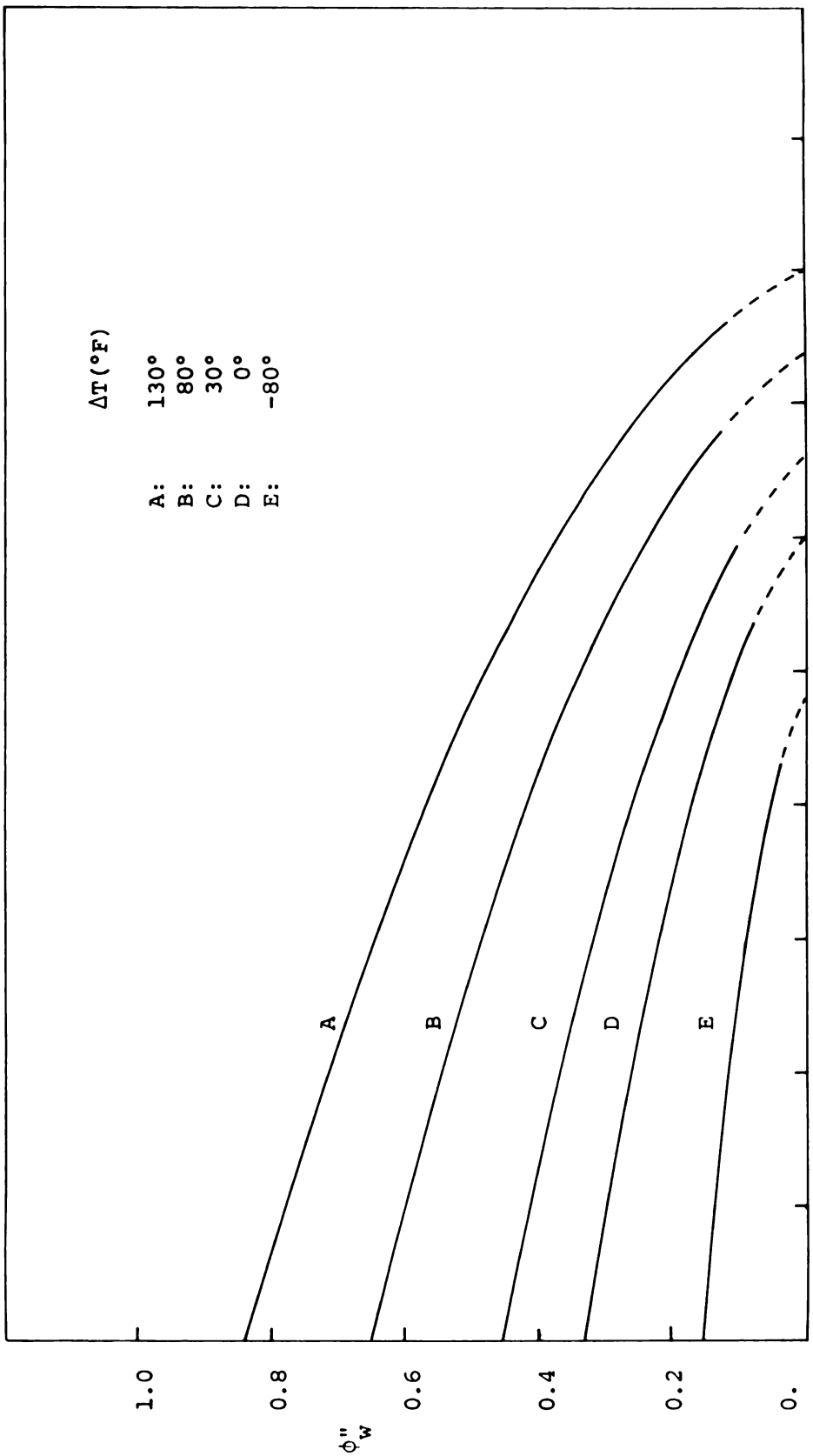

Figure 32. The effect of heating and cooling a flat plate on the velocity gradient at the wall.
$U_e/U_\infty = 1 - \xi$

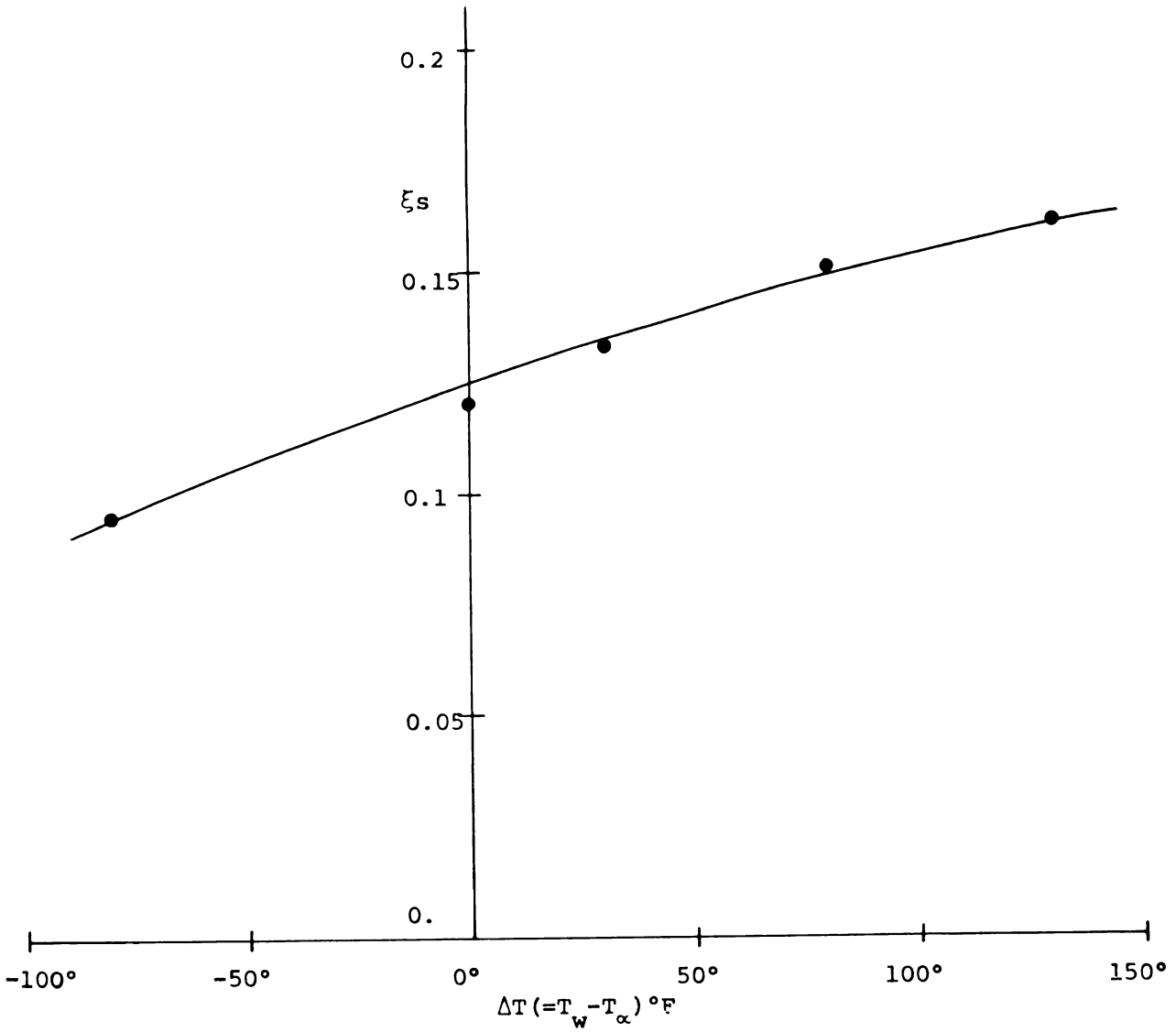

Figure 33. The effect of heat transfer on separation point.
$U_e/U_\infty = 1 - \xi$

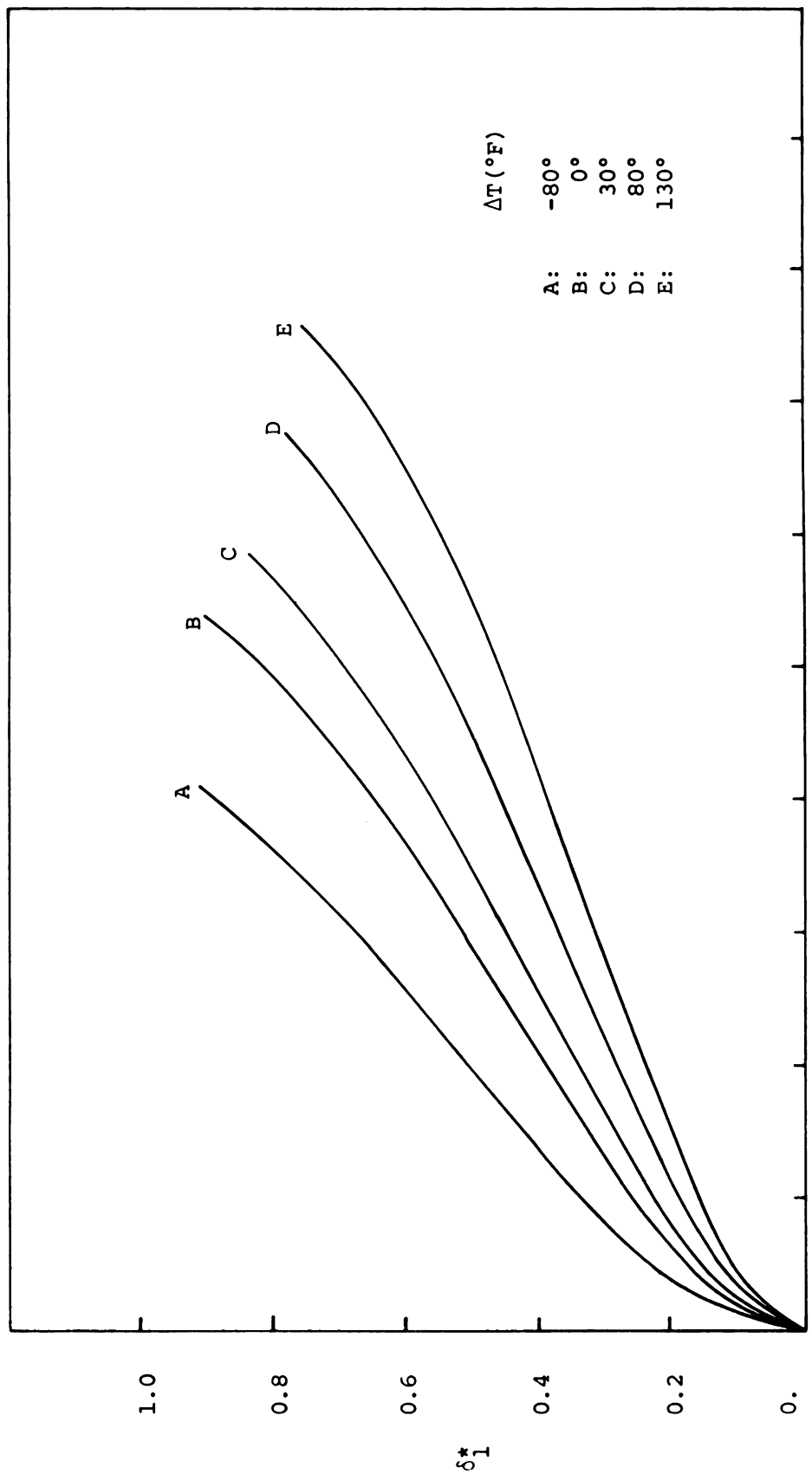

Figure 34. Displacement thickness over heated flat plate. $U_e/U_\infty = 1 - \xi$

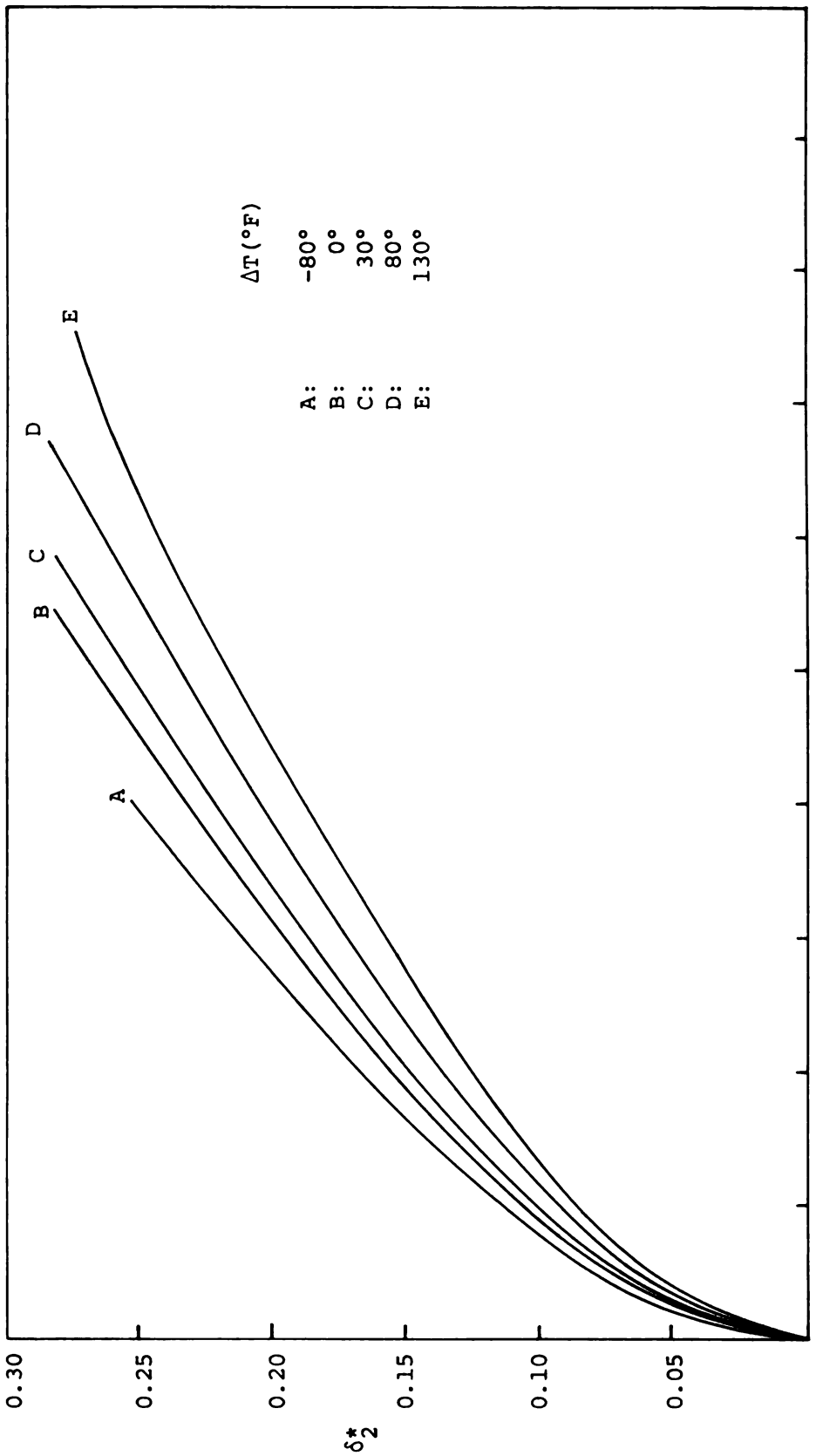

Figure 35. Momentum thickness over a heated flat plate. $U_e/U_\infty = 1 - \xi$

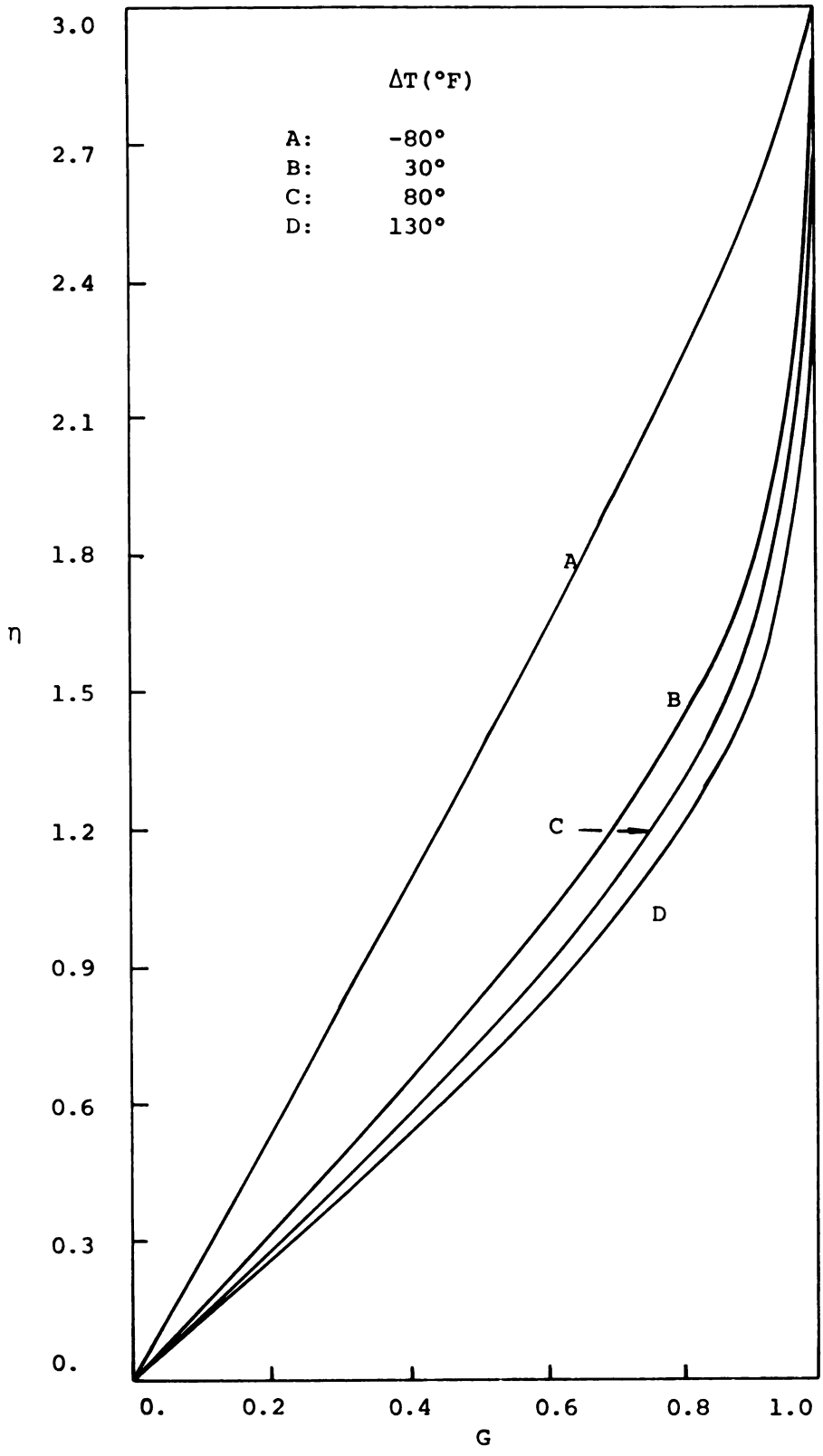

Figure 36. Temperature profiles for a heated flat plate. $U_e/U_\infty = 1 - \xi$, $\xi = .047$

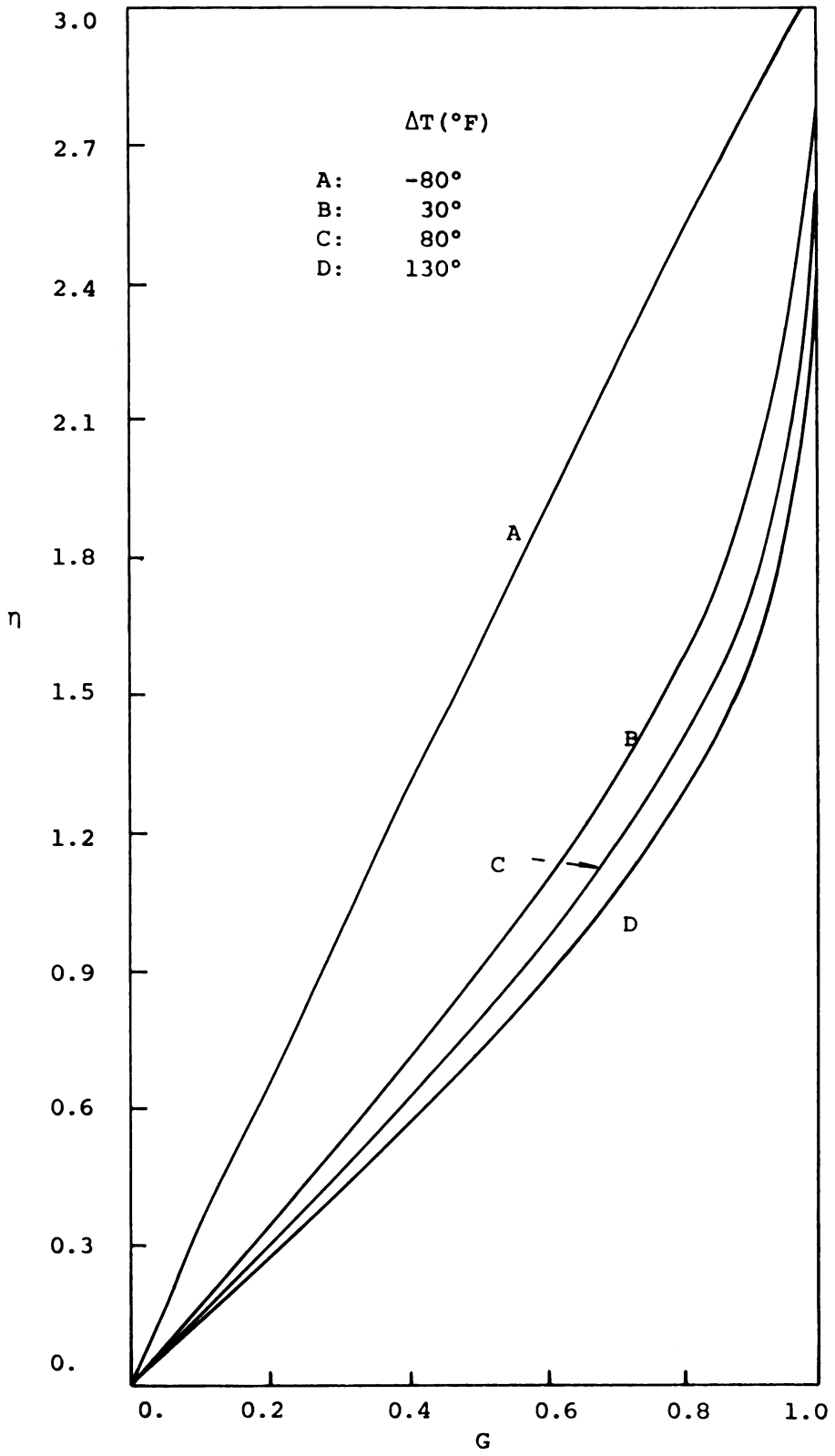

Figure 37. Temperature profiles for a heated flat plate. $U_e/U_\infty = 1 - \xi$, $\xi = .083$

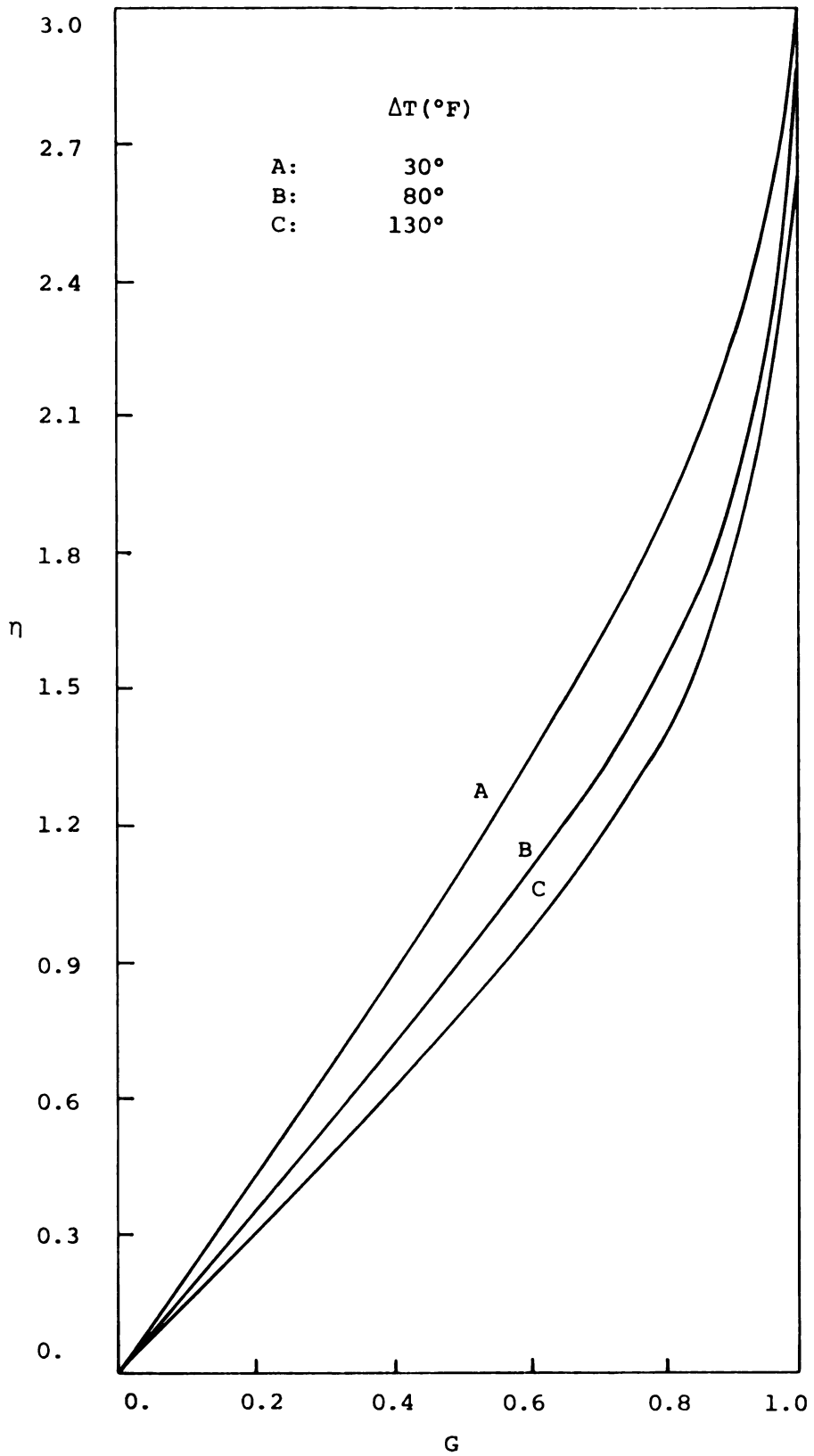

Figure 38. Temperature profiles for a heated flat plate. $U_e/U_\infty = 1 - \xi$, $\xi = .118$

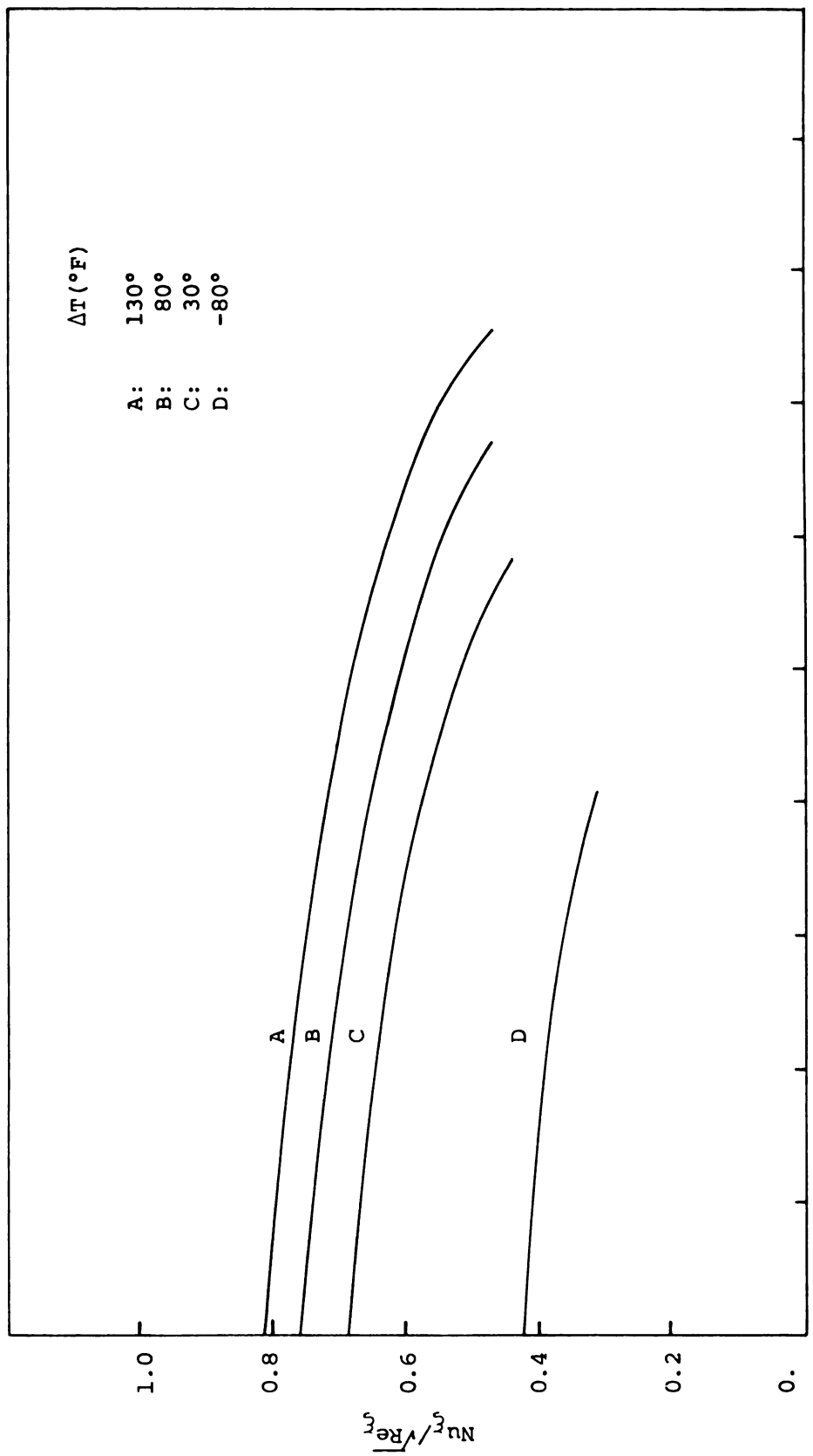

Figure 39. The effect of heating and cooling a flat plate on the local Nusselt Number. $U_e/U_\infty = 1 - \xi$

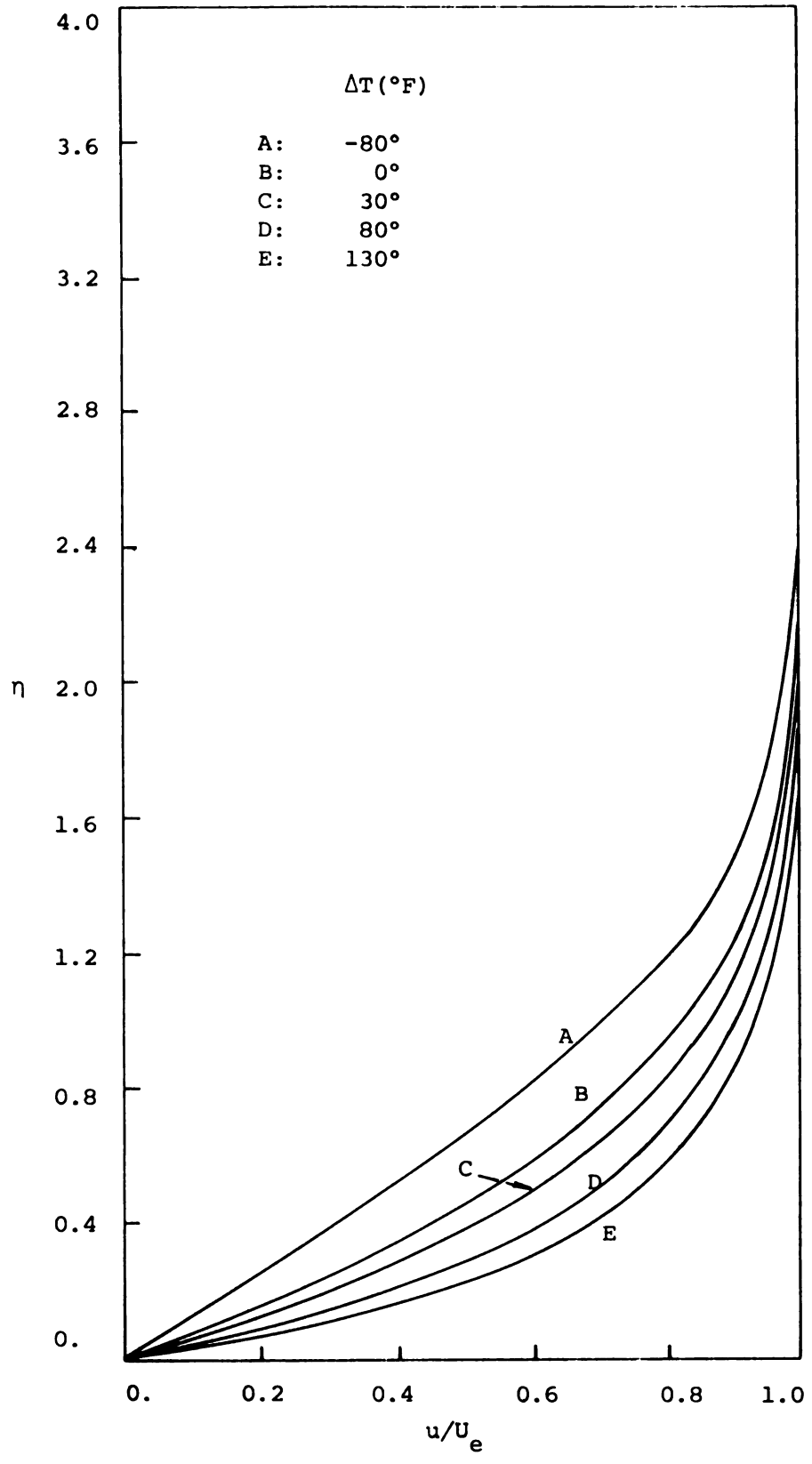

Figure 40. Velocity profiles for a heated sphere. "Above critical" flow, $\alpha = 0°$.

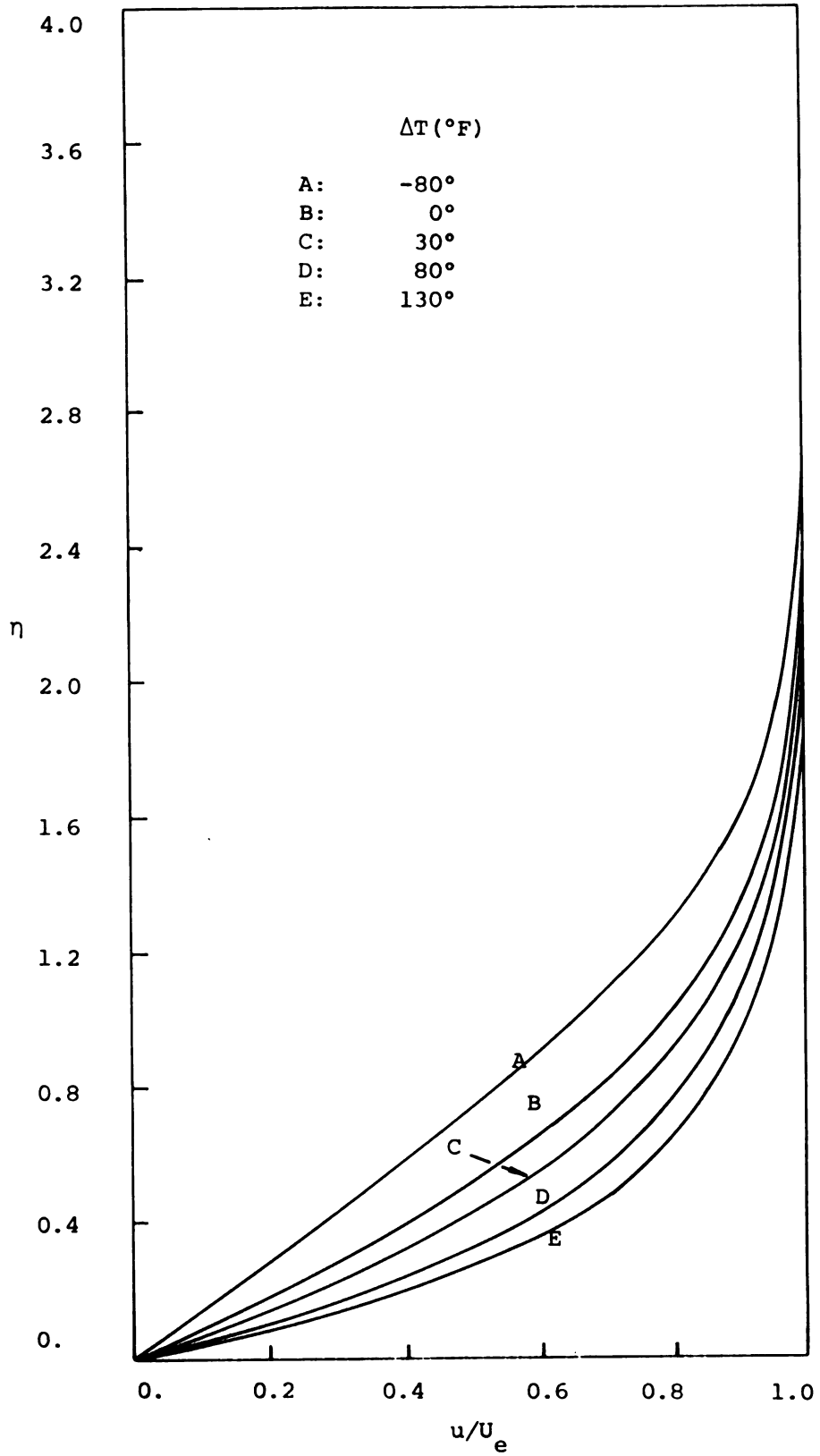

Figure 41. Velocity profiles for a heated sphere. "Above critical" flow, $\alpha = 47.5°$.

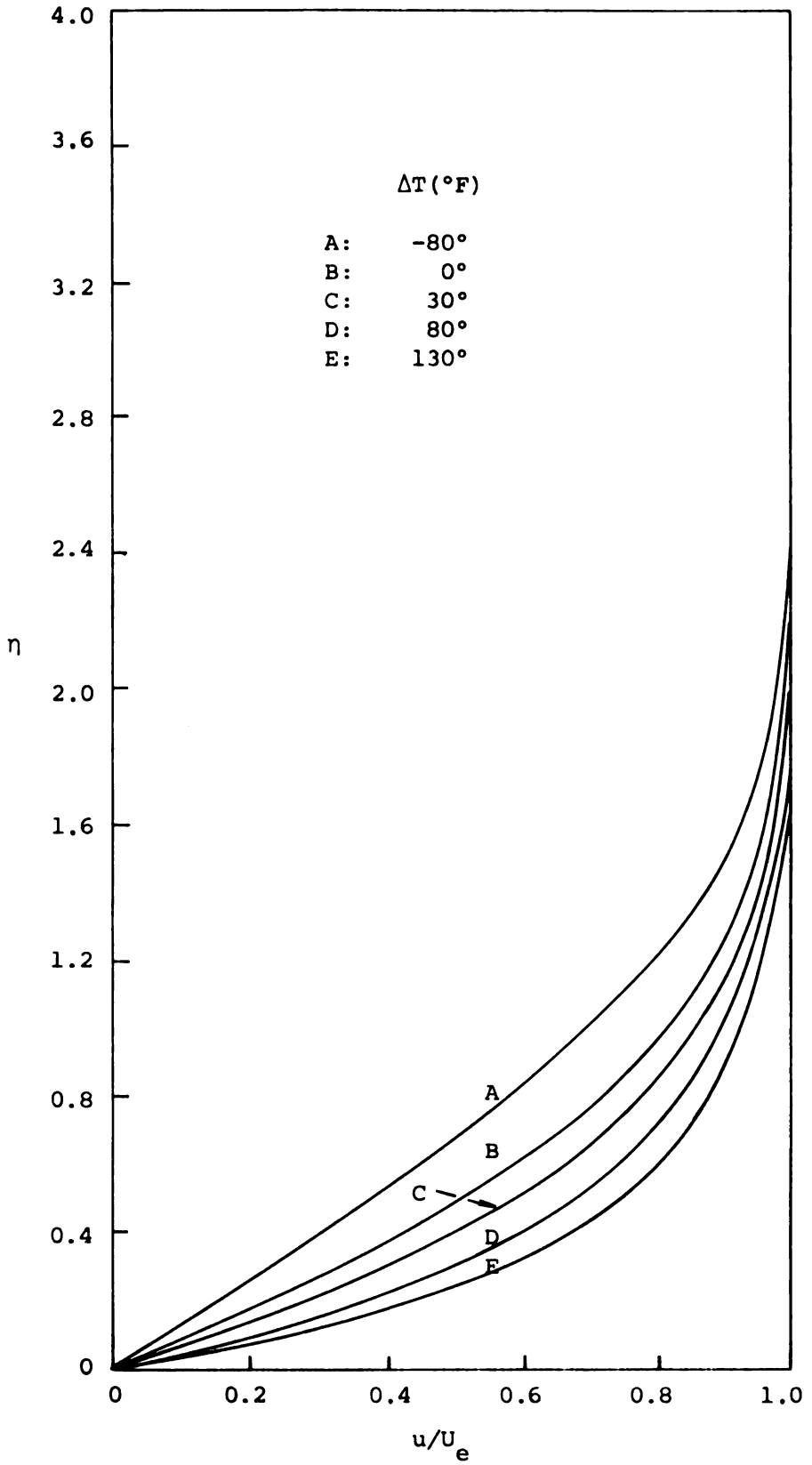

Figure 42. Velocity profile for a heated sphere. "Above critical" flow, $\alpha = 67.8°$.

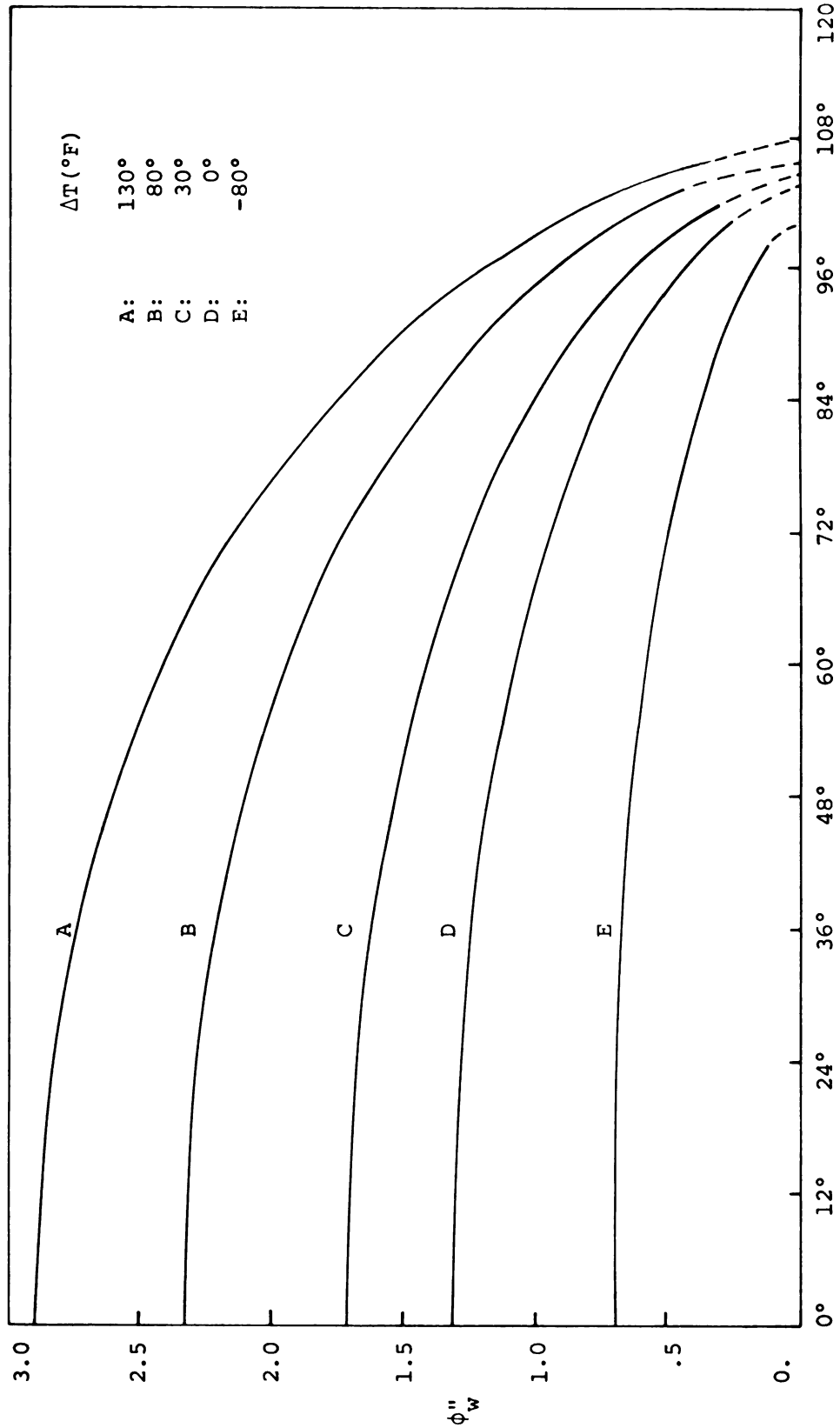

Figure 43. The effect of heating and cooling a sphere on the velocity gradient at the wall. "Above critical" flow.

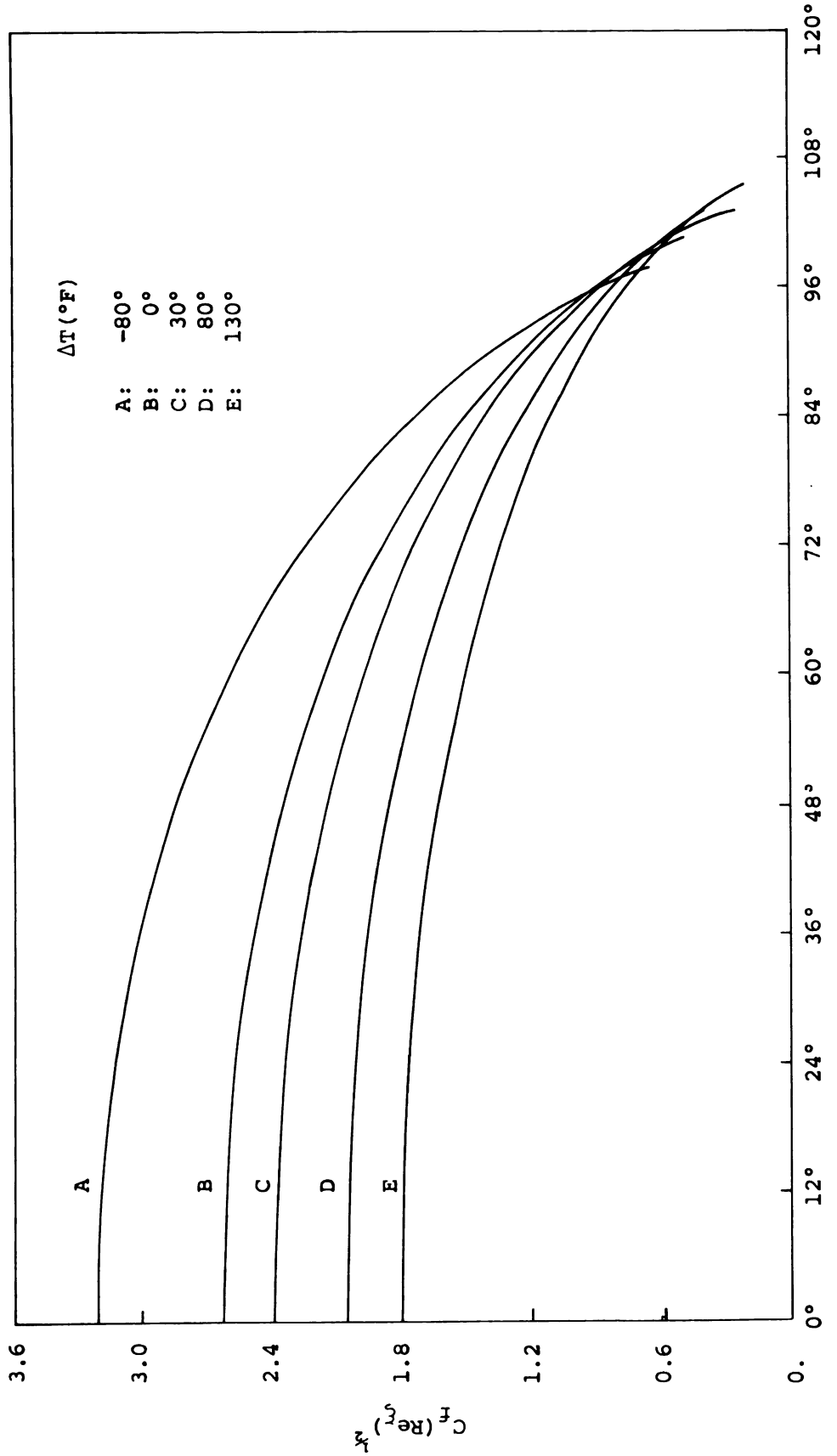

Figure 44. The effect of heating and cooling a sphere on the local skin friction parameter. "Above Critical" flow.

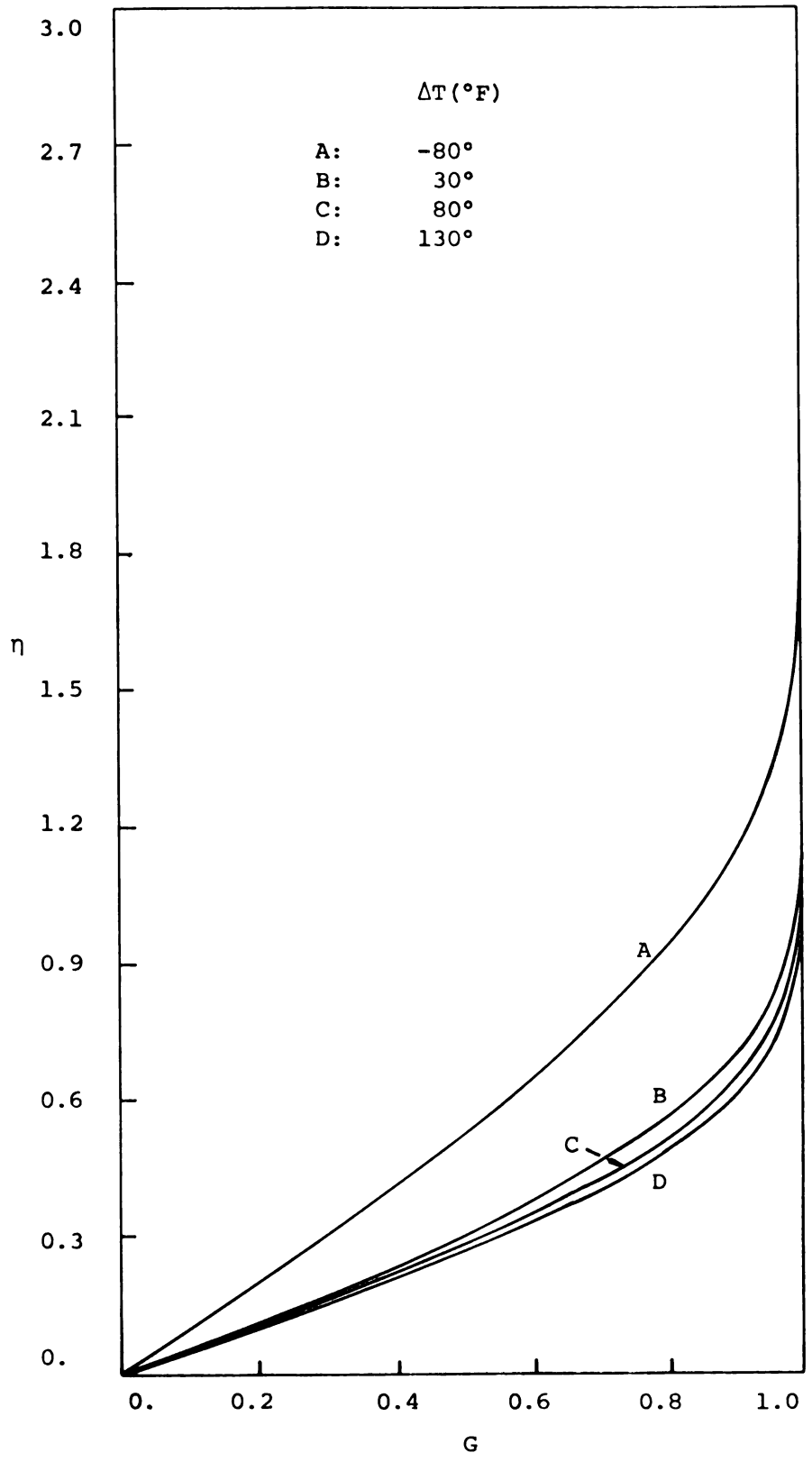

Figure 45. Temperature profiles for a heated sphere. "Above critical" flow, $\alpha = 0°$.

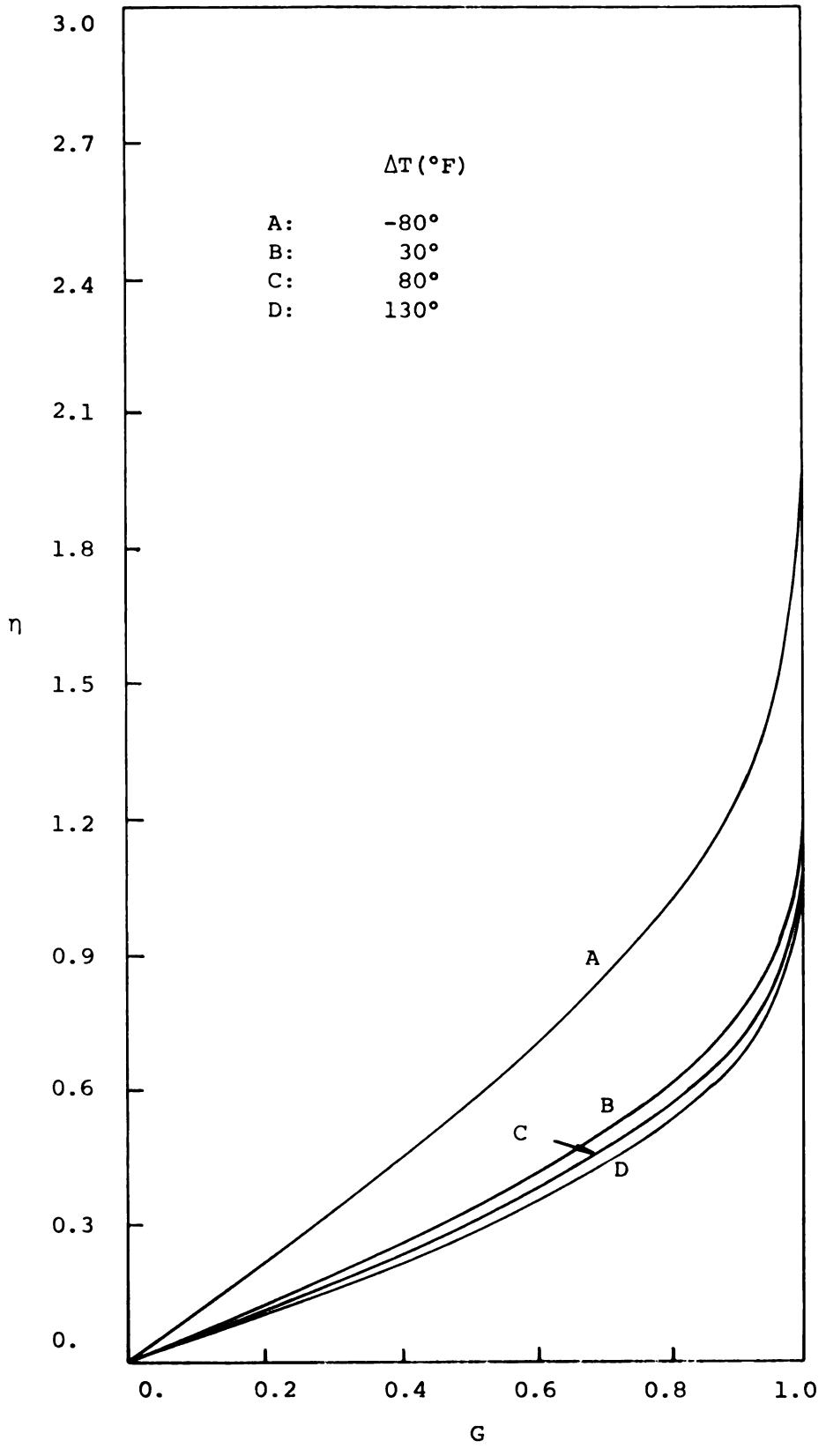

Figure 46. Temperature profiles for a heated sphere. "Above critical" flow, $\alpha = 47.5°$.

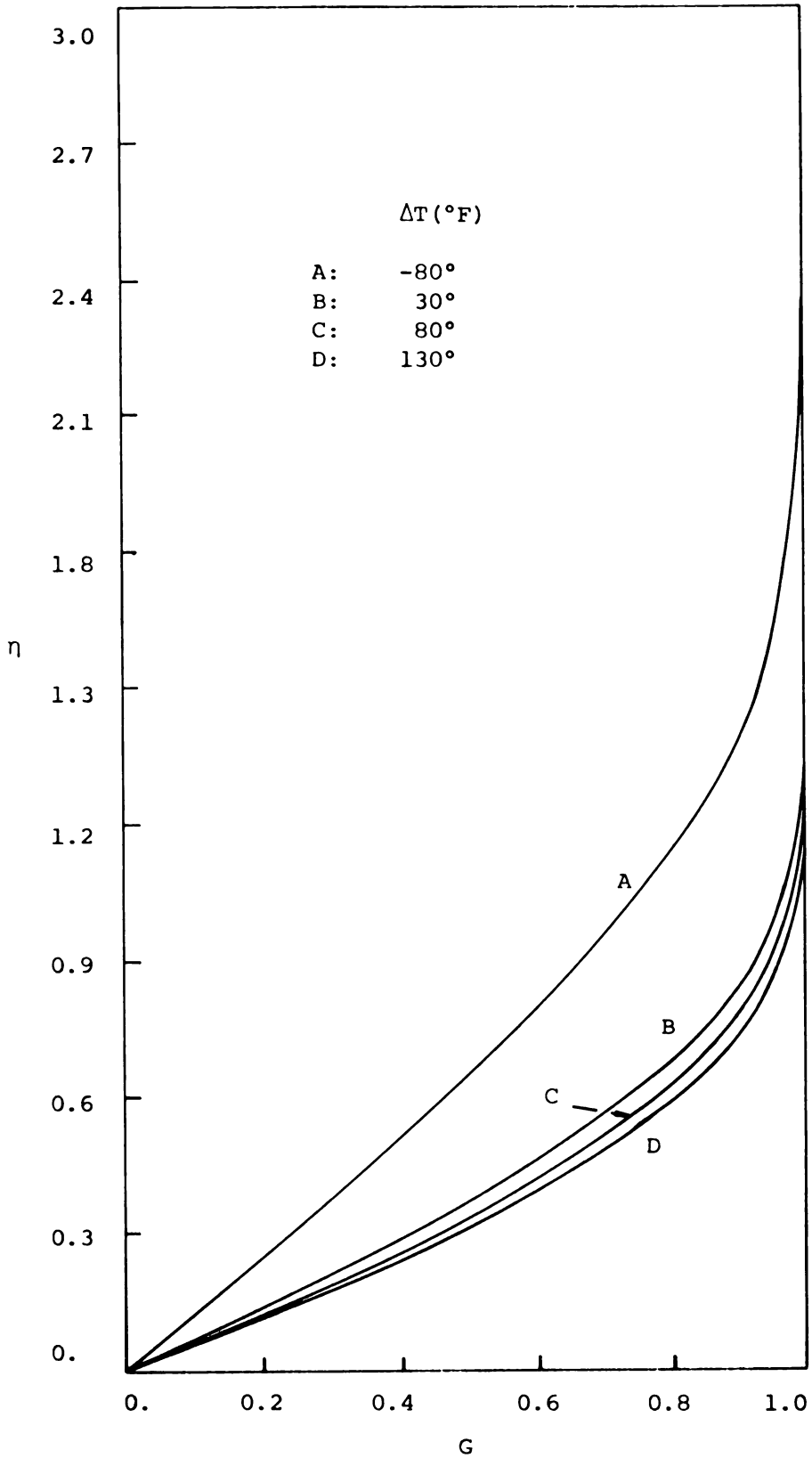

Figure 47. Temperature profiles for a heated sphere. "Above critical" flow, $\alpha = 67.8°$.

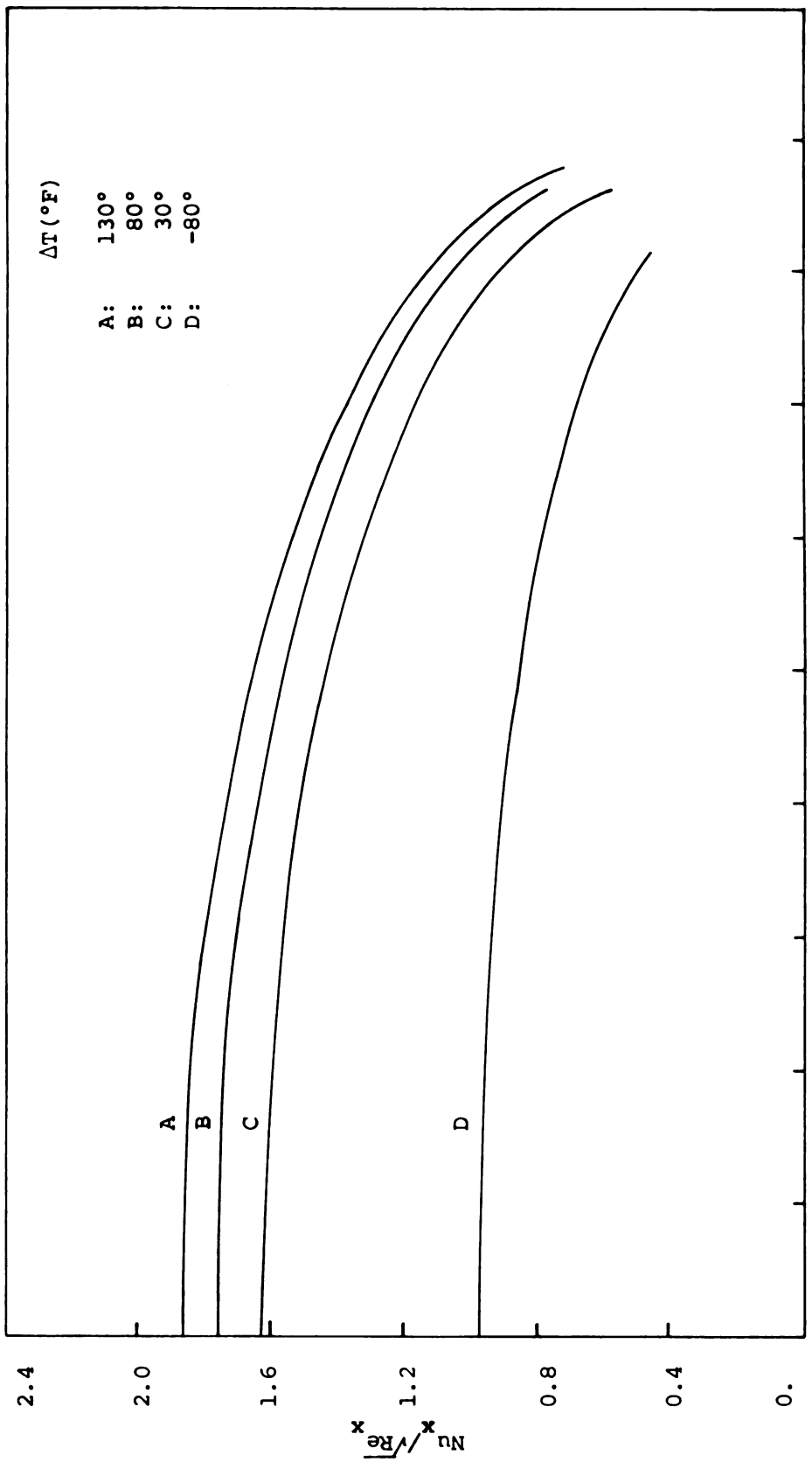

Figure 48. The effect of heating and cooling a sphere on the local heat transfer parameters. "Above critical" flow.

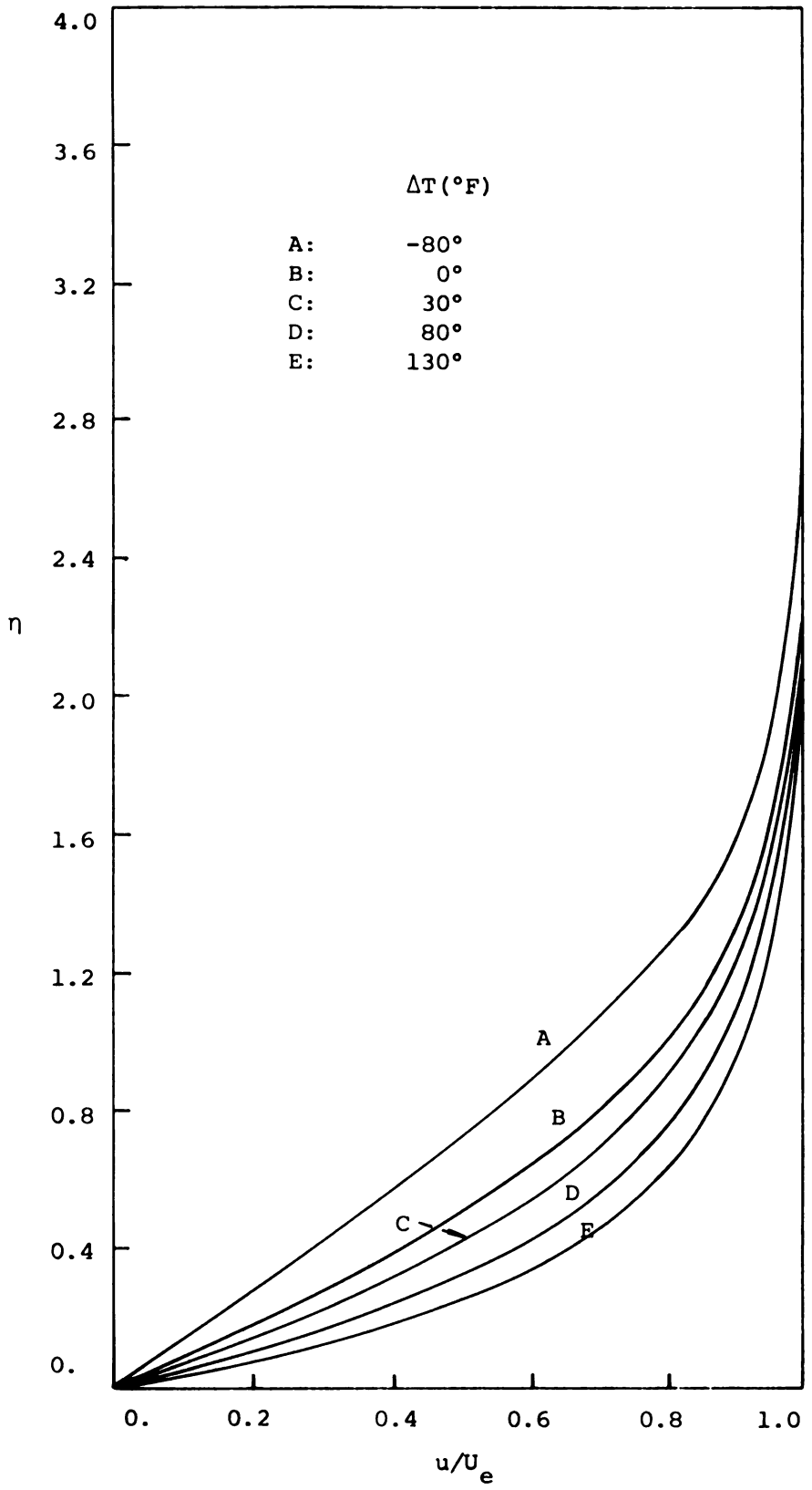

Figure 49. Velocity profiles for a heated sphere. "Below critical" flow, $\alpha = 40°$.

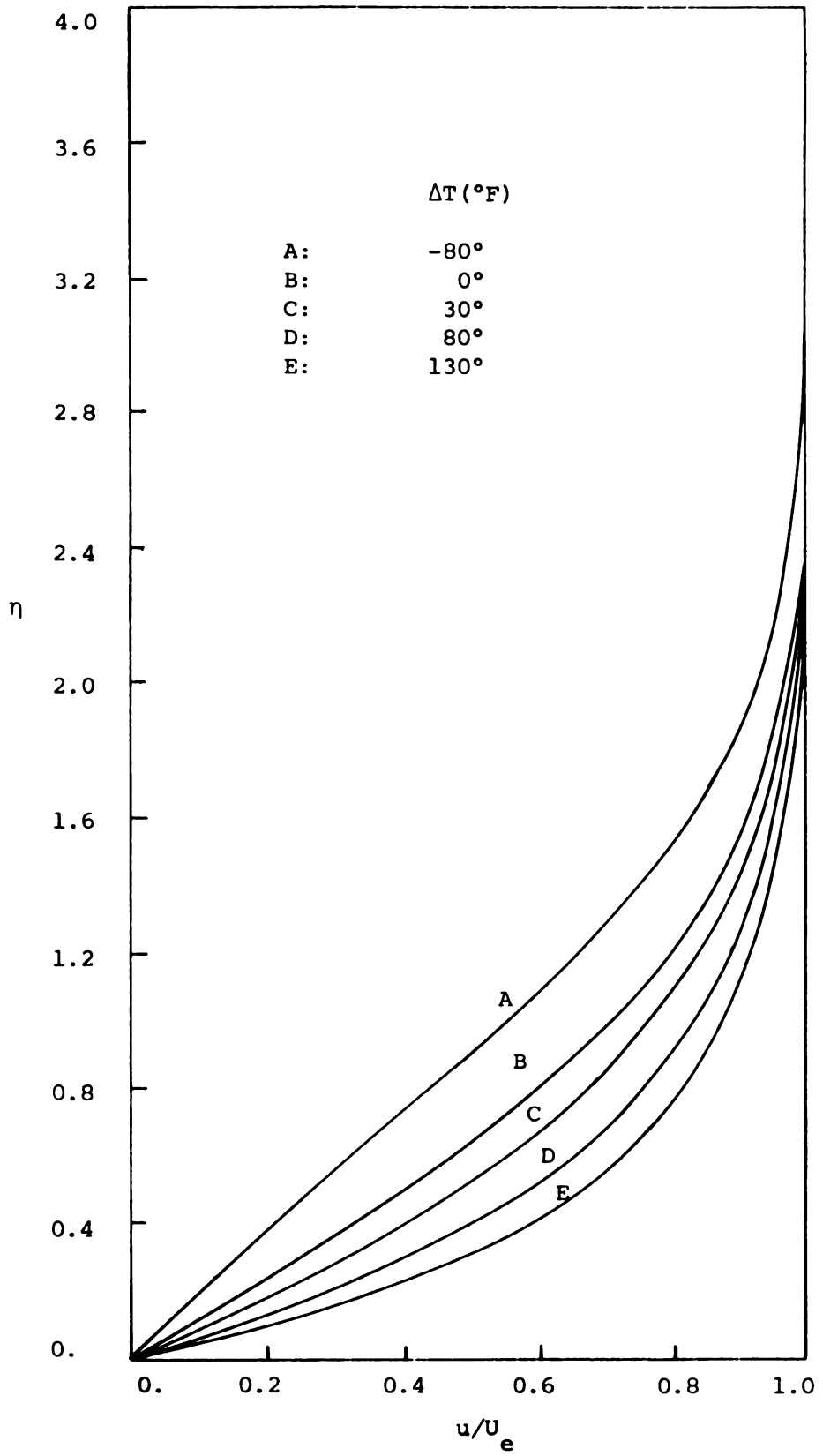

Figure 50. Velocity profiles for a heated sphere. "Below critical flow, $\alpha = 62.6°$.

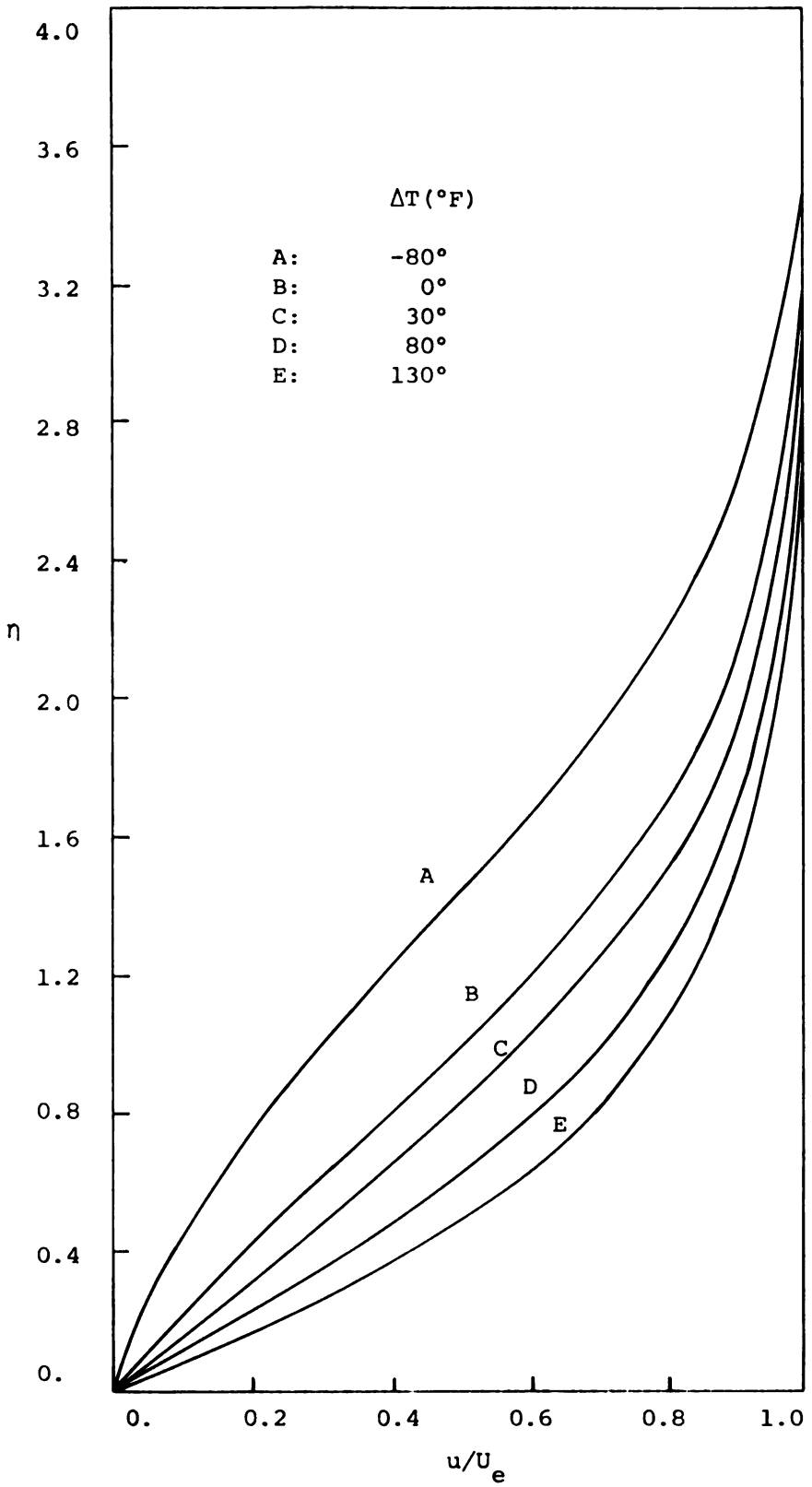

Figure 51. Velocity profiles for a heated sphere. "Below critical" flow, $\alpha = 82°$.

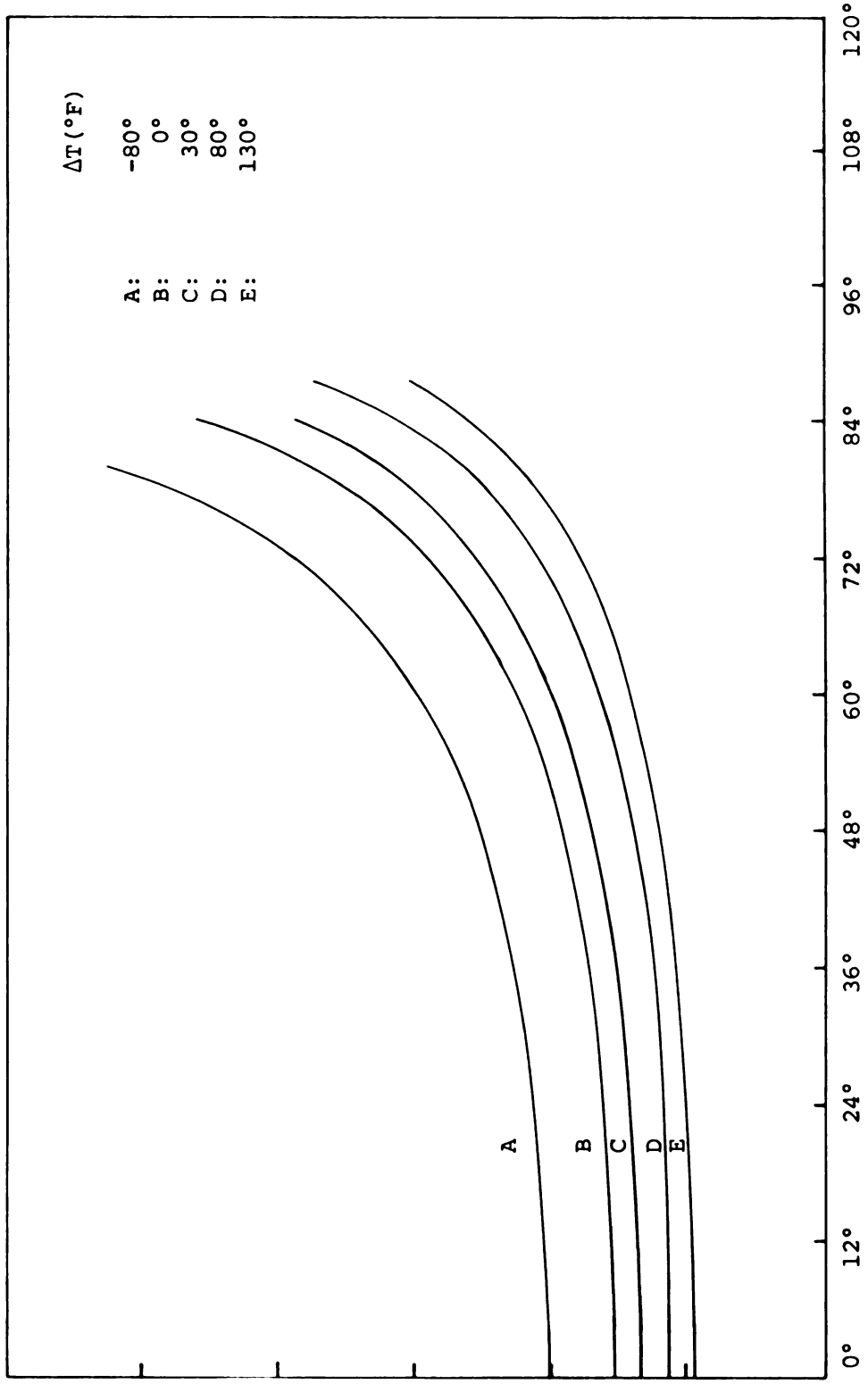

Figure 52. Displacement thickness over a heated sphere. "Below critical" flow.

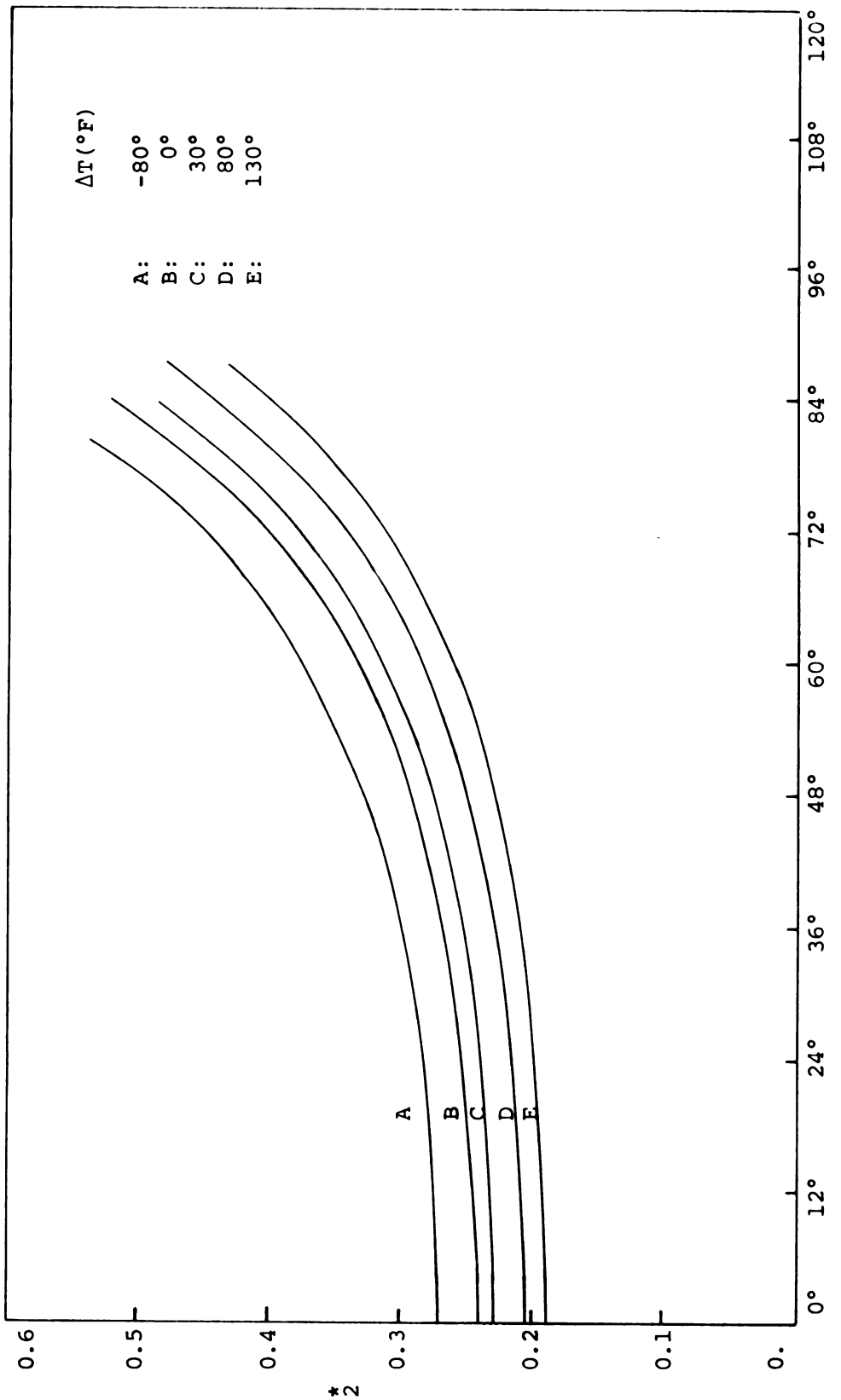

Figure 53. Momentum thickness over a heated sphere. "Below critical" flow.

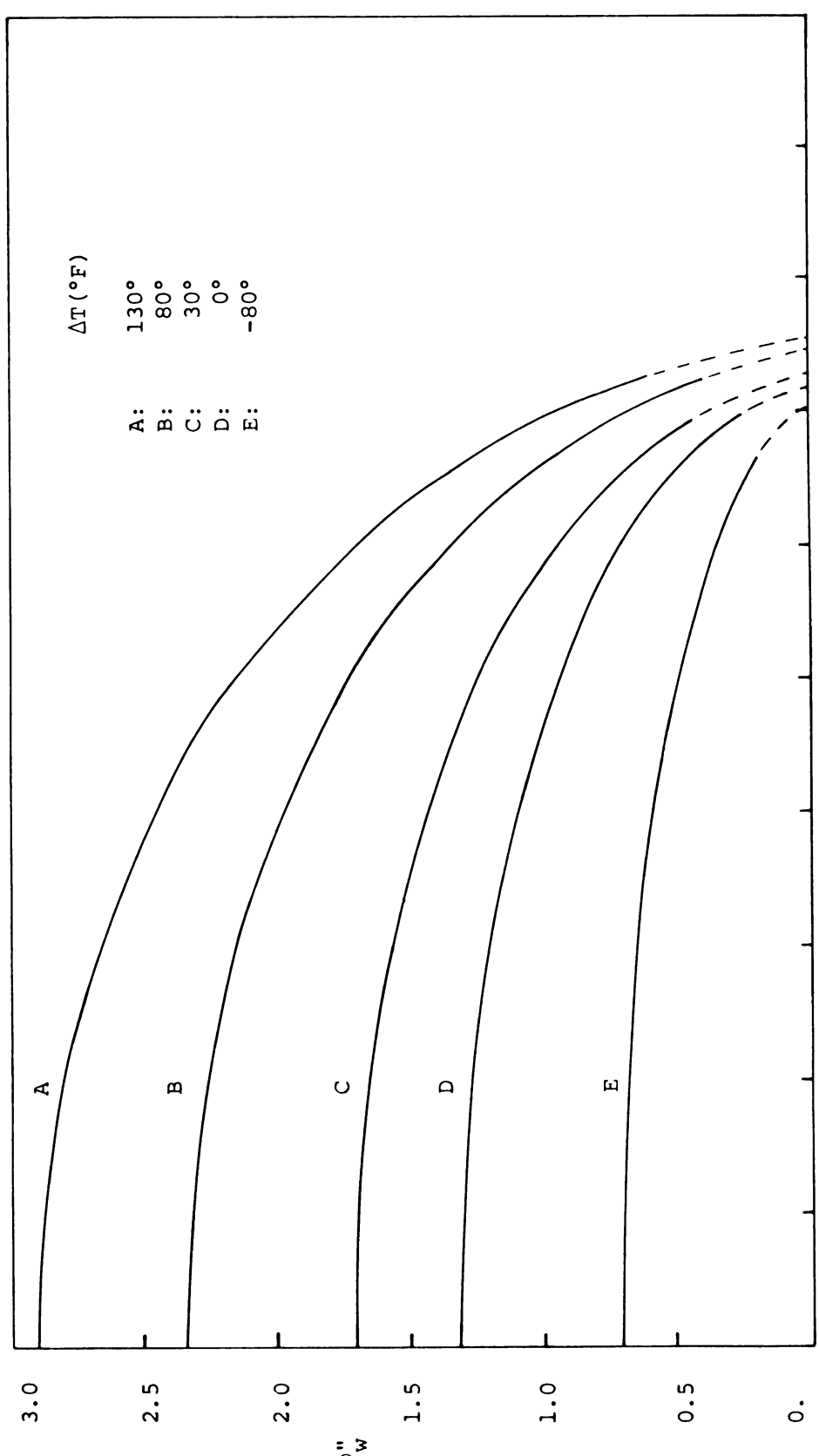

Figure 54. The effect of heating and cooling a sphere on the velocity gradient at the wall. "Below critical" flow.

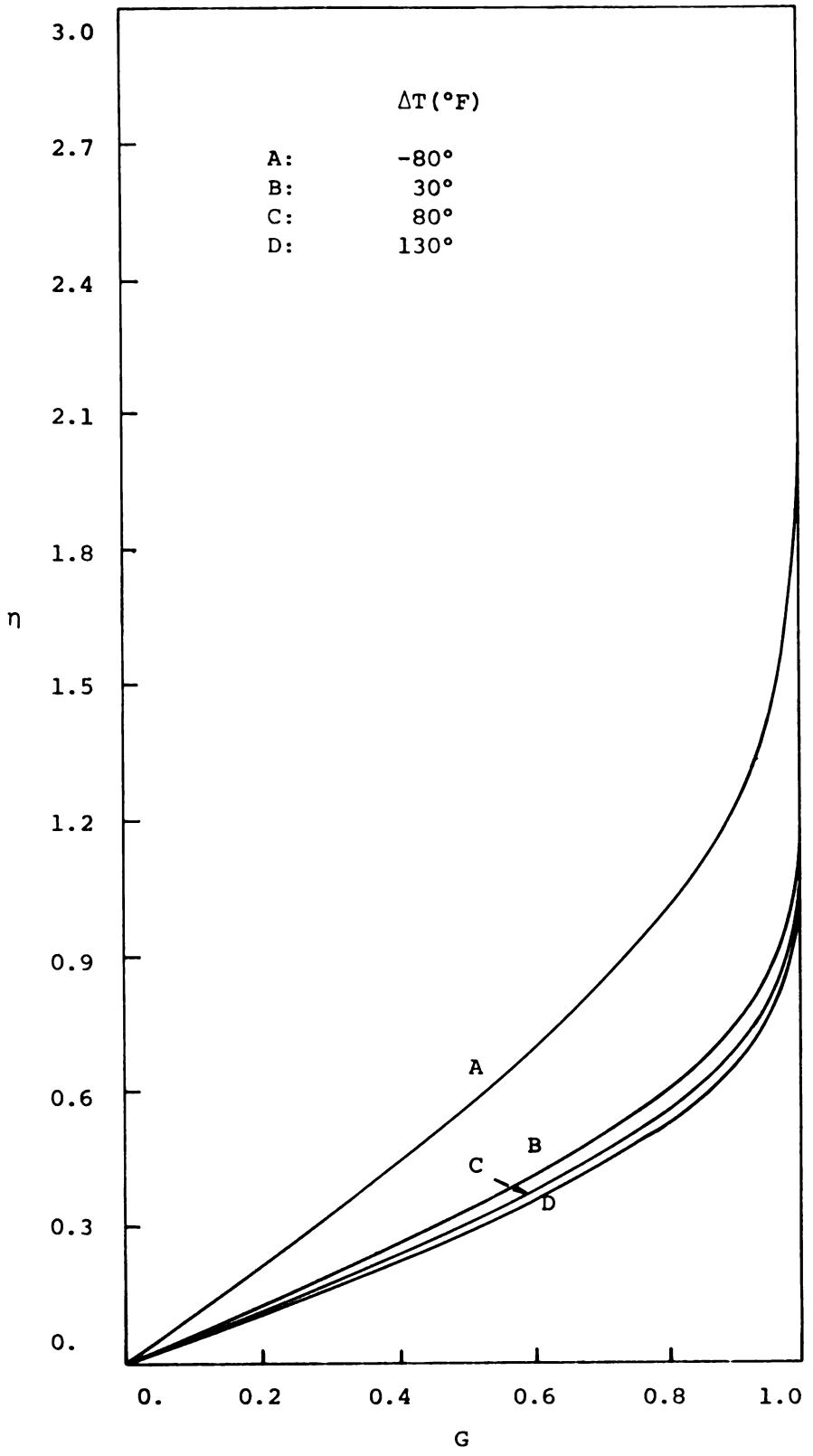

Figure 55. Temperature profiles for a heated sphere. "Below critical" flow, $\alpha = 40°$.

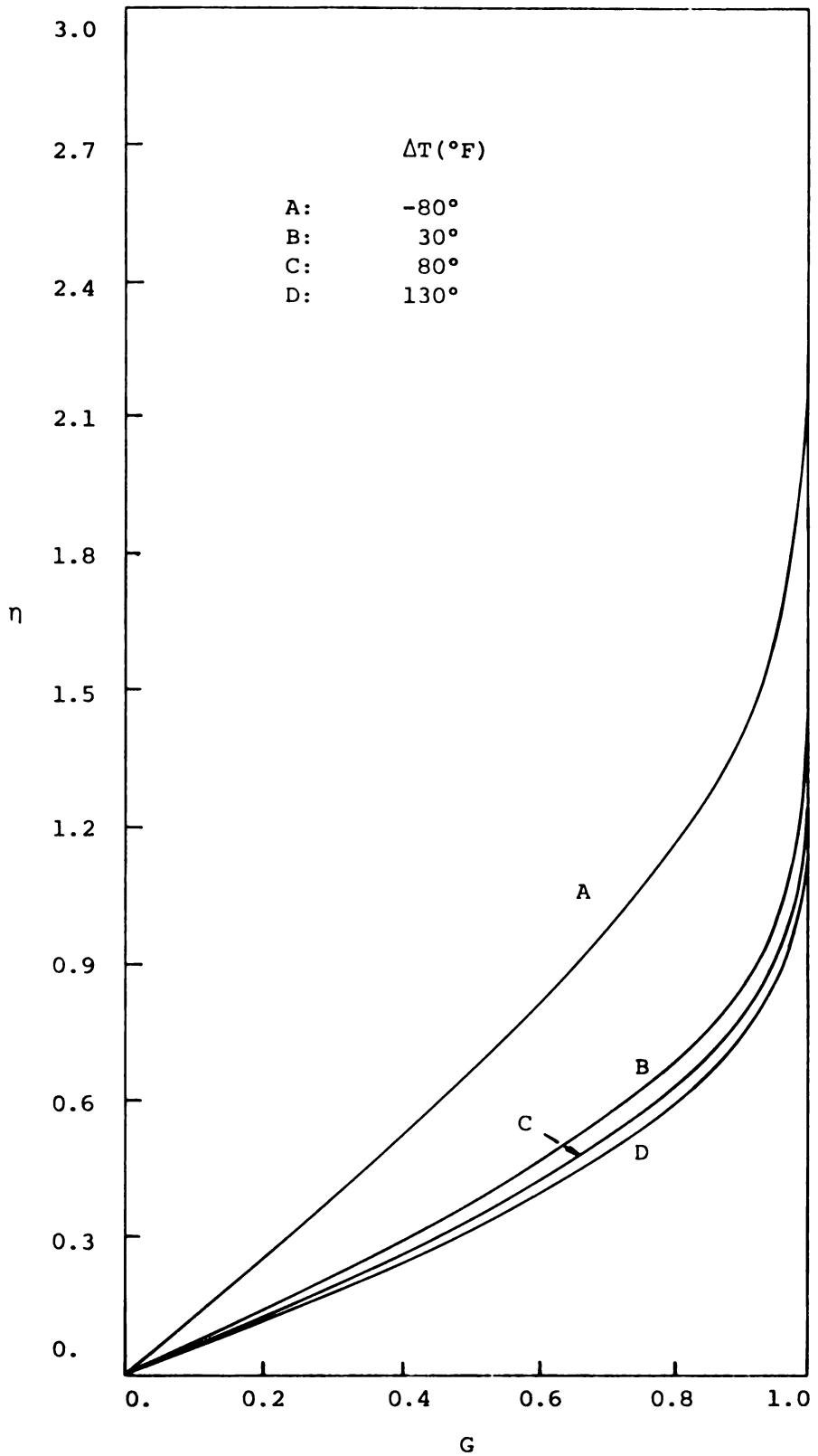

Figure 56. Temperature profiles for a heated sphere. "Below critical" flow, $\alpha = 62.6°$.

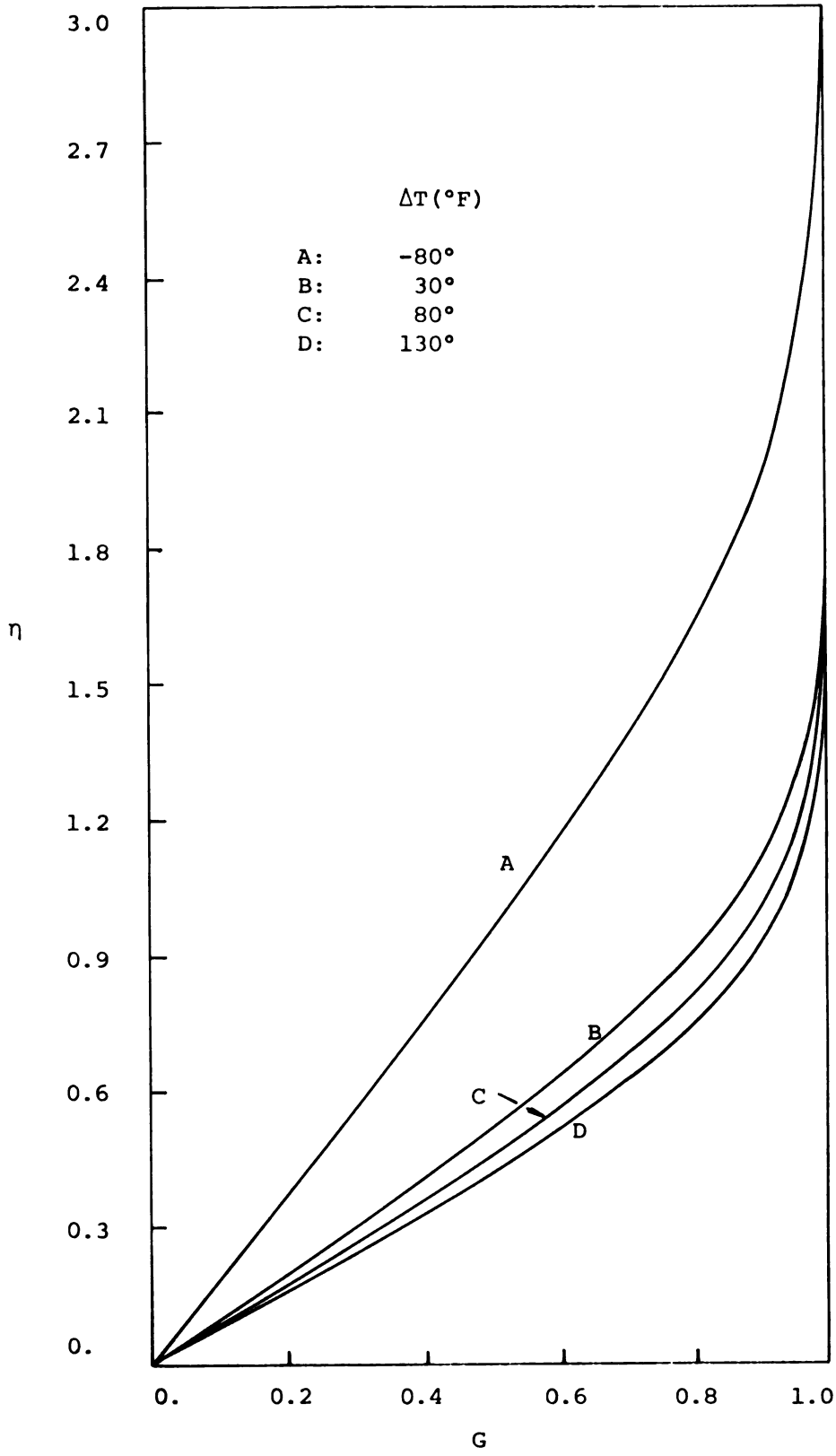

Figure 57. Temperature profiles for a heated sphere. "Below critical" flow, $\alpha = 82°$.

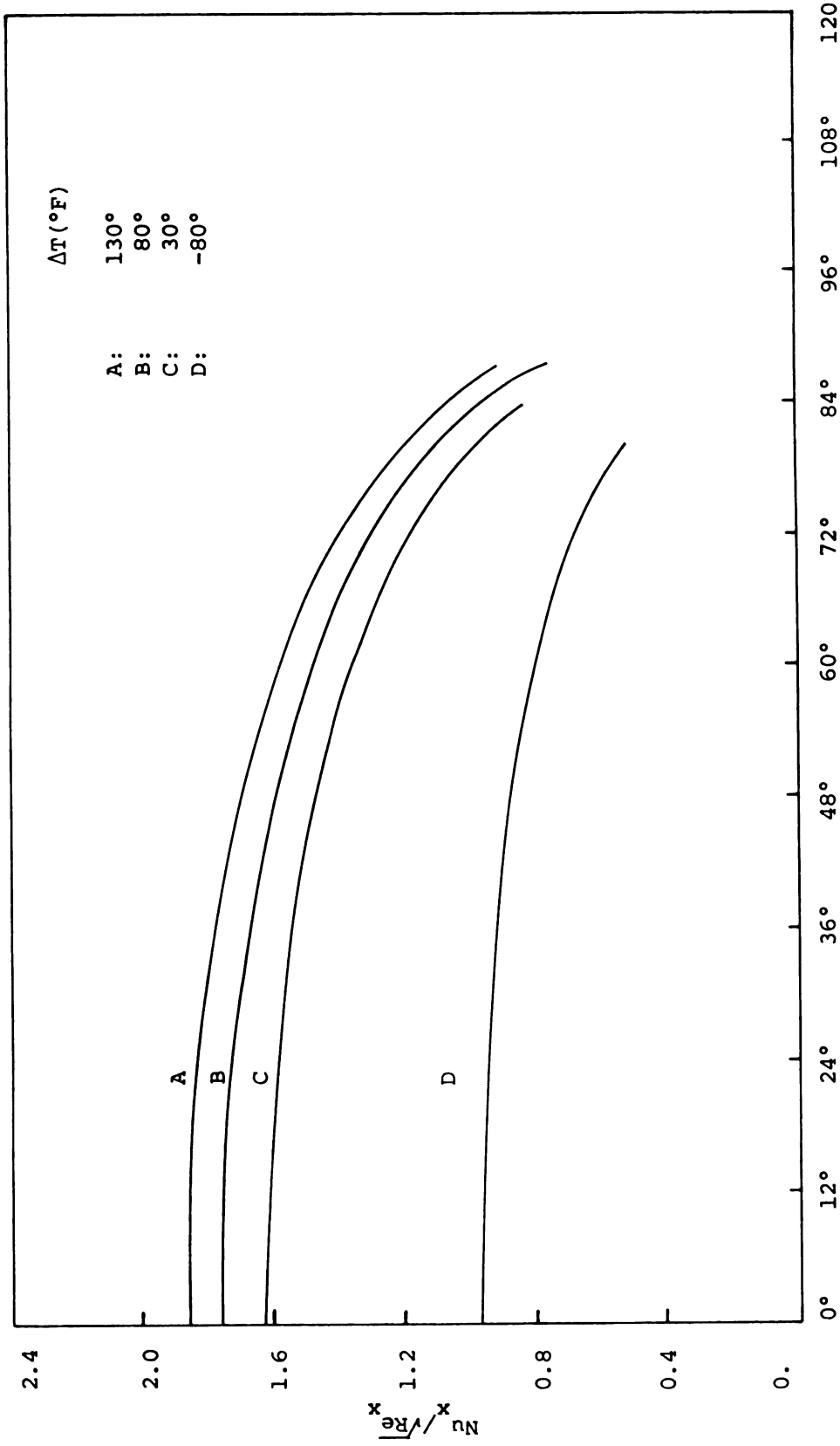

Figure 58. The effect of heating and cooling a sphere on the local heat transfer parameter. "Below critical" flow.

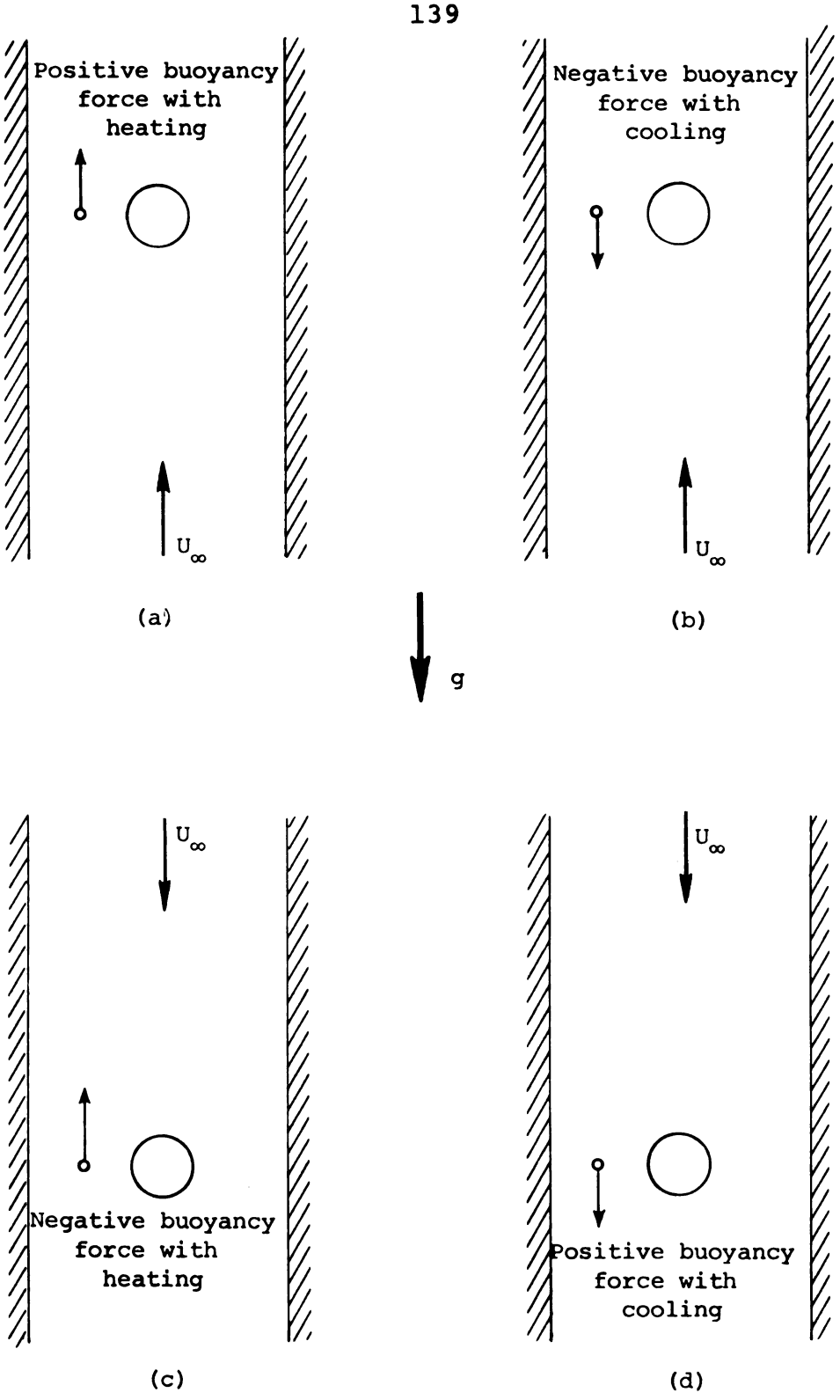

Figure 59. Definition of positive and negative buoyancy forces.

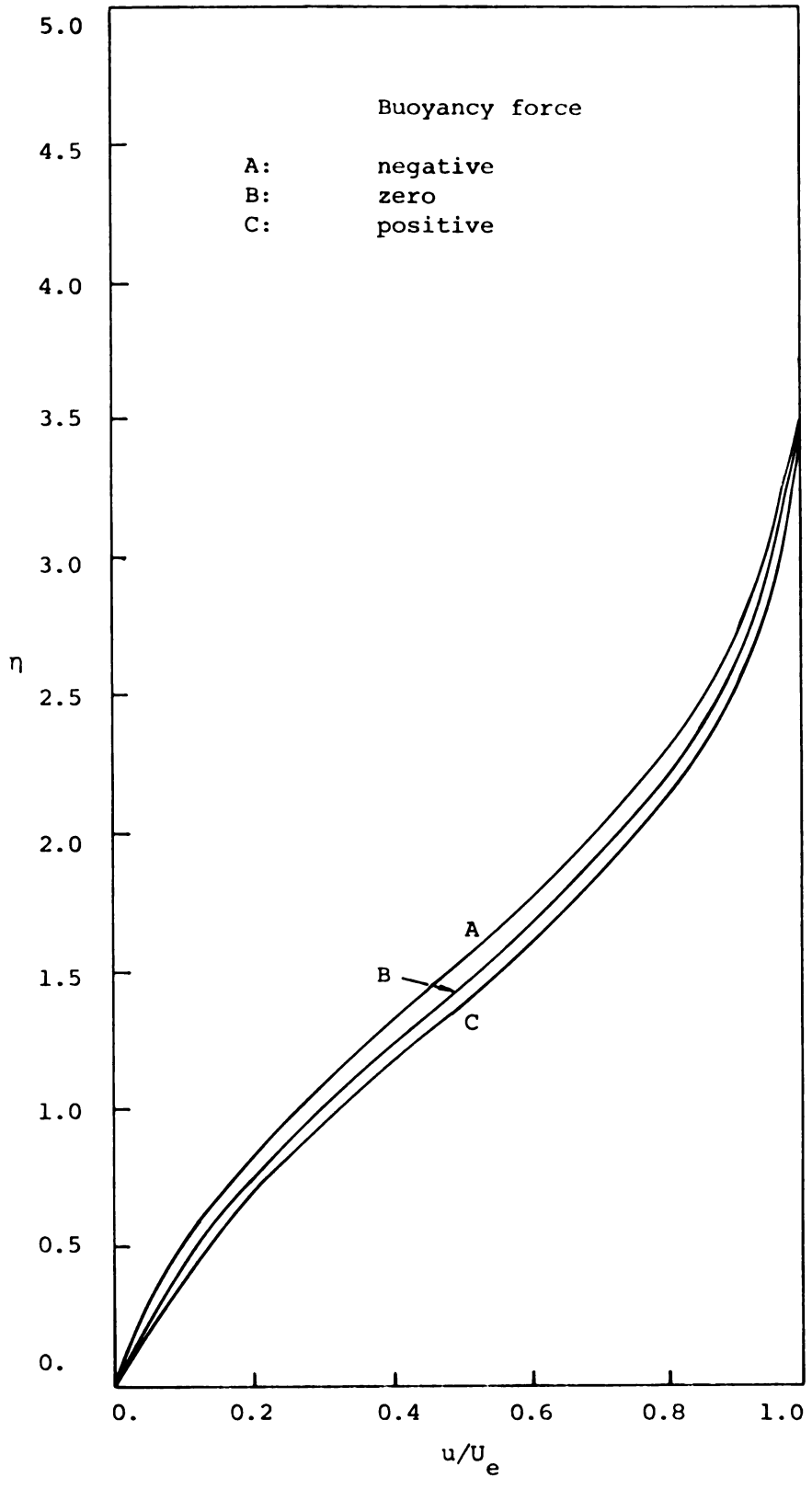

Figure 60. The effect of buoyancy forces on the velocity profiles, when the sphere is cooled. "Below critical" flow, $\alpha = 82°$, $\Delta T = -80°F$.

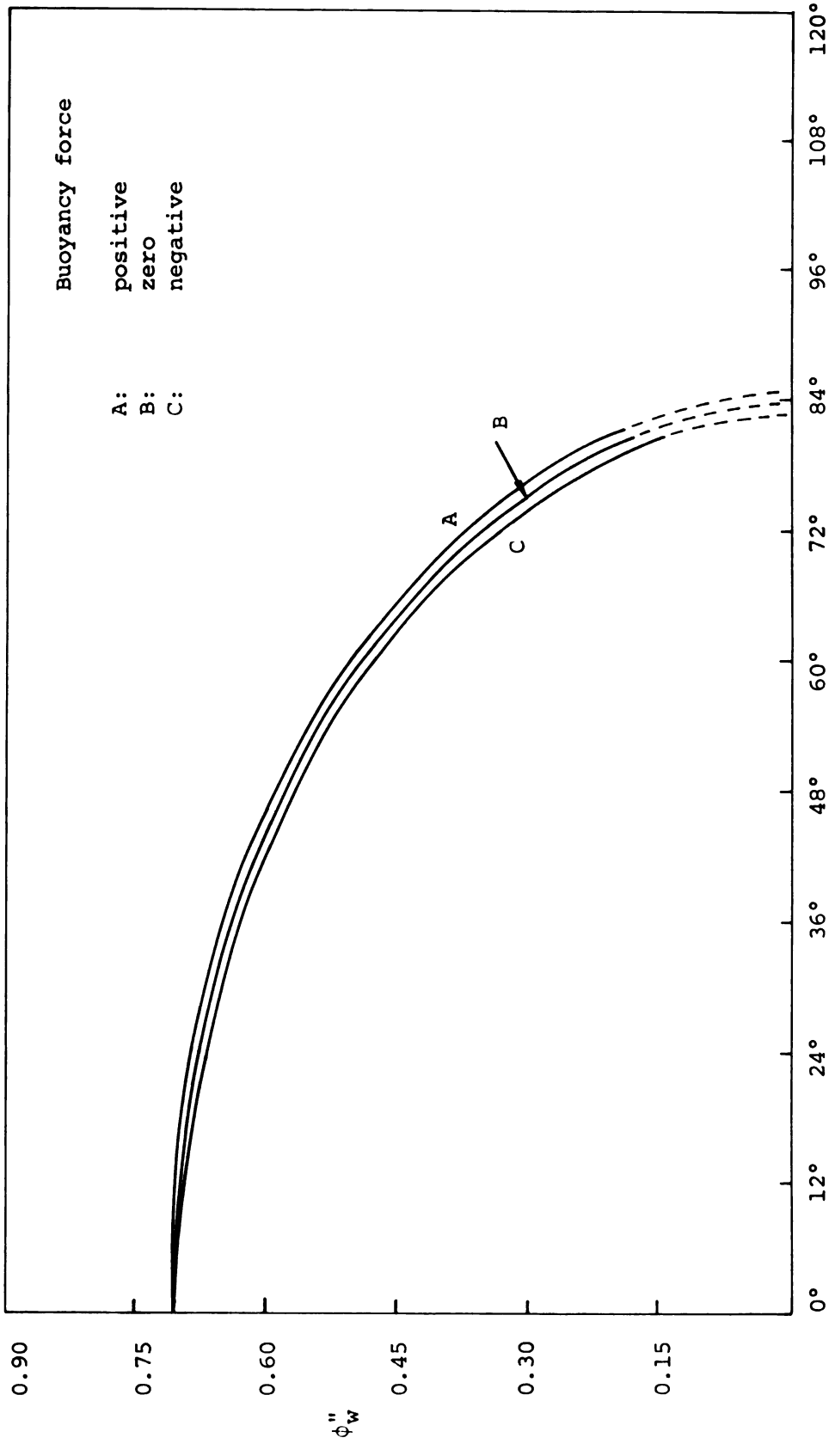

Figure 61. The effect of buoyancy forces on the velocity gradient at the wall, when the sphere is cooled. "Below critical" flow, $\Delta T = -80°F$.

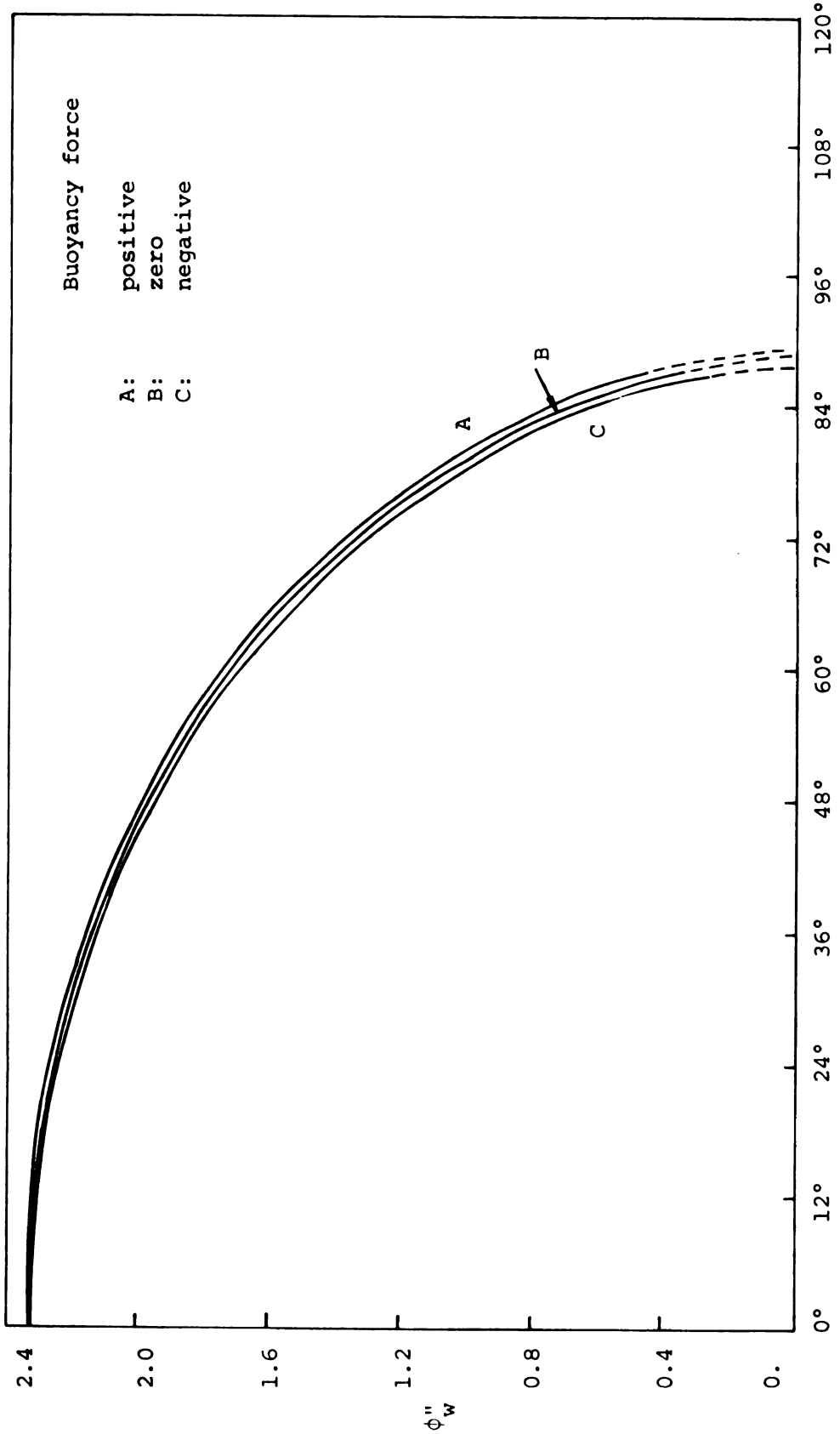

Figure 62. The effect of buoyancy forces on the velocity gradient at the wall, when the sphere is heated. "Below critical" flow, $\Delta T = 80°F$.

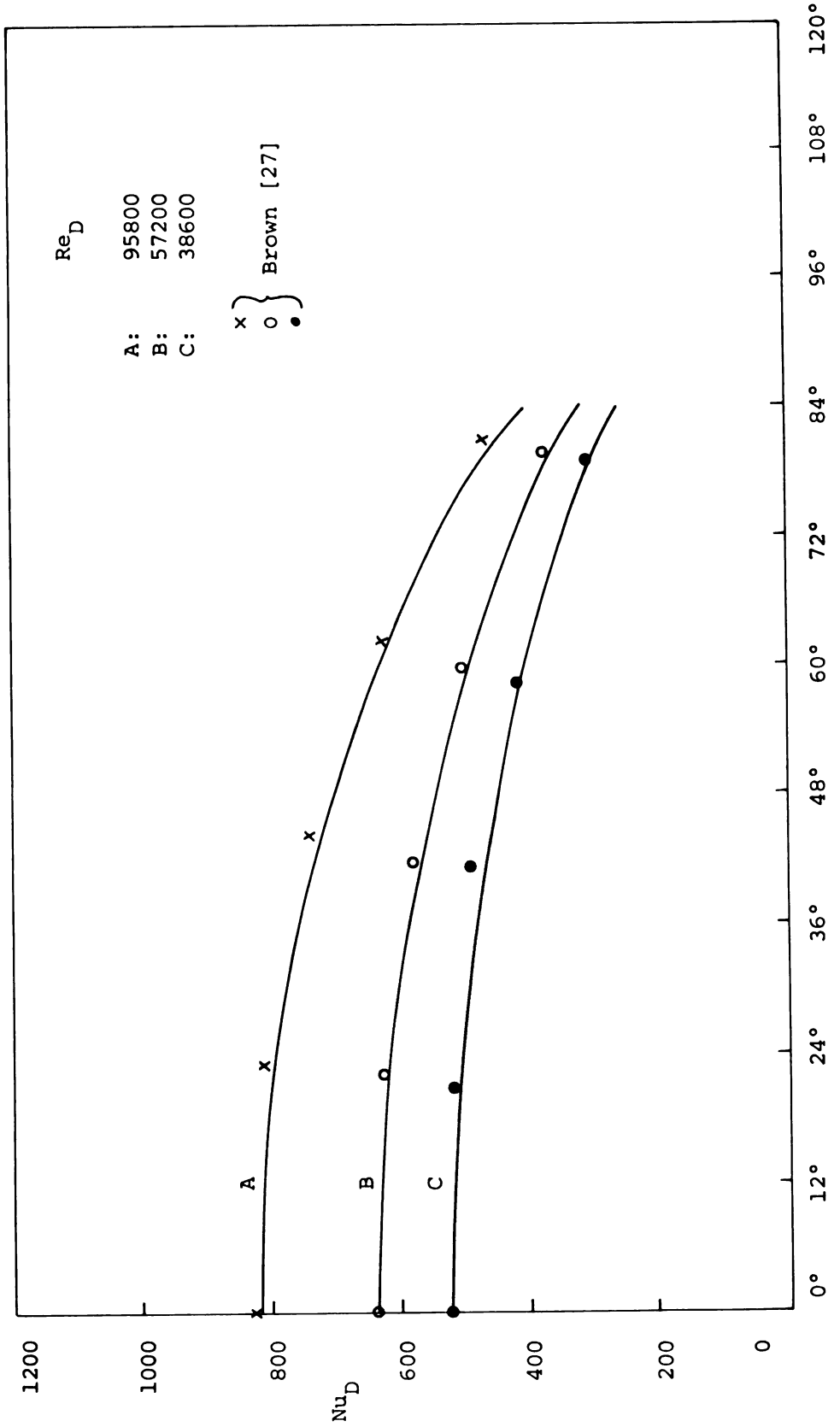

Figure 63. Comparison of local Nusselt Number with experimental results of Brown [27]. T_{wall} = 80°F; T_{water} = 70°F, uniformly heated sphere.

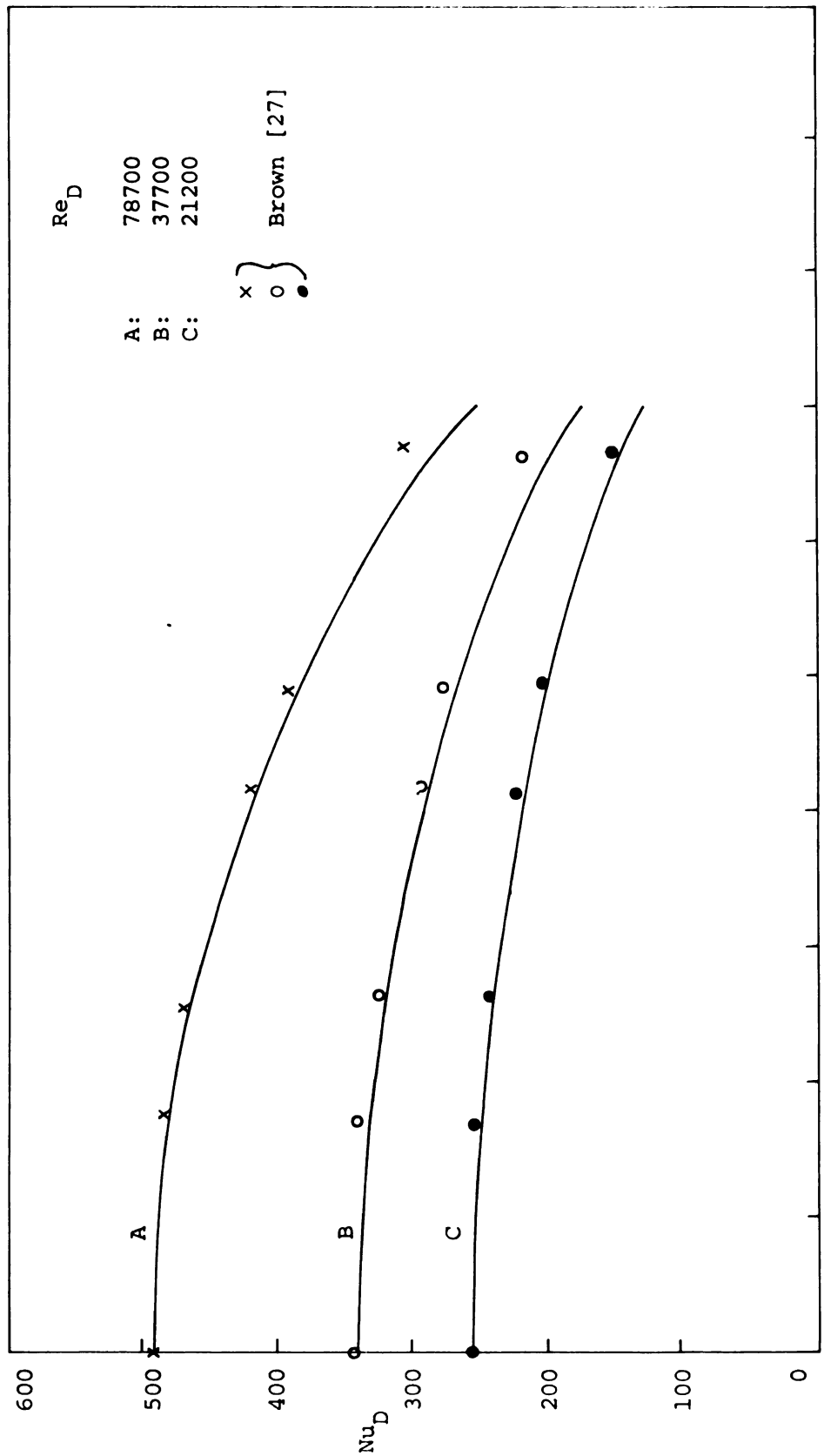

Figure 64. Comparison of local Nusselt Number with experimental results of Brown [27]. T_{wall} = 190°F, T_{water} = 180°F, uniformly heated sphere.

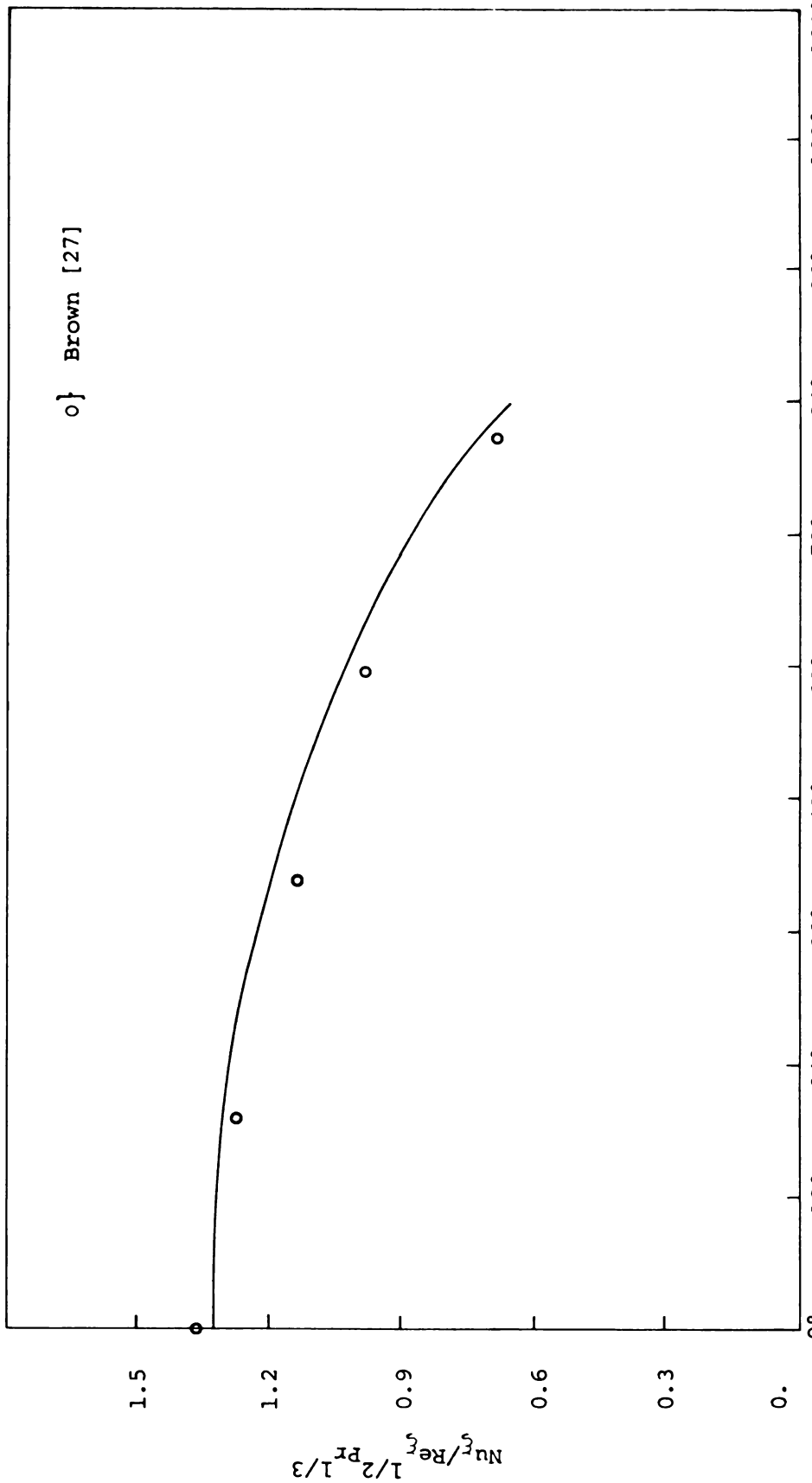

Figure 65. Comparison of heat transfer parameter with experimental results of Brown [27].

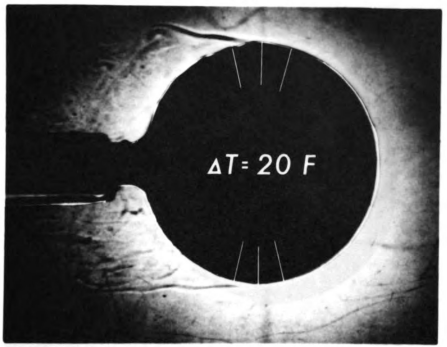

Figure 66. Shadowgraph picture of the heated sphere. $\Delta T = 20°F$

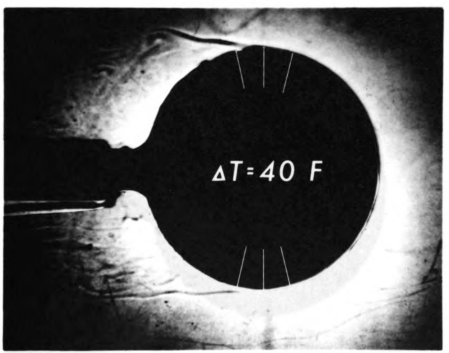

Figure 67. Shadowgraph picture of the heated sphere. $\Delta T = 40°F$

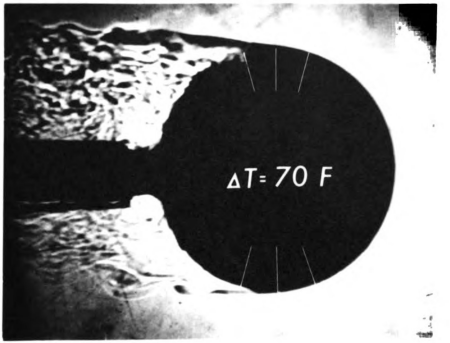

Figure 68. Shadowgraph picture of the heated sphere. $\Delta T = 70°F$

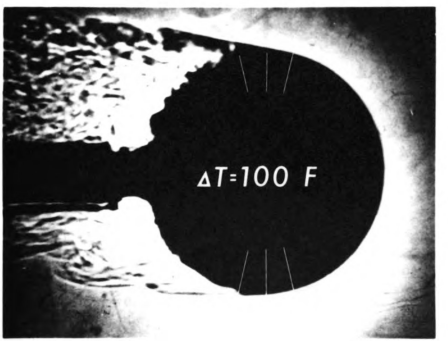

Figure 69. Shadowgraph picture of the heated sphere. $\Delta T = 100°F$

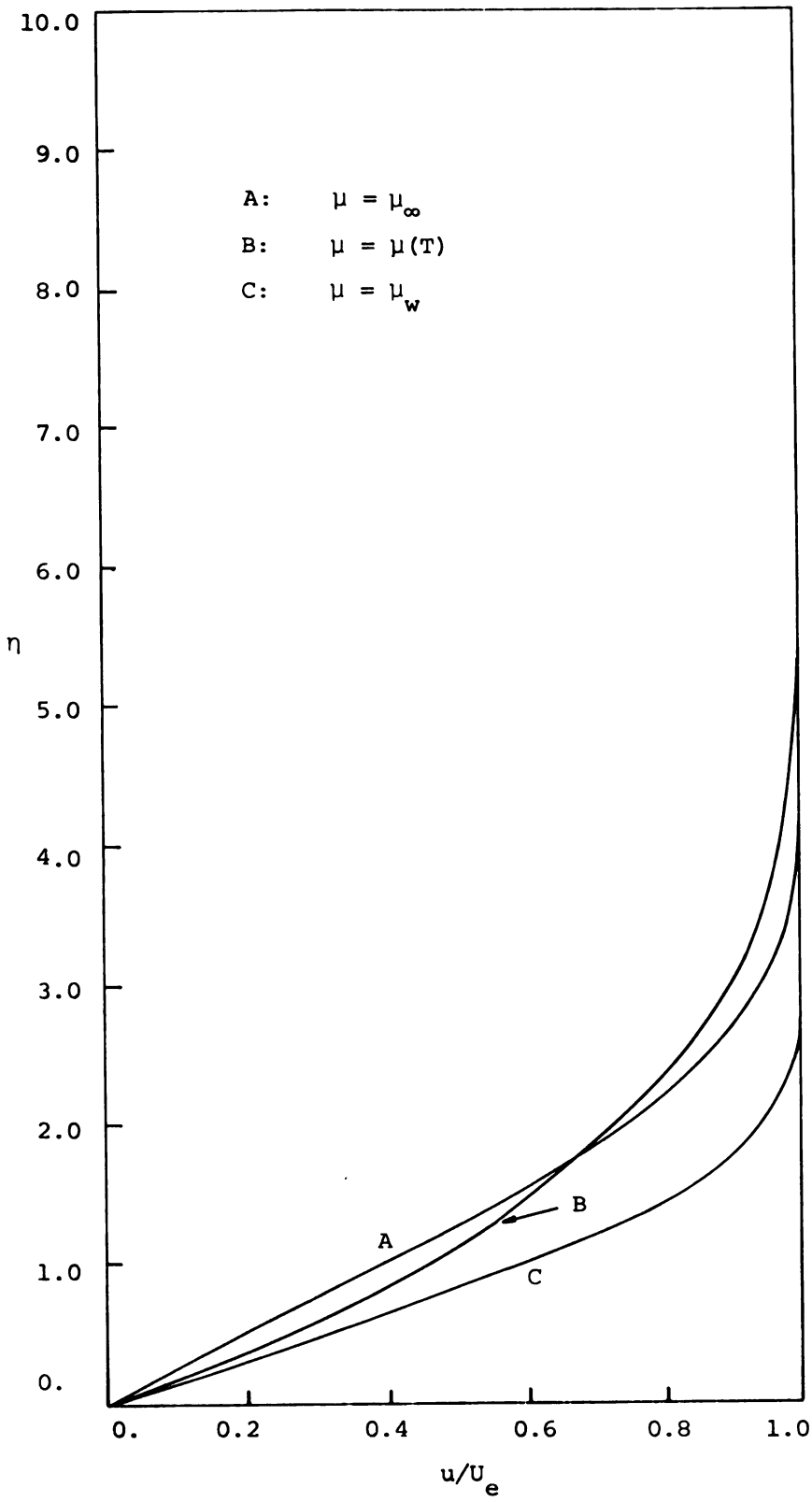

Figure 70. The effect of treating viscosity constant and variable on the velocity profile. $U_e/U_\infty = 1 - \xi$, $\xi = .083$, $\Delta T = 80°F$

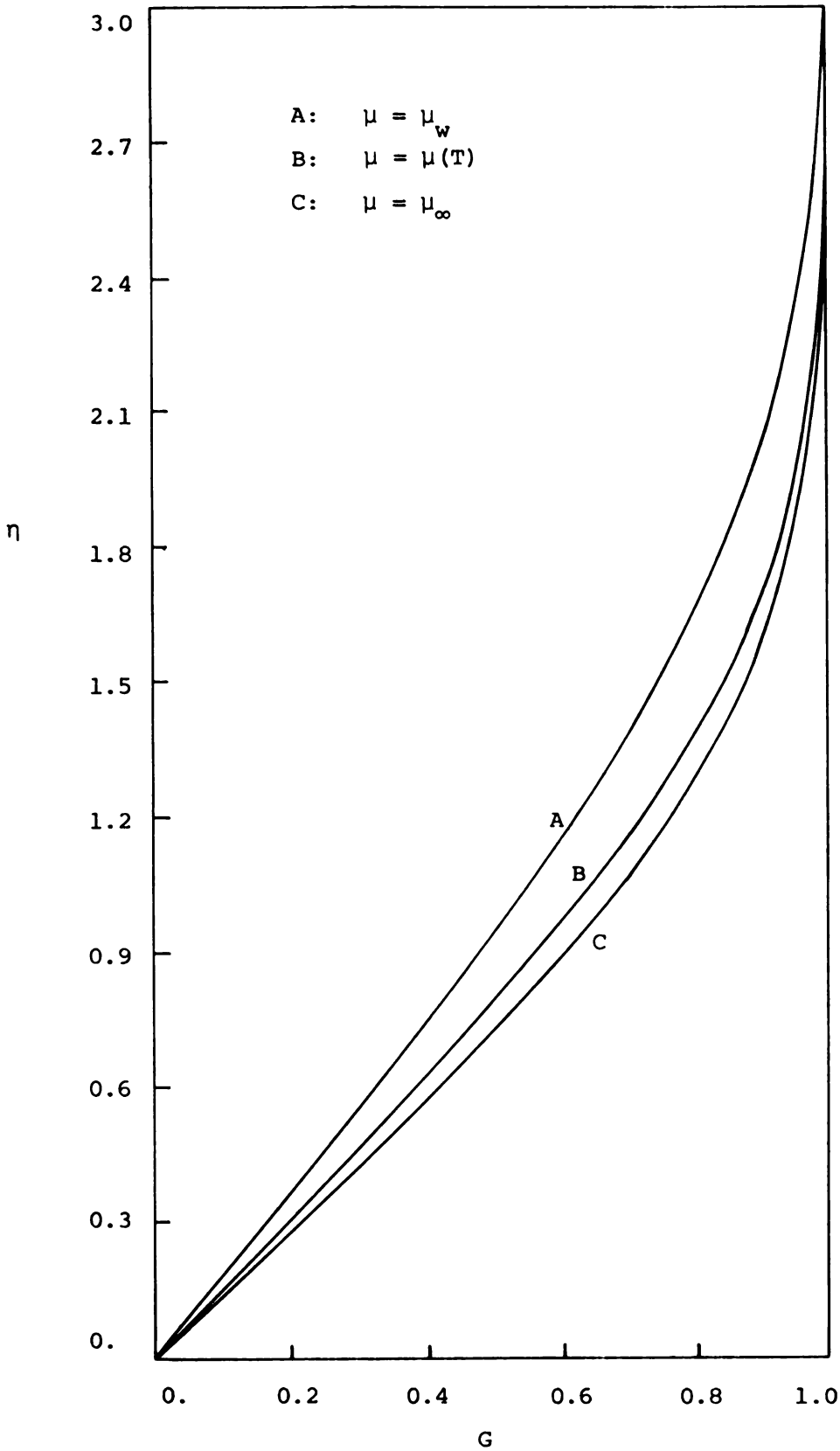

Figure 71. The effect of treating viscosity constant and variable on the temperature profile. $U_e/U_\infty = 1 - \xi$, $\xi = .083$, $\Delta T = 80°F$

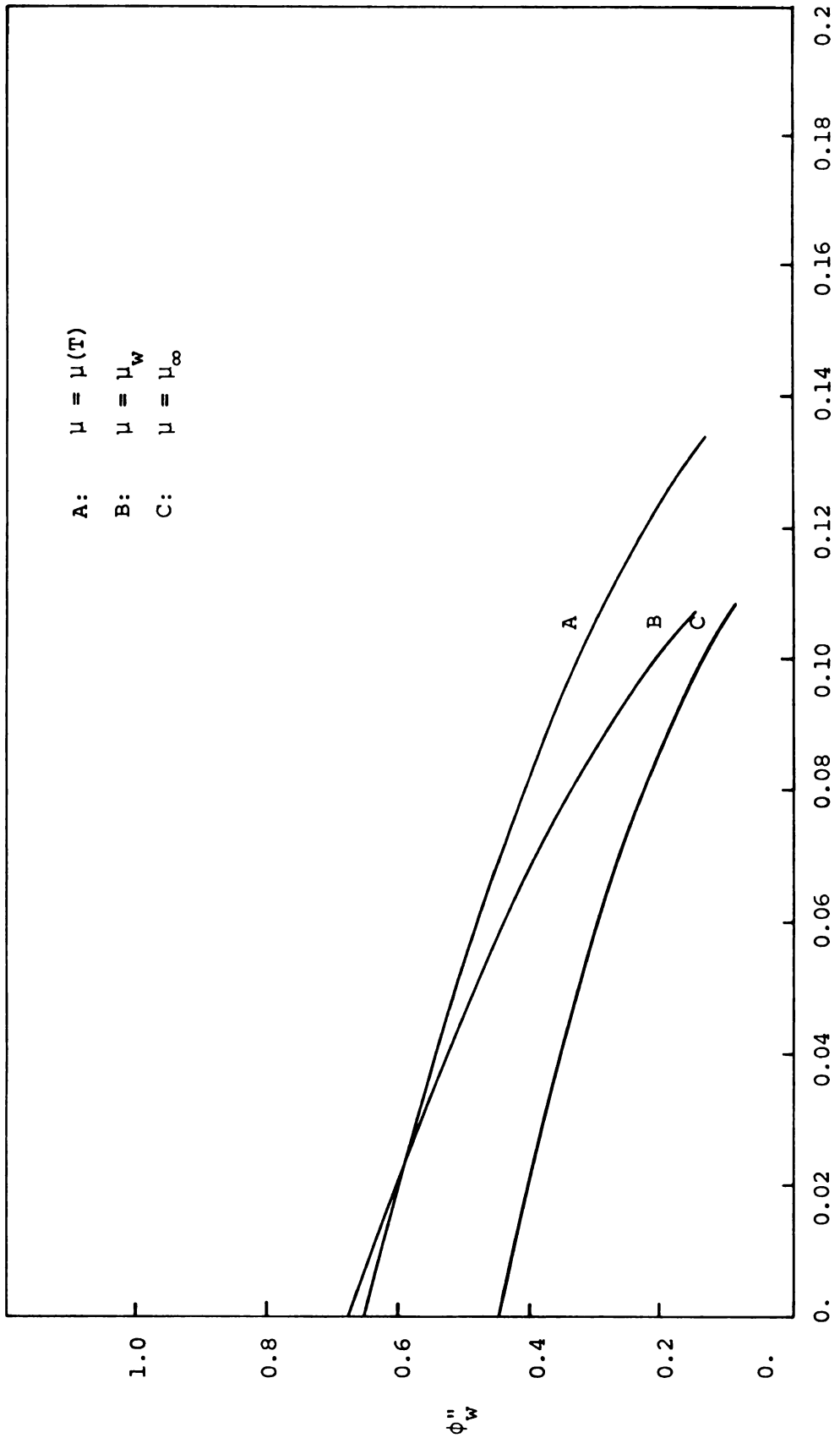

Figure 72. The effect of treating viscosity constant and variable on the velocity gradient at the wall. $U_e/U_\infty = 1 - \xi$, $\Delta T = 80°F$

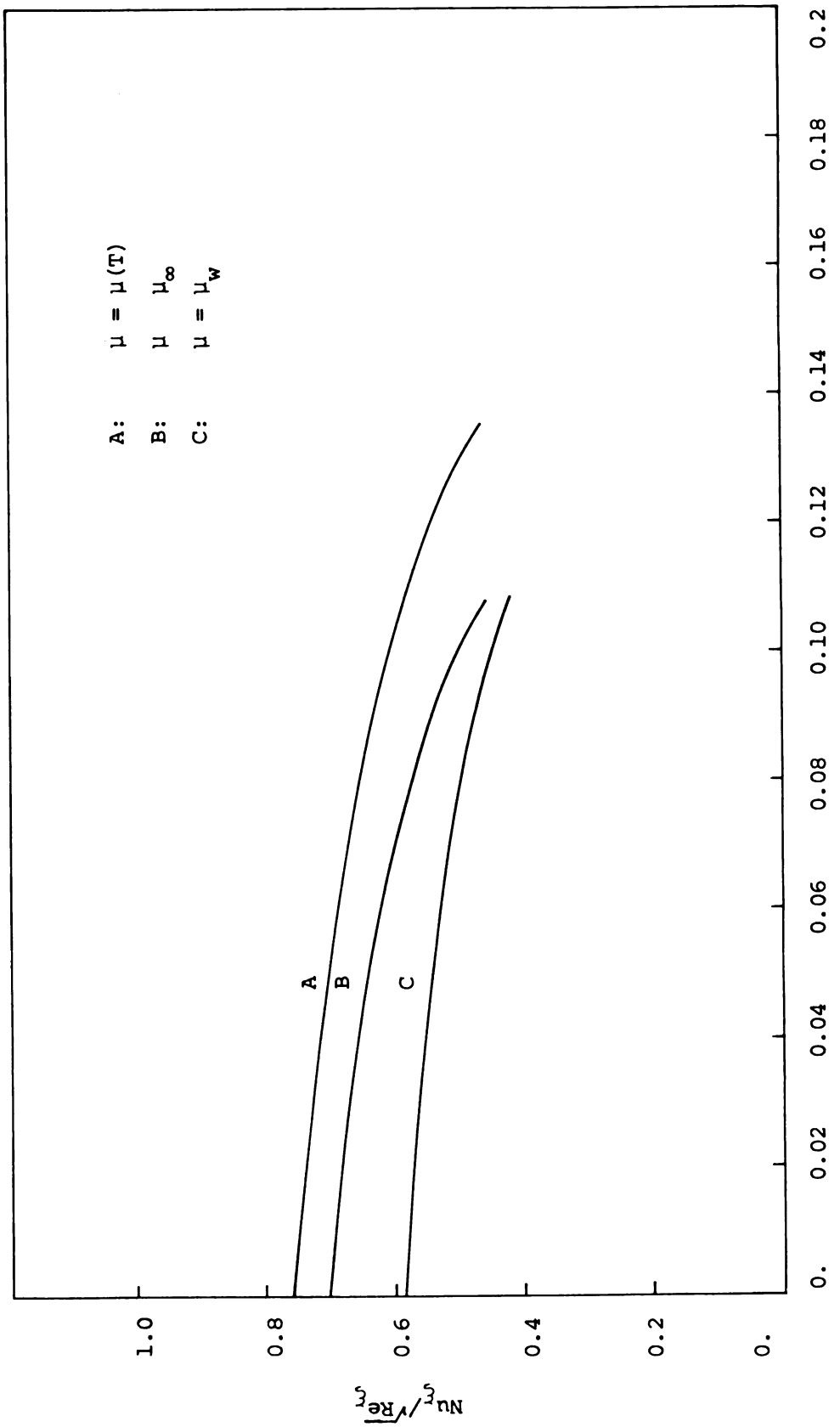

Figure 73. The effect of treating viscosity constant and variable on the local heat transfer parameter. $U_e/U_\infty = 1 - \xi$, $\Delta T = 80°F$

BIBLIOGRAPHY

BIBLIOGRAPHY

[1] Chang, P. K., Separation of Flow, Pergamon Press, New York, 1970.

[2] Prandtl, L., Über Flüssigkeitsbewegung bei sehr kleiner Reiburg. Proc. Third Intern. Math. Congress, Heidelberg, 1904, pp. 484-491.

[3] Prandtl, L., The Mechanics of Viscous Fluids, Aerodynamic Theory, Vol. III, Springer, Berlin, 1924, edited by W. F. Durand.

[4] Morduchow, M., "Review of theoretical investigation on effect of heat transfer on laminar separation," AIAA Journal, 3, 8, 1377-1385 (1965).

[5] Morduchow, M., and Galowin, L., "The compressible laminar boundary layer in a pressure gradient over a surface cooled by fluid injection," Proceedings of the Iowa Thermodynamics Symposium, State University of Iowa, Iowa City, Iowa, 1953, pp. 143-169.

[6] Morduchow, M., and Grape, R. G., "Separation, stability and other properties of compressible boundary layer with pressure gradient and heat transfer," NACA TN 3296 (May, 1955).

[7] Cohen, C. B., and Reshotko, E., "Similar solutions for the compressible laminar boundary layer with heat transfer and pressure gradient," NACA TN 3325 (February, 1955).

[8] Li, T. Y., and Nagamatsu, H. T., "Similar solutions for the compressible boundary layer equations," J. Aeronaut. Sci. 22, 607 (1955).

[9] Stewartson, K., "The Theory of Laminar Boundary Layers in Compressible Fluids, Oxford University Press, New York, 1964.

[10] Illingworth, C. R., "The effect of heat transfer on the separation of a compressible laminar boundary layer," Quart. J. Mech. Appl. Math., VII, 8 (1954).

[11] Luxton, R. E., and Young, A. D., "Generalized methods for the calculation of of the laminar compressible boundary-layer characteristics with heat transfer and non-uniform pressure distribution," British Aeronautical Research Council, R & M 3233 (January, 1960).

[12] Law, G. M., "The compressible laminar boundary layer with heat transfer and small pressure gradient," NACA TN 3028 (October, 1953).

[13] Livingood, J. N. B., and Dononghe, P. L., "Summary of laminar-boundary layer solution for wedge-type flow over connection and transpiration cooled surfaces," NACA TN 3588 (December, 1955).

[14] Gadd, G. E., "A review of theoretical work relevant to the problem of heat transfer effects on laminar separation," Aeronautical Research Council Paper 331 (June 13, 1956).

[15] Curle, N., "The steady compressible laminar boundary layer, with arbitrary pressure gradient and uniform wall temperature," Proc. Roy. Soc. (London), A249, 206-224 (1958).

[16] Poots, G., "A solution of the compressible laminar boundary layer equations with heat transfer and adverse pressure gradient," Quart. J. Mech. Appl. Math. XIII, 57 (1960).

[17] Baxter, D. C., and Flügge-Lozt, I., "The solution of compressible laminar boundary layer problems by a finite difference method," Stanford Univ., Div. of Engineering Mechanics, TR110 (October 15, 1957).

[18] Fannelop, T., and Flügge-Lozt, I., "The laminary compressible boundary layer along a wave-shaped wall," Ing.-Arch., XXXIII, 24-35 (1963).

[19] Schuh, H., "The solution of the laminar boundary layer equations for the flat plate for velocity and temperature fields for variable physical properties and for the diffusion field at high concentration," NACA TM 1275 (May, 1950).

[20] Hanna, O. T., and Myers, J. E., "Laminary boundary layer flow and heat transfer past a flat plate for a liquid of variable viscosity," A.I.Ch.E. Journal, 7, 3, 437-441 (1961).

[21] Johnson, H. A., "Boelter Anniversary Volume Heat Transfer, Thermodynamics and Education, McGraw-Hill Book Co., New York, 1964, pp. 319-379 (chapter on "The Laminar Boundary Layer of a Liquid with Variable Viscosity" by R. A. Saban).

[22] Poots, G., and Raggett, G. F., "Theoretical results for variable property laminar boundary layers in water," Inter. J. Heat Mass Transfer, 10, 597-610 (1967).

[23] Kaups, K., and Smith, A. M. O., "The Laminar Boundary Layer in Water with Variable Properties," Douglas Aircraft Company Paper, Long Beach, Calif. (August, 1967).

[24] Clutter, D. W., and Smith, A. M. O., "Solution of the General Boundary Layer Equations for Compressible Laminar Flow, Including Transverse Curvature," Douglas Aircraft Company Report No. LB 31088, February, 1963.

[25] Kramers, H., "Heat transfer from spheres to flowing media," Physicia, 12, 61 (1946).

[26] Vliet, G. C., and Leppert, G., "Forced convection heat transfer from an isothermal sphere to water," Journal of Heat Transfer, Trans. ASME Series C, 83, 163-175 (1961).

[27] Brown, W. S., Forced Convection Heat Transfer from a Uniformly Heated Sphere to Water, Ph.D. Thesis, Stanford University, Stanford, Calif. (1960).

[28] Boltze, E., "Grenzschichten an Rotantionskörpern in Flüssigkeiten mit Kleiner Reiburg," Dissertation Gottingen (1908).

[29] Millikan, C. B., "The boundary layer and skin friction for a figure of revolution," Trans. Amer. Soc. Mech. Eng., Appl. Mech. Sec., 54, 29-43 (1932).

[30] Schlichting, H., Boundary Layer Theory, McGraw-Hill Book Co., New York (1962).

[31] Tomotika, S., "Laminar boundary layer on the surface of a sphere in a uniform stream," British Aeronautical Research Committee, R and M 1678 (1935).

[32] Hartree, D. R., and Womersley, J. R., "A method for the numerical or mechanical solutions of certain types of partial differential equations," Proc. Royal Soc. Series A, 161, 906, 353 (August, 1931).

[33] Howarth, L., Modern Developments in Fluid Dynamics--High Speed Flow, Vol. 1, Chap. X, Oxford (1953).

[34] Howarth, L., "On the solution of the laminar boundary layer equations," Proc. Royal Society, 164, 547 (1938).

[35] Von Karman, T., and Millikan, C., "On the theory of laminar boundary layers involving separation," NACA Report No. 504 (1934).

[36] Hartree, D. R., "A solution of the laminar boundary layer equation for retarded flow," British R and M No. 2426 (1949).

[37] Smith, A. M. O., and Clutter, D. W., "Solution of Incompressible Laminar Boundary Layer Equations," Douglas Aircraft Company Report No. 40446 (July, 1961).

[38] Levy, S., "Heat transfer to constant-property laminar boundary layer flows with power-function free-stream velocity and wall-temperature variation," Jour. Aero. Sci., 19, 15, 34-348 (1952).

[39] Leigh, D. C. F., "The laminar boundary layer equation: A method of solution by means of an automatic computer," Proc. Camb. Phil. Soc., 51, 320-332 (1955).

[40] Schraub, F. A., Kline, S. J., Hariry, J., Runstadler, P. W., and Little, A., "Use of hydrogen bubbles for quantitative determination of time-dependent velocity fields in low-speed water flows," J. of Basic Engineering, Trans. ASME, 429-444 (June, 1965).

[41] Fage, A., "Experiments on a sphere at critical Reynolds Numbers," British Aeronautical Research Committee R and M 1766 (1936).

APPENDIX

```
      PROGRAM KAPUR(INPUT,OUTPUT,PUNCH)
CCC   THIS PROGRAM PROVIDES A SOLUTION OF THE INCOMPRESSIBLE LAMINAR BOUNDARY
CCC   LAYER EQUATIONS. THE METHOD OF SOLUTION WAS INITIALLY DEVELOPED
CCC   BY SMITH-CLUTTER. THE PROGRAM ALLOWS FOR ARBITRARY CONDITIONS ON THE
CCC   PRESSURE GRADIENT, SURFACE TEMPERATURE AND IT≠S GRADIENT, HEAT
CCC   TRANSFER AND FLUID PROPERTIES.
CCC   THE PROGRAM ALLOWS FOR INCLUDING THE BUOYANCY FORCE TERM AND FOR TREATING
CCC   VISCOSITY CONSTANT ACROSS THE BOUNDARY LAYER THICKNESS.
CCC   THE RESTRICTION ON THE METHOD IS THAT THE BODY BE AXIALLY SYMMETRIC
CCC   OR TWO-DIMENSIONAL.
      INTEGER QMAX
       INTEGER GFLAG
      COMMON/11/FK10,FK14,FK15,FK13/12/ISTA/13/XN/14/X(100)/15/T(400),
     1PRINF,C(400)/16/ETA,II,DETA/17/PH(20)/18/IE1,IE7/19/S1(4),S2(4),
     2S3(4),IFLAG/20/B1(800),B2(800),B3(800)/21/AL(200),BL(200)/22/
     3B7(1600),B8(1600),B15(400)/23/AMBAR,RBAR,SK(100),RP(100)/24/PSIPW,
     4PSIW/25/NMAX,C1,C2,CNIF,QMAX,EPS2/26/FK1,FK25/27/IRH,IRL,IRHL,IRC
     5,ML,MH,MM,MHL,MC,IFLOW,IFIRST,ISW1,ISW2,IPVS,IRET,ITER,IT,IHSW,
     6PHIL,PHIH,ETAH,ETAL,ETAHL,ELSW,EHSW,PHIPP/28/N1,N2,N3,N4/29/NNN
     7/30/INCOMP/31/TINF,TWALL,ETMAX/33/ISK/34/FK26/36/CE/37/DMETA,DEETA
     8/40/KLM/41/EPS3,EPS4,F26
      COMMON/60/IOU/61/GFLAG/62/ILCM,IBOY,BOUY,BETA/63/IVIS/64/IFLAT
      COMMON/75/K1,K2,K3
       DOUBLE PRECISION PH,S1,S2,S3,B1,B2,B3
CCC
CCC   THE FOLLOWING ARE INPUT INTO THE PROGRAM
CCC            TWALL= TEMPERATURE AT WALL
CCC            TINF=TEMPERATURE AT INFINITY
CCC            PSIw=(1-TWALL/TINF)
CCC            NMAX=NUMBER OF X-STATIONS(MAXIMUM)
CCC            X(I)=ARRAY OF X-STATIONS
CCC            SK(I)= ARRAY OF PRESSURE GRADIENT PARAMETERS
CCC            RP(I)=ARRAY OF RADIUS PARAMETERS
CCC            K1,K2,K3= STATION NUMBERS WHERE VELOCITY AND TEMPERATURE
CCC                      PROFILE CARDS ARE TO BE PUNCHED FOR PLOTTING
```

```
CCC
CCC    THE DUMMY INDEX ARE TO BE SET TO
CCC            GFLAG=0          WHEN TEMPERATURE CONSTANT AT SURFACE
CCC                 =1          WHEN HEAT FLUX IS CONSTANT
CCC              N1=1           WHEN ONLY SIMILAR FLOW SOLUTION IS REQUIRED
CCC                =0           NON-SIMILAR SOLUTION
CCC              N3=1           WHEN INTERMEDIATE MOMENTUM SOLUTION TO BE PRINTED
CCC                =0           NO PRINT
CCC              N4=1           WHEN INTERMEDIATE ENERGY SOLUTION TO BE PRINTED
CCC                =0           NO PRINT
CCC              INCOMP=1       WHEN BOTH ENERGY AND MOMENTUM EQUATIONS TO
CCC                             BE SOLVED SIMULTANEOUSLY
CCC                   =0        ONLY MOMENTUM EQUATION SOLUTION
CCC              IBOY=1         WHEN BUOYANCY TERMS TO BE INCLUDED
CCC                  =0         NEGLECT BUOYANCY TERMS
CCC              IVIS=0         WHEN VICOSITY CONSIDERED VARIABLE
CCC                  =1         WHEN VISCOSITY IS CONSTANT AT TINF
CCC                  =-1        WHEN VISCOSITY IS CONSTANT AT TWALL
CCC
CCC    INITIAL GUESSES ARE MADE ON
CCC              PSIW= TEMPERATURE GRADIENT AT WALL AT X=0
CCC              PHIPP=VELOCITY GRADIENT AT WALL AT X=0.
CCC
       N2=0 $ QMAX=5 $ KLM=1 $ ILCM=2 $ ISK=0
       FK1=0.5 $ FK25=9. $ FK26=3. $ F26=3. $ ETMAX=3.
       EPS2=0.000001 $ EPS3=0.00001 $ EPS4=0.00001
       DETA=0.05 $ C1=0.05 $ C2=0.05
CCC      A SAMPLE INPUT IS SHOWN
CCC
      N1=0 $ N2=0 $ N3=0 $ N4=0
      GFLAG=0
      PHIPP=1.0
      TWALL=150. $ TINF=70. $ PSIW=.1509 $ PSIPW=-.12
      TEMP=(TINF+460.)/491.62
      CF=1.0/(35.15539-106.9718715*(TEMP)+107.772037*(TEMP)**2-
     140.59537*(TEMP)**3+5.6391948*(TEMP)**4)
      CINF=CE
      PRINT 100,CINF
```

```
100  FORMAT(10X,E15.5)
     K1=8 $ K2=12 $ K3=16
     X(1)=0.0
      NMAX=25
     X(1)=0. $ X(2)=0.0734$X(3)=0.15414$X(4)=.24295$X(5)=.34065
     X(6)=.44811$X(7)=.55558$X(8)=.66304$X(9)=.77051$X(10)=.87797
     X(11)=.98544$X(12)=1.0929$X(13)=1.1896$X(14)=1.2767$X(15)=1.355
     X(16)=1.4255$X(17)=1.48906$X(18)=1.5461$X(19)=1.5975$X(20)=1.6437
     X(21)=1.6854$X(22)=1.7229$X(23)=1.7566$X(24)=1.7869$X(25)=1.8142
     SK(1)=1. $ RP(1)=1.
      DO 1 I=2,NMAX
     D=X(I) $ DD=D*D $ DDD=DD*D $ DDDD=DDD*D $ DDDDD=DDDD*D
     RP(I)=D*COS(D)/SIN(D)
     SK(I)=D*(1.5-3.*.36402*DD+5.*.024668*DDDD)/(1.5*D-.36402*DDD+
    1.024668*DDDDD)
   1 CONTINUE
     IVIS=1
     IBOY=0 $ BETA=0. $ BOUY=0.
     INCOMP=1 $ CALL SOLVE
     END
     SUBROUTINE CASE(U,X)
     XXX=X*X*X
     XXXXX=XXX*X*X
      U=1.5*X-.36042*XXX+.024668*XXXXX
     RETURN
     END
     SUBROUTINE SOLVE
     INTEGER Q,QMAX,GFLAG
     COMMON/11/FK10,FK14,FK15,FK13/12/ISTA/13/XN/14/X(100)/15/T(400),
    1PRINF,C(400)/16/ETA,II,DETA/17/PH(20)/18/IE1,IE7/19/S1(4),S2(4),
    2S3(4),IFLAG/20/B1(800),B2(800),B3(800)/21/AL(200),BL(200)/22/
    3B7(1600),B8(1600),B15(400)/23/AMBAR,RBAR,SK(100),RP(100)/24/PSIPW,
    4PSIW/25/NMAX,C1,C2,CNIF,QMAX,EPS2/26/FK1,FK25/27/IRH,IRL,IRHL,IRC
    5,ML,MH,MM,MHL,MC,IFLOW,IFIRST,ISW1,ISW2,IPVS,IRET,ITER,IT,IHSW,
    6PHIL,PHIH,ETAH,ETAL,ETAHL,ELSW,EHSW,PHIPP/28/N1,N2,N3,N4/29/NNN
    7/30/INCOMP/31/IINF,IWALL,ETMAX/33/ISK/34/FK26/36/CE/37/DMETA,DEETA
```

```
     8/40/KLM/41/EPS3,EPS4,F26
      COMMON/60/IOU/61/GFLAG/62/ILCM,IBOY,BOUY,BETA/64/IFLAT
      DOUBLE PRECISION EQA,EQB,EQC,EQD,EQE,EQF
      DOUBLE PRECISION PH,S1,S2,S3,B1,B2,B3,A,B,D,CPHIPP,AAA
      DIMENSION B4(1200),B5(1200),B13(1200),B14(1200)
      EQUIVALENCE(IEK,IE1)
      EQUIVALENCE(IJK,IE7)
      LCMAX=ILCM
      FKK=FK25
CCC
CCC   BEGIN MOMENTUM EQUATION SOLUTION.
CCC
   10 ISTA=0
   15 CONTINUE
CCC   COMPUTE STATION CONSTANTS
   25 CALL SC
      Q=0 $ DETA=DMETA
   27 IF(ISTA-1)35,30,35
CCC   COMPUTE INITIAL FLUID PROPERTIES PROFILES.
   30 CALL IC
   35 LC=LCMAX
      LJ=1 $ DETA=DMETA
CCC   INITIALIZE COUNTERS.
      IPVS=0
      MC=1
      ITER=0
      IT=50
      ISW1=0
   40 ETA=0.0
      IF(PHIPP-C1)42,42,41
   42 C1=C1/10.0
      GO TO 40
   41      III=1
      ISW3=0
      IFLAG=0
      IFLOW=0
```

```
      IFIRST=0
      IF1=1
      AL(1)=0.0
      I=1
   45 PH(1)=0.0
      PH(2)=-1.0
      PH(3)=PHIPP
   50 IF(ISTA-1)55,55,60
CCC   COMPUTE X-DERIVATIVES BY FINITE DIFFERENCES.
   55 DER1=0.0
      DER2=0.0
      GO TO 120
   60 IF(IE4.GE.IE1) GO TO 70
   65 PHN1=B4(2*IE4-1)
      PHPN1=0.0
      GO TO 75
   70 PHN1=B4(2*IE1-1)
      PHPN1=B4(2*IE1)
   75 IF(Q) 90,80,90
   80 IF(IE4.GE.IE1) GO TO 90
   85 C(IE1)=C(IE4)
   90 IF(ISTA-3) 115,95,95
   95 IF(IE5.GE.IE1) GO TO 105
  100 PHN2=B5(2*IE5-1)
      PHPN2=B5(2*IE5)
      GO TO 110
  105 PHN2=B5(2*IE1-1)
      PHPN2=B5(2*IE1)
  110 DER1=FK13*PH(1)+FK14*PHN1+FK15*PHN2
      DER2=FK13*PH(2)+FK14*PHPN1+FK15*PHPN2
      GO TO 120
  115 DER1=(PH(1)-PHN1)/FK10
      DER2=(PH(2)-PHPN1)/FK10
  120 CONTINUE
      TNETA=(AMBAR+1.0)/2.0+RBAR
      PH(4)=XN*((PH(2)+1.0)*DER2-PH(3)*DER1)-TNETA*(PH(1)+ETA)*PH(3)+
```

```
     1AMBAR*((PH(2)+1.0)*(PH(2)+1.0)-1.)
      IF(IBOY.NE.1) GO TO 125
CCC   COMPUTE BUOYANCY FORCE TERM
      IB=IFLAG+1 $ IF(ISTA.EQ.1) GO TO 124
      CALL CASE(UU,XN) $ IF(IFLAT.EQ.1) GO TO 123
      BOU=(XN*SIN(XN)*BOUY*T(IB)*TINF)/(UU*UU)
      PH(4)=PH(4)-BOU $ GO TO 125
  123 BOU=(XN*BOUY*T(IB)*TINF)/(UU*UU)
      PH(4)=PH(4)-BOU $ GO TO 125
  124 BOU=BETA*T(IB)*TINF
      PH(4)=PH(4)-BOU
  125 IF(IFLOW) 140,130,140
  130 IF(IFLAG.LE.10) GO TO 140
CCC   USE INTERPOLATION FORMULES.
  135 PH(1)=PH(5)+DETA*PH(6)+(DETA*DETA)/360.0*(38.0*PH(3)+171.0*PH(7)
     1-36.0*PH(11)+7.0*PH(15))
      PH(2)=EQA(PH(6),PH(3),DETA,PH(7),PH(11),PH(15))
      CPHIPP=C(IEK-1)*PH(7)
      PH(3)=EQA(CPHIPP,PH(4),DETA,PH(8),PH(12),PH(16))
      PH(3)=PH(3)/C(IEK)
      IFLOW=1
      GO TO 50
CCC   BLOCKS BELOW CONTAIN THE MOMENTUM EQUATION SOLUTIONS.
  140 IF(MC) 150,155,160
  150 B3(I)=PH(1)
      B3(I+1)=PH(2)
      B3(I+2)=PH(3)
      B3(I+3)=PH(4)
      GO TO 165
  155 B2(I)=PH(1)
      B2(I+1)=PH(2)
      B2(I+2)=PH(3)
      B2(I+3)=PH(4)
      GO TO 165
  160 B1(I)=PH(1)
      B1(I+1)=PH(2)
      B1(I+2)=PH(3)
```

```
      B1(I+3)=PH(4)
  165 IF(ISK.NE.1) GO TO 164
      NNN=N3 $ CALL INTERP
  164 CONTINUE
CCC   CHECK IF OUTER BOUNDARY CONDITIONS ARE MET.
  166 IF(ISK.EQ.1) GO TO 190
  167 IF(ETA.LT.1.0) GO TO 195
  170 IF(PH(2)-FK1) 175,320,320
  175 IF(PH(2)) 180,180,190
  180 IF(PH(2)+FK1) 185,185,190
  185 IF(PH(3))280,190,190
  190 IF(ISK.NE.1) FKK=FK25
  191 IF(ETA-FKK) 195,275,275
CCC   MODIFY ETA AND ETA-STATION COUNTERS.
  195 II=IE1 $ CALL MODETA
      IE1=II
      AL(IE1)=ETA
CCC   USE EXTRAPOLATION FORMULAS.
      CPHIPP=PH(3)*C(IEK-1)
  205 IF(IFLAG.GE.10) GO TO 260
  210 IF(IFLAG.GE.6) GO TO 255
  215 IF(IFLAG-2) 220,240,250
  220 IF(IFLAG) 225,225,230
  225 AAA=PHIPP*C(1)
      A=EQB(AAA,DETA,PH(4))
      B=EQB(PH(2),DETA,PH(3))
      D=PH(1)-DETA/16.0+DETA/512.0*DETA*PH(3)
      GO TO 265
  230 DETAN=DETA/32.0
      DETAM=DETA/16.0
       DETASQ=DETA/1536.0*DETA
  235 A=EQC(CPHIPP,DETAN,PH(4),PH(8))
      B=EQC(PH(2),DETAN,PH(3),PH(7))
      D=EQD(PH(1),DETAM,DETASQ,PH(2),PH(3),PH(7))
      GO TO 265
  240 DETAN=DETA/16.0
      DETAM=DETA/8.0
```

```
      DETASQ=DETA/384.0*DETA
  245 A=EQC(CPHIPP,DETAN,PH(4),PH(12))
      B=EQC(PH(2),DETAN,PH(3),PH(11))
      D=EQD(PH(1),DETAM,DETASQ,PH(2),PH(3),PH(11))
      GO TO 265
  250 DETAN=DETA/8.0
      DETAM=DETA/4.0
      DETASQ=DETA/96.0*DETA
       GO TO 235
  255 A=EQE(CPHIPP,DETA,PH(4),PH(8),PH(12))
      B=EQE(PH(2),DETA,PH(3),PH(7),PH(11))
      D=PH(1)+DETA/2.0*PH(2)+DETA/96.0*DETA*(19.0*PH(3)-10.0*PH(7)+
     13.0*PH(11))
      GO TO 265
  260 A=EQF(CPHIPP,DETA,PH(4),PH(8),PH(12),PH(16))
      B=EQF(PH(2),DETA,PH(3),PH(7),PH(11),PH(15))
      D=PH(1)+DETA*PH(2)+DETA/360.0*DETA*(323.0*PH(3)-264.0*PH(7)+
     1159.0*PH(11)-38.0*PH(15))
  265 CALL SHOFT
  270 PH(1)=D
      PH(2)=B
      PH(3)=A/C(IEK)
      IFLAG=IFLAG+1
       I=I+4
      IFLOW=0
      GO TO 50
  275 IF(ISK.EQ.1) GO TO 342
CCC   MAKE BOUNDARY CONDITION TESTS ON PHIP AND PHIPP.
  276 IF(PH(2)) 280,280,320
CCC   HAVE A LOW SOLUTION
  280 IHSW=-1
      IF(ISW1)285,290,285
CCC   DETERMINE WHAT ETA-INFINITY(MAX) WILL BE
  285 CALL MAXETA
      GO TO(340,40,315) IRET
```

```
  290 PHIL=PHIPP
      PHL=PH(2)
      IRL=IE1
      ETAL=ETA
      ML=MC
      IF(IPVS)300,300,295
CCC   START BISECTION PROCESS ON PHIPP.
  295 PHIPP=PHIL-(PHL/((ABS(PHL-PHH))/(ABS(PHIL-PHIH))))
      MC=0
       IPVS=0
       ISW1=1
      GO TO 40
  300 PHIPP=PHIPP+C1
      IPVS=-1
  305 MC=-MC
      ITER=ITER+1
CCC   CHECK IF MAXIMUM NUMBER OF ITERATIONS HAVE BEEN EXCEEDED.
      IF(ITER.LE.20) GO TO 40
  310 PRINT 99
   99 FORMAT(*    MAX NUMBER OF ITERATIONS HAVE BEEN COMLPLETED*)
  315 IF(ISTA.EQ.1) GO TO 1
      ISTA=ISTA-1
      GO TO 2000
CCC   HAVE A HIGH SOLUTION.
  320 IHSW=1
      IF(ISW1)285,325,285
  325 PHIH=PHIPP
       PHH=PH(2)
      IRH=IE1
      ETAH=ETA
      MH=MC
  330 IF(IPVS)295,335,335
CCC   MAKE CORRECTION ON PHIPP AT WALL
  335 PHIPP=PHIPP-C1
      IPVS=1
      GO TO 305
```

```
CCC    USE LANGRANGIAN INTERPOLATION TO OBTAIN MOMENTUM SOLUTION
  340 CALL LANGINT
      FKK=AL(IE1)
  341 CONTINUE
      PHIPP=B1(3)
      IF(ISK.EQ.1) GO TO 35
  342 CONTINUE
      IF(INCOMP.EQ.1) GO TO 344
      CALL PLT
      GO TO 1035
  344 CONTINUE
CCC
CCC    BEGIN ENERGY SOLUTION
CCC
      ISK=0 $ DETA=DEETA
  350 IF(Q) 360,390,360
  360 IF(Q-QMAX)370,1030,1030
  370 CONTINUE $ QPW=B1(3) $ SSS=ABS(QPW-QPP)
      IF(SSS-EPS2)1030,1030,390
  390 QPP=PHIPP
CCC    INITIALIZE COUNTERS.
  400 LL=0
  410 ISW2=0
  420 IFLAG=0 $ LC=LCMAX $ ETA=0.0 $ IE7=1 $ I=1 $ IFLOW=0
      AL(1)=ETA
      PH(3)=PSIPW $ PH(2)=PSIW$ PH(1)=PH(3)
  440 IF(ISTA-1) 450,450,460
CCC    COMPUTE X-DERIVATIVES BY FINITE DIFFERENCES.
  450 DER1=0.0 $ DER2=0.0 $ GO TO 670
  460 IF(IE13.GE.IE7) GO TO 470 $ PSIN1=0.0 $ GO TO 480
  470 PSIN1=B13(IE7)
  480 IF(IJK.GT.IE4) GO TO 490 $ PHIN1=B4(2*IJK-1) $ GO TO 500
  490 PHIN1=B4(2*IE4-1)
  500 IF(LL) 530,510,530
  510 IF(Q)530,520,530
  520 IF(IE13.GE.IE7) GO TO 530
```

```
      C(IE7)=C(IE13)
  530 IF(ISTA-3)590,540,540
  540 IF(IE7.GT.IE14) GO TO 550 $ PSIN2=B14(IE7) $ GO TO 560
  550 PSIN2=0.0
  560 IF(IJK.GT.IE5) GO TO 570 $ PHIN2=B5(2*IJK-1) $ GO TO 580
  570 PHIN2=B5(2*IE5-1)
  580 DER1=FK13*B1(4*IJK-3)+FK14*PHIN1+FK15*PHIN2
      DER2=FK13*PH(2)+FK14*PSIN1+FK15*PSIN2
      GO TO 670
  590 DER1=(B1(4*IJK-3)-PHIN1)/FK10
      DER2=(PH(2)-PSIN1)/FK10
      TNETA=(AMBAR+1.0)/2.0+RBAR
      PH(4)=XN*((B1(4*IJK-2)+1.)*DER2-PH(3)*DER1)-TNETA*(B1(4*IJK-3)+
     1ETA)*PH(3) $ PH(4)=PH(4)*PRINF
      PH(4)=PH(4)-TTETA*PH(1)
  680 IF(IFLOW.EQ.1) GO TO 700 $ IF(IFLAG-10)700,700,690
CCC   USE INTERPOLATION FORMULAS.
  690 PH(1)=EQA(PH(5),PH(4),DETA,PH(8),PH(12),PH(16))
      PH(2)=EQA(PH(6),PH(3),DETA,PH(7),PH(11),PH(15))
      PH(3)=PH(1)
      IFLOW=1 $ GO TO 440
  700 CONTINUE
  720 IF(ISW2)730,740,730
CCC   BLOCKS CONTAIN ENERGY EQUATION SOLUTIONS.
  730 B8(I)=PH(1) $ B8(I+1)=PH(2) $ B8(I+2)=PH(3) $ B8(I+3)=PH(4)
      GO TO 745
  740 B7(I)=PH(1) $ B7(I+1)=PH(2) $ B7(I+2)=PH(3) $ B7(I+3)=PH(4)
  745 NNN=N4 $ CALL INTERP
  746 IF(I.LE.1) GO TO 750
      IF(ISW2.EQ.1) GO TO 750
      PPU=ABS(B7(I+1)) $ PPUA=ABS(B7(I+2)) $ QPPU=ABS(B7(I-3))
      QPPUA=ABS(B7(I-2))
      IF(PPU.LE.EPS3) GO TO 747
      GO TO 750
  747 IF(PPUA.LE.EPS4) GO TO 748
      GO TO 750
```

```
748 DIFFE=ABS(PPU-QPPU)
    DIFFEA=ABS(PPUA-QPPUA)
    IF(DIFFE.LE.EPS4) GO TO 749
    GO TO 750
749 IF(DIFFEA.LE.EPS4) FK26=ETA
750 IF(ETA-FK26)755,880,880
755 II=IE7 $ CALL MODETA $ IE7=II $ AL(IJK)=ETA
760 IF(IFLAG.GE.10) GO TO 860
770 IF(IFLAG.GE.6) GO TO 850
780 IF(IFLAG-2) 790,830,840
790 IF(IFLAG) 800,800,810
800 A=EQB(PH(1),DETA,PH(4)) $ B=EQB(PH(2),DETA,PH(3)) $ GO TO 870
810 DETAN=DETA/32.0
820 A=EQC(PH(1),DETAN,PH(4),PH(8)) $ B=EQC(PH(2),DETAN,PH(3),PH(7))
    GO TO 870
830 DETAN=DETA/16.0
    A=EQC(PH(1),DETAN,PH(4),PH(12)) $ B=EQC(PH(2),DETAN,PH(3),PH(11))
    GO TO 870
840 DETAN=DETA/8.0 $ GO TO 820
850 A=EQE(PH(1),DETA,PH(4),PH(8),PH(12))
    B=EQE(PH(2),DETA,PH(3),PH(7),PH(11))
    GO TO 870
860 A=EQF(PH(1),DETA,PH(4),PH(8),PH(12),PH(16))
    B=EQF(PH(2),DETA,PH(3),PH(7),PH(11),PH(15))
870 CALL SHOFT
    PH(1)=A $ PH(2)=B $ PH(3)=PH(1)
    IFLAG=IFLAG+1
    I=I+4
    IFLOW=0 $ GO TO 440
880 IF(ISW2)960,890,960
890 ISW2=1 $ QPS1=PH(2) $ IF(GFLAG-1)900,930,900
900 IF(QPS1)910,920,920
910 PSIPW=B7(3)+C2 $ GO TO 420
920 PSIPW=B7(3)-C2 $ GO TO 420
930 IF(QPS1)940,940,950
940 PSIW=B7(2)+C2 $ GO TO 420
```

```
  950 PSIW=B7(2)-C2 $ GO TO 420
CCC   ADD TWO SOLUTIONS OF ENERGY EQUATION TO FORM GENERAL SOLUTION.
  960 CALL ENERINT
      FK26=F26 $ PSIW=B7(2) $ PSIPW=B7(3)
  970 CALL ENERPT
CCC   COMPUTE NEW FLUID PROPERTIES FROM ENERGY SOLUTION.
  980 CALL FPWNS
  990 IF(LL-LCMAX) 1000,1010,1010
 1000 LL=LL+1 $ GO TO 410
 1010 CONTINUE
 1020 PHIPP=B1(3) $ Q=Q+1 $ GO TO 35
 1030 CALL PLT $ CALL FINAPLT
 1035 IF(N1.EQ.1) GO TO 2000
 1040 IF(ISTA.GT.1) GO TO 1050
      IE4=0 $ IE13=0
 1050 IE5=IE4 $ IE4=IE1 $ IE14=IE13 $ IE13=IE7 $ N=2*IE5 $ DO 1060 I=1,N
 1060 B5(I)=B4(I)
      N=IE4 $ DO 1070 I=1,N  $ B4(2*I-1)=B1(4*I-3)
 1070 B4(2*I)=B1(4*I-2)
      FKK=FK25 $ ISK=0
 1075 IF(INCOMP.EQ.0) GO TO 1115
 1080 N=IE14 $ DO 1090 I=1,N
 1090 B14(I)=B13(I)
 1100 N=IE13 $ DO 1110 I=1,N
 1110 B13(I)=B15(I)
 1115 IF(ISTA-1-NMAX)25,2000,2000
 2000 RETURN
      END
      SUBROUTINE IC
      INTEGER GFLAG
      COMMON/15/T(400),PRINF,C(400)/16/ETA,II,DETA/37/DMETA,DEETA
     1/30/INCOMP/31/TINF,TWALL,ETMAX/36/CE/34/FK26
     2/61/GFLAG/24/PSIPW,PSIW/63/IVIS/64/IFLAT
      EQUIVALENCE(CE,CCIU)
      TREF=491.69
      IF(IVIS.EQ.1) GO TO 27
```

```
      IF(IVIS)27,1,27
    1 CONTINUE
      IF(INCOMP.EQ.0) GO TO 25
      DETA=DEETA
      ETA=0.0
       II=1 $ I=1
   10 IF(ETA.GE.ETMAX) GO TO 30
      IF(GFLAG.EQ.1) GO TO 100
      IF(I.EQ.1) GO TO 20
      CALL MODETA $ GO TO 21
   20 TEMP=(TINF+460.)/TREF
      CCIU=1.0/(35.15539-106.9718715*(TEMP)+107.772037*(TEMP)**2-
     140.59537*(TEMP)**3+5.6391948*(TEMP)**4)
      CE=CCIU
   21 TEMP=TWALL-((TWALL-TINF)/ETMAX)*ETA
      T(I)=(TEMP/TINF-1))
       TEMP=(TEMP+460.0)/TREF
  101 CONTINUE
      C(I)=1.0/(35.15539-106.9718715*(TEMP)+107.772037*(TEMP)**2-
     140.59537*(TEMP)**3+5.6391948*(TEMP)**4)
      C(I)=C(I)/CCIU
      I=I+1
      GO TO 10
  100 CONTINUE
      T(I)=PSIPW*(ETA-ETMAX)
      TEMP=(T(I)+1.)/TREF
      TEMP=(TEMP+460.)/TREF
      CALL MODETA
      GO TO 101
   25 DO 26 J=1,300
   26 C(J)=1.0
      IF(IVIS.EQ.0) GO TO 30
   27 II=1 $ ETA=0. $ J=1
      IF(IVIS) 40,41,40
   40 TEMP=(TWALL+460.)/TREF
      CCIU=1.0/(35.15539-106.9718715*(TEMP)+107.772037*(TEMP)**2-
```

```
     140.59537*(TEMP)**3+5.6391948*(TEMP)**4)
      GO TO 28
   41 TEMP=(TINF+460.)/TREF
      CCIU=1.0/(35.15539-106.9718715*(TEMP)+107.772037*(TEMP)**2-
     140.59537*(TEMP)**3+5.6391948*(TEMP)**4)
   28 T(J)=PSIw-((PSIw-1.)*ETA)/ETMAX
      C(J)=CCIU
      IF(ETA.GE.ETMAX) GO TO 29
      CALL MODETA $ J=4+1 $ GO TO 28
   29 TEMP=(TINF+460.)/TREF  $ I=J
   30 IF(INCOMP.EQ.0) GO TO 35
      DO 31 J=I,400
      T(J)=T(J-1)
   31 C(J)=C(J-1)
  110 IAA=-1  $ IF(IVIS.EQ.IAA) TEMP=(TWALL+460.)/TREF
      PRINF=1.0/(73.376906-208.7474538*TEMP+197.7604676*(TEMP)**2
     1-68.8626186*(TEMP)**3+7.4779458*(TEMP)**4)
      PRINF=PRINF*13.66
   35 RETURN
      END
      SUBROUTINE SC
      COMMON/11/FK10,FK14,FK15,FK13/13/XN/14/X(100)/12/ISTA/23/AMBAR,
     1RBAR,SK(100),RP(100)
      ISTA=ISTA+1
      XN=X(ISTA)
      AMBAR=SK(ISTA)
      RBAR=RP(ISTA)
      IF(ISTA.NE.1) GO TO 20
   10 RETURN
   20 FK10=X(ISTA)-X(ISTA-1)
      IF(ISTA.LT.3) GO TO 10
      FK13=X(ISTA)-X(ISTA-2)
      FK15=X(ISTA-1)-X(ISTA-2)
      FK14=-FK13/(FK10*FK15)
      FK15=FK10/(FK13*FK15)
      FK13=1.0/FK10+1.0/FK13
```

```
      RETURN
      END
      SUBROUTINE INTERP
      COMMON/16/ETA,I,DETA/18/IE1,IE7/17/PH(20)/29/NNN
      DOUBLE PRECISION PH
C
C     THIS SUBROUTINE PRINTS INTERMEDIATE VALUES
C
      IF(NNN.EQ.0) GO TO 50
      IF(IE1-1) 1,1,2
    1 PRINT 10
      PRINT 20, ETA,PH(1),PH(2), PH(3), PH(4),PH(3)
      GO TO 50
    2 PRINT 30, ETA,PH(1),PH(2),PH(3),PH(4)
   10 FORMAT(//3HETA,12X,2HPH,13X,3HPHP,12X,4HPHPP,11X,6HCPHPPP,9X,
     15HPHPPW)
   20 FORMAT(E15.5,5D15.5)
   30 FORMAT(E15.5,4D15.5)
   50 RETURN
      END
      SUBROUTINE SHOFT
      COMMON/17/PH(20)/19/S1(4),S2(4),S3(4),IIFLAG
      DOUBLE PRECISION PH,S1,S2,S3
      IFLAG=IIFLAG
      IF(IFLAG.GT.0) GO TO 5
      DO 1 I=1,4
    1 S1(I)=PH(I)
      GO TO 55
    5 IF(IFLAG.NE.2) GO TO 10
      DO 6 I=1,4
    6 PH(I)=S1(I)
      GO TO 55
   10 IF(IFLAG.NE.4) GO TO 15
      DO 11 I=1,4
   11 S2(I)=PH(I)
      GO TO 55
```

```
   15 IF(IFLAG.NE.5) GO TO 20
      DO 16 I=1,4
       PH(I)=S2(I)
   16 PH(I+4)=S1(I)
      GO TO 55
   20 IF(IFLAG.NE.6) GO TO 25
       DO 21 I=1,4
   21 S3(I)=PH(I)
      GO TO 55
   25 IF(IFLAG.NE.9) GO TO 55
      DO 26 I=1,4
      PH(I)=PH(I+4)
      PH(I+4)=S3(I)
   26 PH(I+8)=S1(I)
   55 I=16
      J=12
   60 PH(I)=PH(J)
      I=I-1
      J=J-1
      IF(J)75,75,60
   75 RETURN
      END
      SUBROUTINE MODETA
      COMMON/16/ETAXX,IEX,DETAX
CSUBROUTINE TO MODIFY ETA TO BE UESD IN THE NEW EQUATIONS
C     ETAX= TRANSFORMED NORMAL COORDINATE
C     IEX =NUMBER OF ETA INTERVALS
C     DETA = DENOTES THE ETA INTERVAL
C
      ETAX=ETAXX
      DETA=DETAX
      IF(IEX-11) 2,25,25
    2 GO TO (5,5,10,15,15,15,20,20,20,20) IEX
    5 ETAX=ETAX+DETA/16.
      GO TO 30
   10 ETAX=ETAX+DETA/8.
```

```
      GO TO 30
   15 ETAX=ETAX+DETA/4.0
      GO TO 30
   20 ETAX=ETAX+DETA/2.0
      GO TO 30
   25 ETAX=ETAX+DETA
   30 IEX=IEX+1
      ETAXX=ETAX
      RETURN
       END
      SUBROUTINE LANGINI
      COMMON/13/XN/18/IE1,IE7/20/B1(1200),B2(1200),B3(1200)/21/AL(300)
     1,BL(300)/33/ISK/12/ISTA
      DOUBLE PRECISION B1,B2,B3,A,B,D,A20,A21,A22
      KK=4*IE1-2
      JJ=KK+2
      A=B1(KK)
      B=B2(KK)
      D=B3(KK)
      A20=(B*D)/((A-B)*(A-D))
      A21=(A*D)/((B-A)*(B-D))
      A22=(A*B)/((D-A)*(D-B))
       PRINT 1
       DO 10 II=1,JJ
   10 B1(II)=A20*B1(II)+A21*B2(II)+A22*B3(II)
      ILK=JJ-7
      PRINT 4,IE1
    4 FORMAT(60X,* I AT ETMAX=*,I5)
      J=1
    1 FORMAT(*            FINAL     INTERPOLATED      ANSWERS*)
      DO 11 I=1,JJ,4
      BL(J)=B1(I+1)
   11 J=J+1
      IE1=J-1
      PRINT 2,XN,B1(3)
    2 FORMAT(10X,*  XN=======*,E15.5,*FPPWALL====*,D25.15)
```

```
      ISK=1
      RETURN
      END
      SUBROUTINE FPWNS
      COMMON/15/T(400),PRINF,C(400)/18/IE1,IE7/31/TINF,TWALL,ETMAX/36/CE
     1/63/IVIS
      IF(IVIS.NE.0) GO TO 30
      DO 1 I=1,IE7
      TEMP=(T(I)*(TINF+460.))/491.69
      C(I)=1.0/(35.15539-106.9718715*(TEMP)+107.772037*(TEMP)**2-
     140.59537*(TEMP)**3+5.6391948*(TEMP)**4)
      C(I)=C(I)/CE
    1 CONTINUE
      II=IE7+1
      DO 2 J=II,400
    2 C(J)=C(IE7)
   30 CONTINUE
      RETURN
      END
      SUBROUTINE FINAPLT
      COMMON/21/AL(200),BL(200)/15/T(400),PRINF,C(400)/18/IE1,IE7
      COMMON/37/D,DEETA/16/ETA,J,DETA/31/TINF,TWALL,ETMAX
      COMMON/60/IOU
      DIMENSION U(400)
      DETA=DEETA $ J=1 $ ETA=0.
      IF(IOU.EQ.1) GO TO 25
      DO 3 I=1,IE7
      TW=T(I)*(TINF+460.) $ TW=TW-460.
      U(I)=(TW-TWALL)/(TINF-TWALL)
      PUNCH 10,ETA,U(I)
    3 CALL MODETA
   10 FORMAT(10X,E15.5,10X,E15.5)
   25 IOU=1
      RETURN
       END
```

```
      SUBROUTINE ENERPT
      COMMON/13/XN/15/T(400),PRINF,C(400)/18/IE1,IE7/22/B7(1600),B8(1600
     1),B15(400)
      DO 3 I=1,IE7
    3 T(I)=B15(I)
      PRINT 4,T(1),T(IE7)
    4 FORMAT(10X,*TEMPERATURES AT WALL AND INFINITY*,E15.5,5X,E15.5)
      RETURN
       END
      SUBROUTINE ENERINT
      COMMON/18/IE1,IE7/22/B7(1600),B8(1600),B15(400)
      J=4*IE7 $ K=J-2 $ A1=B7(K)-B8(K) $ A=B7(K)/A1 $ A1=-B8(K)/A1
      DO 10 I=1,J,4
CCCCCCCCC            NEW    PSI
      B7(I+1)=A1*B7(I+1)+A*B8(I+1)
CCCCCCCC             NEW     PSI   PRIME
   10 B7(I+2)=A1*B7(I+2)+A*B8(I+2)
      DO 20 I=1,IE7
       B15(2*I-1)=B7(4*I-2)
   20 CONTINUE
      RETURN
      END
      SUBROUTINE MAXETA
       COMMON /16/ETA,I,DETA/26/FK1,FK25/27/IRH,IRL,IRHL,IRC
     1,ML,MH,MM,MHL,MC,IFLOW,IFIRST,ISW1,ISW2,IPVS,IRET,ITER,IT,IHSW,
     6PHIL,PHIH,ETAH,ETAL,ETAHL,ELSW,EHSW,PHIPP
     7/12/ISTA
     8/18/IE1,IE7
      EQUIVALENCE(PHIPP,PHIW)
   90 FORMAT(//*TWO SUCCESSIVE VALUES OF PHIPP AT WALL HAVE APP THE SAME
     1 VALUE AT STATION*,I2,/*ETA INFINITY WAS SET EQUAL TO *,E15.5)
  999 FORMAT( I5,15X,E15.5,*   MAX NO OF BISECTIONS---TERMINATE   *)
   10 MHL=MC
      ETAHL=ETA
      IRHL=IE1
   20 IF(IFIRST) 100,30,100
```

```
 30 IF(ETAH-FK25)40,40,50
 40 EHSW=0.0
    GO TO 60
 50 EHSW=1.0
 60 IF(ETAL-FK25)70,70,80
 70 ELSW=0.0
    GO TO 900
 80 ELSW=1.0
900 IFIRST=1
100 DIF=ABS(PHIH-PHIL)/(ABS(PHIH)+ABS(PHIL))
    IF(DIF.GT.0.00001) GO TO 200
110 IF(IRH.GE.IRL) GO TO 130
120 IF(IRH-IRHL) 160,150,150
130 IF(IRHL.LT.IRL) GO TO 150
140 ETA=ETAL
    IRH=IRL
    IRHL=IRL
    IRC=IRL
    IE1=IRL
     GO TO 170
150 ETA=ETAHL
    IRH=IRHL
    IE1=IRHL
    IRC=IRHL
    IRL=IRHL
    GO TO 170
160 ETA=ETAH
    IRHL=IRH
    IRL=IRH
    IF1=IRH
    IRC=IRH
170 KL=ISTA-1
    PRINT 999, KL,ETA
180 IRET=1
190 RETURN
200 IT=II-1
```

```
      IF(IT.GT.5) GO TO 210
      IRET=3
      PRINT 999
      GO TO 190
  210 IF(ETA-FK25) 220,220,260
  220 IF(IHSW)230,230,250
  230 MM=MC
      MC=ML
      ML=MM
      IRL=IRHL
       ETAL=ETA
      PHIL=PHIW
  240 PHIW=(PHIL+PHIH)/2.0
      IRET=2
      GO TO 190
  250 MM=MC
      MC=MH
      MH=MM
      ETAH=ETA
      PHIH=PHIW
      IRH=IRHL
      GO TO 240
  260 IF(IHSW) 310,270,270
  270 IF(ELSW) 290,280,290
  280 EHSW=1.0
      GO TO 250
  290 IF(EHSW)300,280,300
  300 IRL=IRHL
      IRH=IRHL
       GO TO 180
  310 IF(EHSW) 330,320,330
  320 ELSW=1.0
      GO TO 230
  330 IF(ELSW.EQ.0.0) GO TO 320
       GO TO 300
      END
```

```
      SUBROUTINE FINALP
CCC   THIS SUBROUTINE CALCULATES THE BOUNDARY LAYER PARAMETERS AT EACH
CCC   X-STATION ALONG THE BOUNDARY
      COMMON/13/XN/18/IE1,IE7/16/ETA,I,DETA/20/B1(800),B2(800),B3(800)
     1/15/T(400),PR,C(400)/22/B7(1600),B8(1600),B15(400)/30/INCOMP
     2/37/DMETA,DEETA
     3/31/TINF,TWALL,ET
      DOUBLE PRECISION B1,B2,B3
      DIMENSION FR(10)
      IFLAG=0
      CALL CASE(UEUSQ,XN)
      IF(UEUSQ.EQ.0.0.OR.XN.EQ.0.) GO TO 1
      DENOM=SQRT(UEUSQ/XN)
      GO TO 5
    1 DENOM=0.0
      DO 4 J=1,5
    4 FR(J)=0.0
      GO TO 60
    5 ETA=0. $ DETA=DEETA
       I=1
      IF(INCOMP-0)11,13,11
   11 GP=B7(4*I-2)
      IF(GP-.01)3,3,10
   10 CALL MODETA
      GO TO 11
    3 CALL MODETA
       FR(1)=ETA/DENOM
      GO TO 15
   13 FR(1)=0.
   15 ETA=0. $ DETA=DMETA $ I=1
   16 FP=B1(4*I-2)+1.
      IF(FP-.99)17,18,18
   17 CALL MODETA
       GO TO 16
   18 CALL MODETA
      FR(2)=ETA/DENOM
```

```
      ETA=0. $ I=1
      DO 20 J=1,IE1
   20 CALL MODETA
      FRR=ETA/DENOM
   30 F=B1(4*IE1-3)*ETA
       FR(3)=FRR-F/DENOM
   40 DO 50 I=1,IE1
      FP=B1(4*I-2)*1.
      FPSQ=FP*FP
       CALL INTEG(IFLAG,DMETA,FPSQ,ANS)
   50 IFLAG=IFLAG+1
      RES=0.
      FR(4)=(F-ANS)/DENOM
      FR(5)=(F-RES)/DENOM
   60 FR(6)=2.*C(1)*B1(3)
      IF(DENOM.EQ.0.) GO TO 70
      FR(7)=2.*((UEUSQ)**1.5)*(SQRT(1./XN))*C(1)*B1(3)
   70 CONTINUE
      IF(INCOMP.EQ.0) GO TO 80
      FR(8)=-B7(3)/B7(2)
      IF(DENOM.EQ.0.) GO TO 71
      TEMP=TWALL*460. $ TEMP=TEMP/491.62
      PW=1./(73.376906-208.7474538*TEMP+197.7604676*(TEMP)**2-68.862618
     16*(TEMP)**3+7.4779458*(TEMP)**4)
      PW=PW*13.66 $ FR(9)=FR(8)/(2.*PW*UEUSQ*B1(3))
   71 CONTINUE
      FR(10)=B1(3)
      GO TO 90
   80 FR(8)=0. $ FR(9)=0. $ FR(10)=B1(3)
   90 CONTINUE
      PRINT 100,FR(1),FR(2),FR(3),FR(4),FR(5)
       PRINT 100,FR(6),FR(7),FR(8),FR(9),FR(10)
  100 FORMAT(10X,5E15.5)
      DO 111 I=1,10
  111 PUNCH110,XN,FR(I)
  110 FORMAT(10X,E15.5,10X,E15.5)
      RETURN
      END
```

```
      SUBROUTINE PLT
CCC   THIS ROUTINE PUNCHES VELOCITY AND TEMPERATURE PROFILES
      COMMON/21/A(200),B(200)/18/IE1,IE7/12/ISTA/28/N1,N2,N3,N4
     1/23/AMBAR,RBAR,SK(100),RP(100)
     2/13/XN/27/IRH,IRL,IRHL,IRC
     5,ML,MH,MM,MHL,MC,IFLOW,IFIRST,ISW1,ISW2,IPVS,IRET,ITER,IT,IHSW,
     6PHIL,PHIH,ETAH,ETAL,ETAHL,ELSW,EHSW,PHIPP
      COMMON/60/IOU
      COMMON/30/INCOMP
      PRINT 3,AMBAR
    3 FORMAT( *PRESSURE PARAMETER= *,E15.5)
      N=IE1
      PRINT 11,N,IE7
   11 FORMAT( *   IE1=    *,I5,*       IE7=    *,I5)
      IF(ISTA.EQ.1) IOU=0
      IF(ISTA.EQ.11) IOU=0
      IF(ISTA.EQ.21) IOU=0
      IF(ISTA.EQ.31) IOU=0
      IF(ISTA.GE.41) IOU=0
      IF(IOU.EQ.0) GO TO 12
      GO TO 22
   12 DO 13 I=1,N
      C=B(I)+1.
   13 PUNCH 14,A(I),C
   14 FORMAT(10X,E15.5,10X,E15.5)
   22 CONTINUE
      CALL FINALP
      IF(INCOMP.EQ.0) IOU=1
      RETURN
      END
*DECK INTEG
      SUBROUTINE INTEG(IFLAG,DDETA,FFX,AAY)
      DETA=DDETA
      FX=FFX
      IF(IFLAG)5,20,5
    5 IF(IFLAG.GT.11) GO TO 100
```

```
   10 GO TO(30,30,40,50,60,60,70,80,80,80,90),IFLAG
   20 NFLAG=0
   30 DETAX=DETA/16.
      CALL SIMPS(NFLAG,DETAX,FX,AY)
      AYY=AY
      GO TO 110
   40 NFLAG=0
      DETAX=DETA/8.
      CALL SIMPS(NFLAG,DETAX,FXX,AY)
      CALL SIMPS(NFLAG,DETAX,FX,AY)
      AYY=AY+A1
      GO TO 110
   50 NFLAG=0
      A2=A1
      CALL SIMPS(NFLAG,DETAX,FXX,AY)
   60 DETAX=DETA/4.
      CALL SIMPS(NFLAG,DETAX,FX,AY)
      AYY=AY+A2
      GO TO 110
   70 NFLAG=0
      A2=A1
      CALL SIMPS(NFLAG,DETAX,FXX,AY)
   80 DETAX=DETA/2.
      CALL SIMPS(NFLAG,DETAX,FX,AY)
      AYY=AY+A2
      GO TO 110
   90 NFLAG=0
      A2=A1
      CALL SIMPS(NFLAG,DETA,FXX,AY)
  100 CALL SIMPS(NFLAG,DETA,FX,AY)
       AYY=AY+A2
  110 FXX=FX
      A1=AYY
      AAY=AYY
        RETURN
       END
```

```
      SUBROUTINE SIMPS(NFLAG,DX,F,SUM)
      NFLAG=NFLAG+1
      IF(NFLAG-4)2,20,20
    2 GO TO (5,10,15),NFLAG
    5 SUM=0. $ SUM1=0. $ GO TO 80
   10 SUM=((F2+F)/2.)*DX
      GO TO 80
   15 SUM=SUM1+DX*(F1+4.*F2+F)/3.
       SUM1=SUM $ ASSIGN 25 TO K
      GO TO 80
   20 GO TO K,(25,15)
   25 SUM=SUM+DX*((-0.25*F1)+2.*F2+1.25*F)/3.
      ASSIGN 15 TO K
   80 F1=F2 $ F2=F
  100 RETURN
      END
      DOUBLE PRECISION FUNCTION EQA(A,B,DETA,C,D,E)
      DOUBLE PRECISION A,B,C,D,E
C     INTERPOLATION FORMULAS USED WHEN STEP SIZE OF FOUR DELYA HAS
C      BEEN BUILT UP
      EQA=A+DETA/24.0*(9.0*B+19.0*C-5.0*D+E)
      RETURN
      END
      DOUBLE PRECISION FUNCTION EQB(A,DETA,B)
      DOUBLE PRECISION A,B
      EQB=A+DETA/16.0*B
      RETURN
  902 END
      DOUBLE PRECISION FUNCTION EQC(A,DETA,B,C)
      DOUBLE PRECISION A,B,C
C     TAYLOR SERIES STEP SIZE DETA/16.0
C     THIS FUNCTION VALID FOR ALL TWO POINT FORMULA
      EQC=A+DETA*(3.0*B-C)
      RETURN
      END
      DOUBLE PRECISION FUNCTION EQD(A,DETAN,DETASQ,B,C,D)
      DOUBLE PRECISION A,B,C,D
```

```
      EQD=A+DETASQ*(4.0*C-D)+DETAN*B
      RETURN
      END
      DOUBLE PRECISION FUNCTION EQE(A,DETA,B,C,D)
      DOUBLE PRECISION A,B,C,D
C     FUNCTION VALID FOR ALL THREE POINT EXTRAPOLATION FORMULAS
C     WITH STEP SIZE DETA/2.0
      EQE=A+(DETA/24.0)*(23.0*B-16.0*C+5.0*D)
      RETURN
      END
      DOUBLE PRECISION FUNCTION EQF(A,DETA,B,C,D,E)
      DOUBLE PRECISION A,B,C,D,E
C     FOUR POINT EXTRAPOLATION
C      FULL STEP SIZE
      EQF=A+DETA/24.0*(55.0*B-59.0*C+37.0*D-9.0*E)
      RETURN
      END
```